UNIVERSITÉ DE SHERBROOKE
Faculty of Applied Sciences
Department of Civil Engineering

REMOTE MONITORING OF UNDERGROUND EXCAVATIONS BY MEANS OF DEFORMATION MEASUREMENTS (CIUS)

by

Vahid Reza Hajiabdolmajid

A Thesis submitted for the degree
of Master of Sciences in Civil Engineering

April, 1996

Sherbrooke (Québec), CANADA

ABSTRACT

The Niobec mine is located in St-Honoré 15 km north-east of Chicoutimi (Quebec, Canada) and produces Niobium at a rate of 815,000 metric tones annually. Exploitation is done using the Long Hole method with sill and crown pillars at the levels 300-600 (90-180m) and 700-1000 (200-300m). For economic reasons, no backfill has been used at this mine. As a result, stopes with a minimum 100 meters in height have been left open since excavation. Mining activity take places in a carbonatite pluton located in the Pre-Cambrian Shield. The carbonatite and host rocks are capped by flat lying limestone. The carbonatite, which is rich in carbonate minerals, contains small vertical zones of Niobium enrichment.

Six CIUS (Cylindre Instrumenté de l'Université de Sherbrooke) have been installed at this mine. The CIUS is a cylindrical concrete inclusion, instrumented with vibrating wires, installed in a borehole and used to follow the variations of stress and deformation in the host medium (rock mass). The objectives of instrumentation at this mine by the CIUS are to monitor the variations of stress and deformation, which can lead to a better understanding of the stability of underground openings and detection of the instabilities which can endanger stability of the underground excavations by triggering the warning signals.

The thesis presents the development and application of a probabilistic model for prevention and prediction of in-situ rock mass failure. The programming procedure of a rock failure warning system (Alarm System) using the CIUS' data has also been presented. The algorithm of this model operates on the basis of the detection of the anomalies on the deformation rates, recorded by the CIUS. The warning system contains the CIUS and an acquisition system, developed at the Université de Sherbrooke (CAIUS), in which the algorithm of the preventive model can be implanted. It has been shown that this unit can offer the continuous remote monitoring of underground structures, regardless where they are located.

The thesis also presents the last results of monitoring by the installed CIUS at the different levels of the Niobec mine.

SOMMAIRE

La mine Niobec exploite un gisement de Niobium par la méthode des longs-trous sur deux niveaux, un troisième devant être prochainement mis en exploitation. Ceci engendre la création d'immenses excavations de plus de 100 mètres de hauteur, excavations dont le gigantisme peut mettre en défaut leur stabilité. La roche est une carbonatite légèrement métamorphisée et peu fissurée, ce qui lui a permis de ne pas céder sous les charges appliquées.

Ainsi, pour comprendre les mécanismes de transfert de charges dans cette mine, un total de six instruments (cylindre instrumenté de l'Université de Sherbrooke, CIUS) ont été installés depuis 1989. Ces CIUS ont pour but de:

- faire le suivi des variations de contrainte et de déformation afin de pouvoir analyser le comportement de massif.
- prévoir les instabilités et déclencher des alarmes en cas de danger.

Ce mémoire présente le développement et l'application d'un modèle probabilistique pour la prévention et la prévision de ruptures dans les massifs rocheux. L'algorithme de ce modèle a été utilisé pour programmer un système d'alarme qui déclenche les alarmes en cas d'instabilités imminentes. Cet algorithme fonctionne sur le principe de la détection d'anomalies sur les courbes de variations de déformations mesurées par les CIUS. Il possède l'avantage d'être probabiliste, ce qui le rend plus facile d'utilisation; il n'est pas nécessaire de fixer un seuil de déclenchement.

Cet algorithme peut être programmé sur le système d'acquisition développé à l'Université de Sherbrooke (CAIUS). Ce système CAIUS peut ainsi être inséré dans le même forage que le CIUS (diamètre 96 mm ou 152 mm), ce qui est la meilleure protection pour lutter contre tous les aléas existant dans les mines: chutes de blocs, dynamitages, circulation d'engins,...

Ce mémoire présente aussi les résultats de l'auscultation de la mine Niobec par les CIUS de 1993 à 1995, ainsi qu'une illustration du type d'application d'un tel modèle probabiliste.

ACKNOWLEDGMENTS

I would like to express my sincere thanks to my supervisor Professor Gérard Ballivy for his encouragement and assistance, without whom it would have been impossible to accomplish this study. Thanks are also due to Dr. Kaveh Saleh at IREQ who provided his generous help and guidance during my graduate studies.

I would like to acknowledge a fellowship from the Ministry of Culture and Higher Education of IRAN which made my graduate studies possible at the Université de Sherbrooke.

Ghislain Pomerleau at the Niobec mine, Trimbak Pavate, Danick Charbonneau and Martin Lizotte at the Laboratory of Rock Mechanics and Applied Geology of the Université de Sherbrooke are also acknowledged for their help and cooperation.

TABLE OF CONTENTS

LIST OF ILLUSTRATIONS

LIST OF TABLES

CHAPTER 1

1. INTRODUCTION

1.1 Stability monitoring of underground structures

Monitoring of rock performance is one of the most important activities in hard rock mining which characterizes the operational response of the rock mass to mining activity. The intention is to establish a comprehension of the roles of the various elements of the rock mass in the load-deformational behavior of the rock medium. The data required to generate this understanding can be obtained by displacement and stress measurements made at key locations in the mine structures. The measurements include closures across pillars, slip on faults, and leveling and horizontal displacement measurement in and around the active mining zone. States of stress may be measured in pillars, abutments and in the interior of any rock units showing signs of excessive stress. Also visual inspections may be undertaken regularly to locate any structurally controlled failures and areas of anomalous response.

The most desirable goal in underground mining is the control of the deformability, movement and stresses in the rock surrounding mine excavation. It is necessary to be able to predict excessive movement or stresses since these can endanger the safe excavation of rock and production of ore. Various types of instruments are being used to determine the stability of openings and rock properties.

Rock mechanics instrumentation is indispensable for detecting potential ground instability and has become an integral part of the mining operation, particularly with regard to the planning and design of safe underground structures.

The monitoring of rock mass where the potential exists either for ground falls due to separation along a plane or planes of weakness or sudden and violent rock failure due to high stress concentration (rock burst), is particularly important and should not be omitted from any ground control program. In such cases, protective measures can be taken in order to prevent adverse phenomena.

The philosophy of rock monitoring should emphasize the preventative aspects rather than the remedial aspect of the instability of mine excavations.

1.2 Objectives of the study

The engineering mechanics problem posed in all structural design is the prediction of the performance of the structure under the loads imposed on it during its prescribed functional operation.

Clearly, the subject as defined is of fundamental relevance to mining engineering because the act of creating mining excavations changes the force fields of the rock's physical environment. The study of the response of the rock to these changes requires the application of analytical techniques and instruments developed specifically for this purpose.

Starting in 1985, the Laboratory of Rock Mechanics and Applied Geology of the Université de Sherbrooke began the development of the CIUS (Cylindre Instrumenté de l'Université de Sherbrooke). The objective has been to obtain a simple, reliable and robust technique which can meet the requirements of the principles for monitoring the variations of stresses and deformation over a long period of time. This technique is based on the application of an inclusion device, instrumented with vibrating wires, installed in a borehole in the host medium (rock mass or concrete structure).

Several studies have been conducted in order that the fabrication, installation, and data interpretation be done perfectly and correctly. Several civil structures have been instrumented so far by the CIUS. For the first time an underground mine has been instrumented using this instrument in 1989. Six CIUS have been installed at the Niobec mine, located 13 km north-east of Chicoutimi, Quebec. The goals of instrumentation at this mine have been as follows:

1- Monitoring the variations of stresses and those of deformations, which would lead to a better understanding of the stability of stopes and the pillars in different levels.

2- Detection of the instabilities which endanger stability of underground openings by triggering the warning signals when an instability is anticipated.

Previous studies have been considered to achieve the final objective of instrumentation at the mine under consideration. In addition, real time programs were prepared to operate specially developed acquisition system and an intelligent system. Further, the present work makes the use of CIUS' data for automated remote monitoring of the mining structures at the study site. All aspects of mining structures instrumentation will be fully explored through this thesis in subsequent chapters.

Chapter 2 describes the principal instruments which are used in the mines. They are used to assure the stability of underground openings. Chapter 3 reviews the instruments which are used for in-situ stress measurements in underground mines. Chapter 4 provides a description of the developed technique and the instrument, designed at the Laboratory of Rock Mechanics and Applied Geology of the Université de Sherbrooke (CIUS) for monitoring variations of stresses and deformation.

Chapter 5 provides a discussion of approaches for development of a rock failure warning system (discussing the possible methods for programming a rock failure warning system). Chapter 6 presents the development of a probabilistic and statistical preventive model for the detection of anomalies in the rate of deformation. It includes also the decision making regarding the warning signals to be triggered.

Chapter 7 gives the theoretical presentation of the possibility of failure-time prediction in the rocky mediums of underground mining openings by means of deformation measurements. The development of the remote monitoring system at the Niobec mine have been reported in chapter 8. This chapter also describes the application of the probabilistic preventive model, for programming a rock failure warning system, using the CIUS' data at the Niobec mine. The latest results of monitoring by the installed CIUS at different levels of the mine are also presented.

CHAPTER 2

2. ENSURING STABILITY BY MEANS OF INSTRUMENTATION

2.1 Introduction

Instrumentation of excavations for the safety of underground and surface mines is normally carried out during the construction of these structures. The measurements of the instrumentation should provide warnings of potential problems so that remedial measures can be taken before the problems have developed to a stage where the remedial measures are either very expensive or impossible to execute. They also provide information which can be used to check the validity of the design and to permit the completion of on-going design work.

Londe [43], Bieniawski and Maschek [6] consider that the measurement of displacement is the most effective means of monitoring the rock mass behavior during the construction of an underground excavation. Therefore, principal types of ground movement would first be briefly discussed, prior to the description of individual instrumentation techniques.

2.2 Mechanism of ground movement

There are theoretically four possible types of ground movement as represented in the displacement curves of Figure 2.1 and Figure 2.2. The convergence is that of a stope back and may be described by the following ground conditions:

(a) No deformation: the stope back has a low level of stress which does not produce any measurable displacement (stable ground conditions).

(b) Creep deformation: the stope back has a higher level of stress which produces a creep deformation which decreases with time (stable ground conditions).

(c) Linear deformation: the stope back experiences a build-up of stress which could eventually result in a rock burst failure (dangerous ground conditions).

(d) Accelerated deformation: the stope back experiences dilation of the planes of weakness resulting in an increased downward movement of blocks due to gravity and the potential for a sudden fall of ground (dangerous ground conditions) [39].

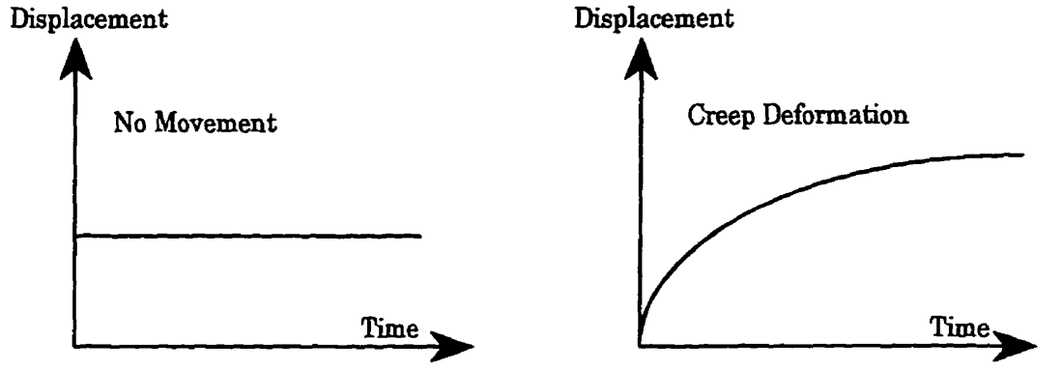

Figure 2.1 Two types of stable ground conditions

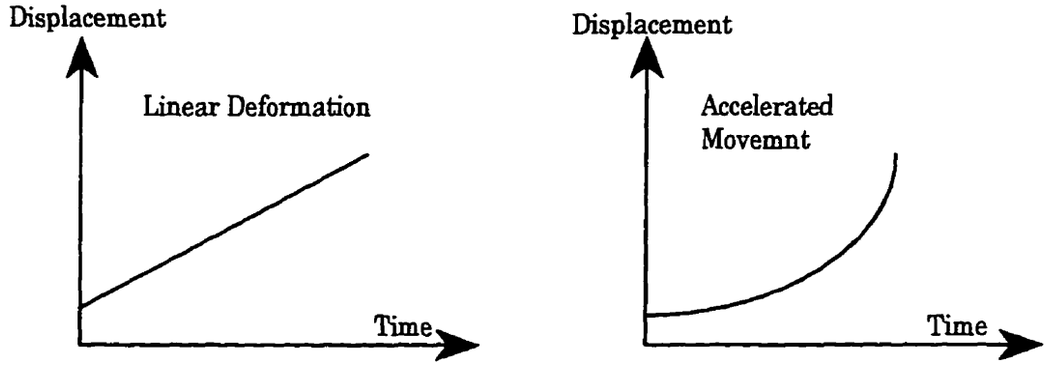

Figure 2.2 Two types of dangerous ground conditions

2.3 Ground movement instrumentation

There are many instruments which may be used to assure the safety and the stability of underground openings by means of measuring ground movement. To understand and correctly interpret the measured data of ground movement is of paramount importance so that the correct preventative measures may be taken in order to avoid an accident in underground. The following instruments are among the most important ones which may be used for monitoring an underground structure.

2.4 Multi-wire extensometer

This instrument measures the axial displacement of a borehole in which a number of violin or piano wires have been anchored at different depths. The most common is the six-wire extensometer. The anchors are usually made of aluminum wedges and constant tension is applied to each wire. A measuring device physically measures the position of the anchor relative to the collar station within 0.025mm.

The installation of multi-wire extensometers is usually perpendicular to the ore body or to other geological structures. It is the most commonly used to measure the movements of crown pillars and stope walls [66].

2.5 Multi-rod extensometer

This instrument also measures the axial displacement of a borehole similar to the wire extensometer. It is suitable for monitoring the movements of stope and drift backs. There are several types of multi-rod extensometers currently on the market but only two are described below.

2.5.1 Rod extensometer with snap-ring anchors

This type of rod extensometer is suitable for monitoring rock mass displacement and rock separation and can be installed in any orientation. It consists of steel rods which extend from each anchor up to the collar anchor which is set inside the mouth of the borehole (Figure 2.3). This type of extensometer is particularly suitable for upward directed holes in hard or competent rock where the borehole are smooth and will remain open.

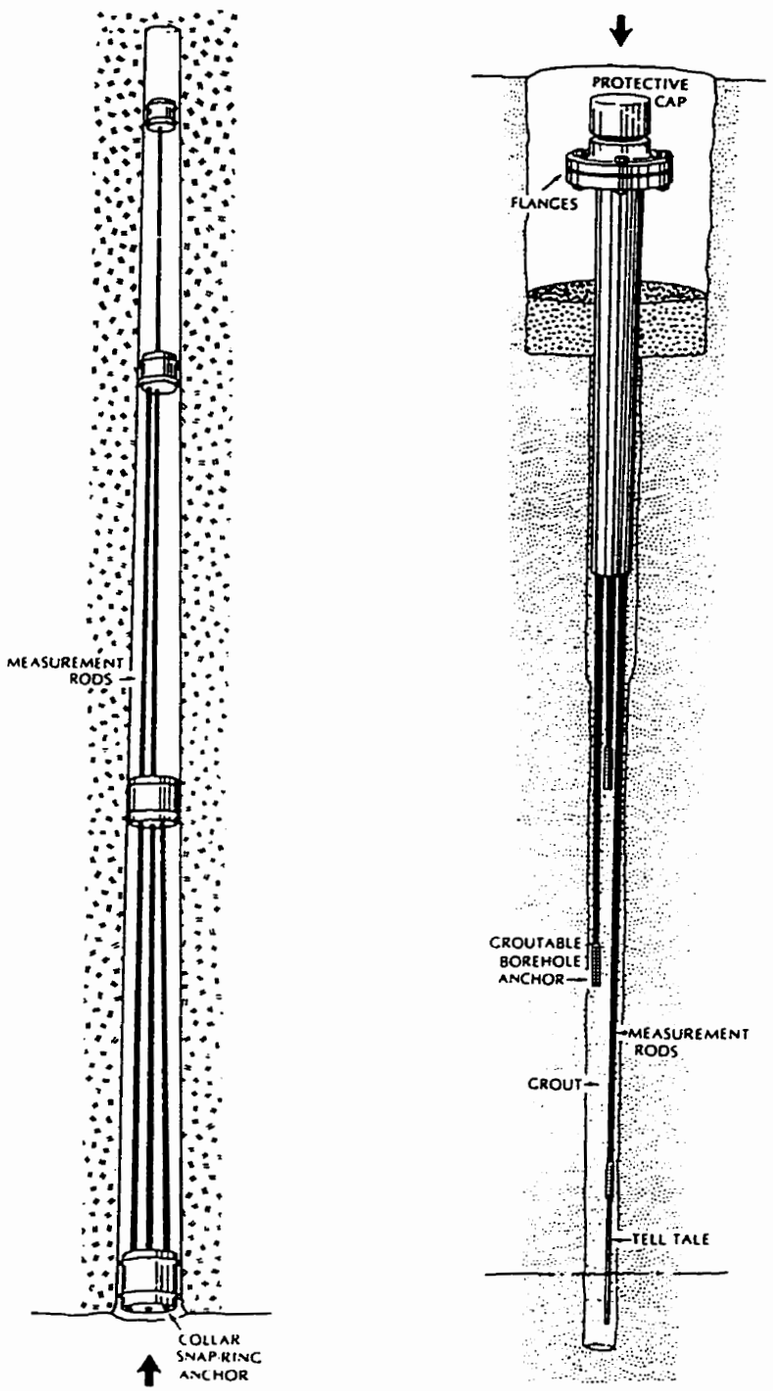

Figure 2.3 Rod extensometer with snap-ring anchors (left), Rod extensometer with groutable anchors (right) [39]

2.5.2 Rod extensometer with groutable anchors

This instrument is also suitable for monitoring rock mass displacement and rock separation. In this case the anchors consist of lengths of steel reinforcing bars which are connected to the measuring rods. The rods are sheathed in plastic pipes to protect them from the grout and the rods may be filled with oil to lubricate the rods. The rods follow the movements of the anchors which are determined by measuring the distance from the upper tip of the measuring rod to the stainless steel reference plate in the instrument head. Up to six of these rod assemblies of different lengths can be installed in the borehole. That makes it possible to measure the displacements and deduce the approximate depth of potential failure planes (Figure 2.3).

In the case of rock displacement due to strain, it is possible to convert the measured data to stress magnitudes if the elastic constants of the rock mass, as well as those of the extensometer wires or rods, are known.

2.5.3 Measuring system

The instrument may be read using either a dial gauge or a remote read-out system. The latter consists of steel mounting rods attached to the extensometer rods and a number of linear position transducers (LPT), one for each anchor. As the ground around the anchor moves, the position of the mounting rod in the LPT changes altering its electrical resistance. The change in electrical resistance (ΔR) can be translated to linear displacement (l), if the conversion factor (K) for the particular LPT is known. Actual displacement can be found from the following relation:

$$l_{(cm)} = \frac{\Delta R(k\Omega)}{K(k\Omega/cm)} \qquad (2\text{-}1)$$

The installed apparatus should be left in place during the entire monitoring period or until such time as it is threatened by blasting operations. The displacement readings for all the anchors in a borehole should be taken simultaneously [39].

2.6 Rock-bolt dynamometer

Rock-bolts can be used to measure ground movements by incorporating dynamometers. It is necessary to determine not only the load on the rock-bolts, but also whether the load is increasing, decreasing or remaining constant. The principal requirements of rock-bolt dynamometers are that they should be inexpensive and simple to install and operate since the instruments can be used in large numbers to obtain the load readings for a particular rock-bolt pattern. An important consideration in mining operations should be given to areas where large numbers of bolts are used for support purposes [38].

There are several types of rock-bolt dynamometers and two of the main types are described below.

2.6.1 Photo-elastic rock-bolt dynamometer

An example of this type is made by Tele-dyne Company-Terrametrics and is described as follows:

(a) The photo-elastic rock-bolt extensometer is a simple, rugged device for direct monitoring of initial tensioning and subsequent changes of tension in rock-bolts. In use, tension meters will give a rapid visual indication of increasing bolt loads in unstable ground and will also indicate any relaxation of bolt tension and resulting ineffectiveness. In addition, tension meters can be used to evaluate the efficiency of rock-bolt installation procedure.

(b) The dynamometer consists of a disc of optical glass enclosed in a hollow steel cylinder. When the steel cylinder is loaded across its diameter, the deformation of the cylinder causes a corresponding strain on the glass disc. The strain on the disc is visible in the form of photo-elastic interference fringes when the disc is illuminated with polarized light and observed through a hand viewer. The extensometer with photo-elastic disc should be installed between the rock-bolt nut or forged-head and the anchor plate (Figure 2.4).

Spherical cup and dome washers must be used, and can be supplied, to ensure uniform loading of the meter. Hardened washers are also available for use between the meter and rock-bolt nut or

forged-head to prevent 'digging in' under high loads. The instrumental rock-bolt is tensioned in the same manner as any other bolt. whether by hand, hydraulic means, or using any type of impact wrench.

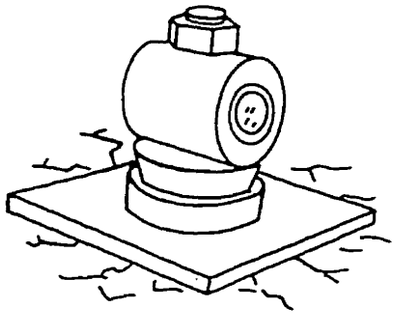

Figure 2.4 The photo elastic extensometer installed between the rock-bolt nut and the anchor plate

(c) Reading the photo-elastic disc is done by hand viewers. For example, the precision hand viewer is fitted with a standard miner lamp housing which polarizes the light from the cap lamp. The viewing aperture has a rotating compensation scale marked from 0 to 1.0 with 0.01 subdivisions. Other hand viewers of a simpler design are also available which make the fringes visible and will permit the fringe order to be estimated to within 0.25 fringes. Calculation of extension in the rock-bolt is very simple. The observed fringe count should be multiplied by the appropriate meter sensitivity factor, and from this rock-bolt tension is obtained.

2.6.2 Mechanical rock-bolt dynamometer

These are manufactured by several companies (Interfels of Austria, Goodyear, Geokon and others) but here the discussion is limited to the rock-bolt dynamometer which is widely used in the underground mines of Canada. It is illustrated in Figure 2.5.

The instrument consists of a linear potentiometer enclosed in an aluminum housing. As movement of the rock surface occurs, the resistance of the potentiometer changes and displacement can be calculated using the following equation [39]:

linear displacement = change in resistance (kΩ)/1.2

The monitor is installed on the end of a rock-bolt that is placed inside a drill hole and anchored at the base of the hole. If movement takes place anywhere between the anchor and the open face, it is registered by the ground movement monitors.

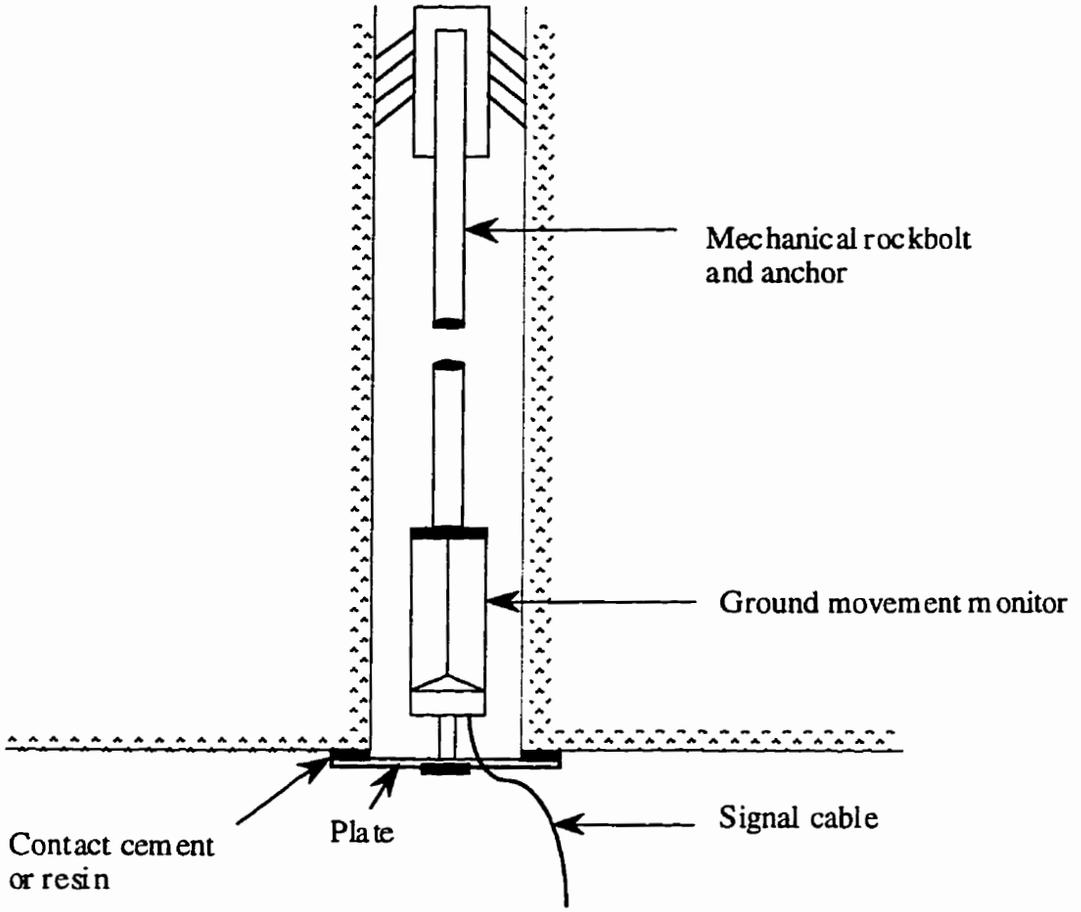

Figure 2.5 Sketch of mechanical rock-bolt extensometer

Ground movement monitors are very popular because they are easy to install, and because readings, which are very accurate, are easy to take and to interpret. One of the disadvantage to these monitors is the fact that when they are installed in sulfides they become corroded and unusable in about six months.

Another main disadvantage of this type of ground movement monitoring is that rock-bolt dynamometers have a limited sphere of influence, and that movement beyond their influence can be undetected, as is illustrated in Figure 2.6. For example, the dynamometer has been installed from the level above through the ore body into the stope back revealed that ground movement had

occurred. The amount of movement taking place suggested that there is a ground slip located in the back and that movement was taking place at an increasing rate.

There are rock-bolt dynamometers located in the back of the stope monitoring local movement but no movement was registered on the monitor.

This case history is very instructive and clearly suggests that ground movement monitoring cannot solely depend on the rock-bolt extensometer. If the slip had not been detected by the rod extensometer the stope back may have fallen on an unsuspecting miner and/or expensive equipment.

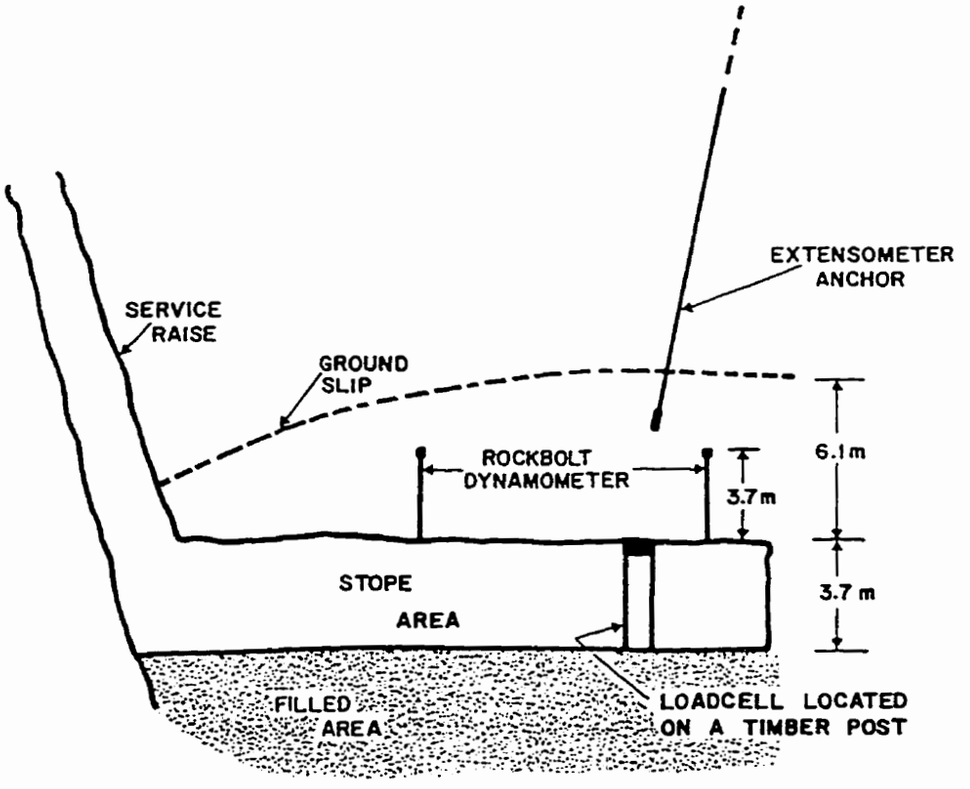

Figure 2.6 Model of instrumentation of cut and fill stope (cross-section)

2.7 Convergence meter

Convergence measurements normally carried out by means of a tape or rod extensometer between targets attached to the walls and roof of an excavation as illustrated in the margin sketch (Figure 2.7).

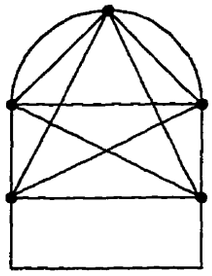

Figure 2.7 Typical convergencemetry

A number of convergence measuring instruments are available. Basically, the convergence measurements are made by two types of instrumentation [37].

2.7.1 Convergence rods

These instruments are commonly used to measure closure deformation between the floor and roof of mine openings. In the cases of larger lateral pressure, they have been successfully used for closure measurements between two walls (Figure 2.8) [38]. The instrument consists of telescoping tubes of Invar steel, mounted with a indicator which reads directly to 0.025mm for range of 50 mm. Telescoping tubes are limited to measuring openings up to 3.5m. Because of the use of pin connectors at the joints of telescoping tubes, the range of measurements was found to be within 0.0125mm. Normally, the apparatus is left in place during the entire monitoring period, and reading of deformation is by remote read-out.

2.7.2 Tapes

These are usually used for measuring closure between drift walls. They can be used for spans greater than 3 m, and usually up to 8 m. It could be a useful tool for determination of lateral

convergence of any mine opening with a relative accuracy. Most commonly used is a steel pipe with punched holes every 37.5mm. The convergence could be measured from a remote location by a resistor, where any resistance change in turn is correlated to an actual displacement.

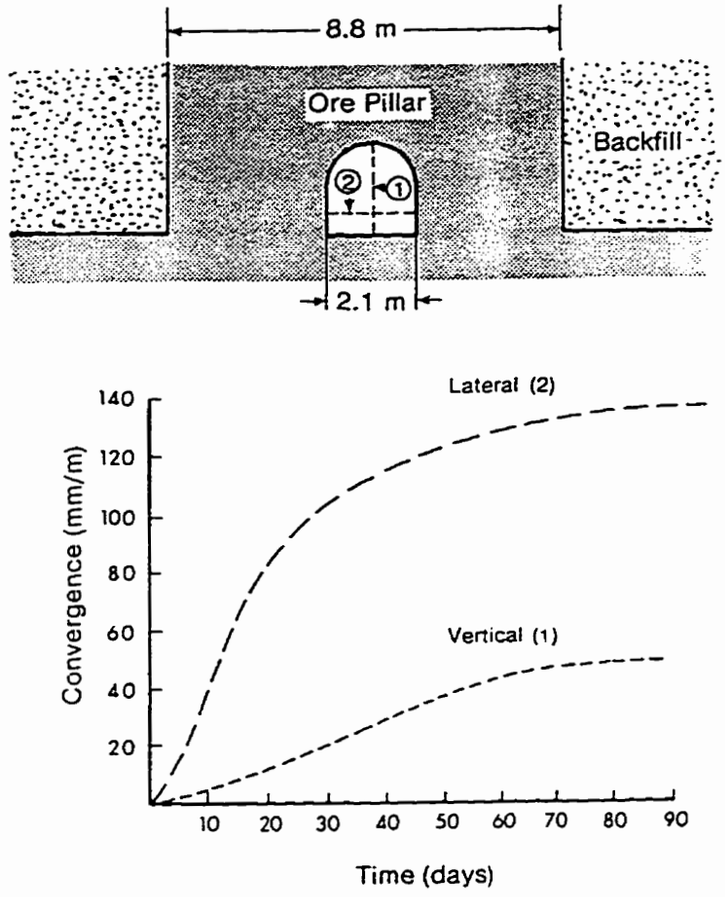

Figure 2.8 Drift closure measured by convergence rod [39]

2.8 Crack extension meter

This type of instrumentation is well developed at Kid Creek Mine, in Timmins, Ontario, and its description and implementation is based on the experience from this mine. Yu [66], describes three principal types of crack extension meters as follows.

2.8.1 Crack gauge

This instrument was assembled from parts of wire extensometers previously used for pit wall monitoring. A dial gauge is attached between an aluminum sleeve and a movable steel rod, or copper tube, to display a change of displacement as small as 0.025 mm. An aluminum coil spring of adjustable tension keeps the rod against the sleeve at any desired tension without affecting the dial reading, and also makes the device readily recoverable.

The crack gauge, installed between two anchors across a crack in the wall or back of a drift, monitors the relative movement of the discontinuity.

2.8.2 Crack meter

This is a device used to monitor a shear zone ranging from 1.0 to 1.6cm in width which is too wide for the crack gauge. The device (Figure 2.9) consists of an aluminum channel and an aluminum angle, which are installed across the shear zone. A threaded steel rod is fastened at an angle and extends across the zone to the channel. A push-button switch is mounted on the channel for triggering by movements of the rod.

The triggering level can be set as small as 0.25mm by adjusting the threaded rod. A hazard flasher is incorporated with a switch to provide warning signals visible at a distance.

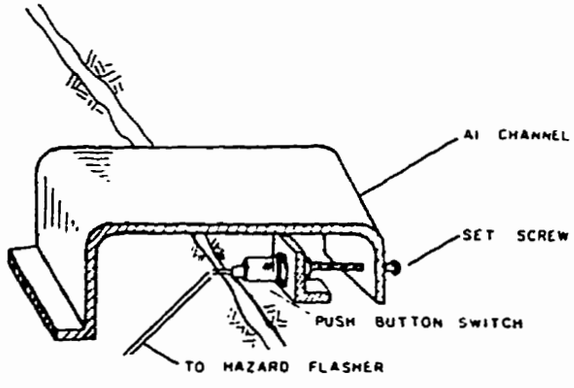

Figure 2.9 Crack meter device [39]

2.8.3 Slough meter

The device was developed to monitor the failure of stope walls causing an electric switch to trigger audio and/or visual warning signals. Figure 2.10 illustrates the whole unit consisting of a sensor, an electronic switch (inside the flasher) and an alarm system.

The sensor, assembled from plastic tube or hose, has conductor wires tied to the tube at any selected spacing. The lead wires can be colored for the whole length, or only at the very end of the tube for wire identification [39].

The electronic switch uses a silicon controlled rectifier to regulate the flow of current through the alarm system when a discontinuity in the sensor wire takes place.

The sensor is installed and grouted with cement slurry in a hole drilled from a crosscut toward the stope opening to be monitored. Should the stope wall fail, the slough meter will not only give warning signals, but also indicates the approximate extent of wall failure by identifying the location of the broken sensor wire.

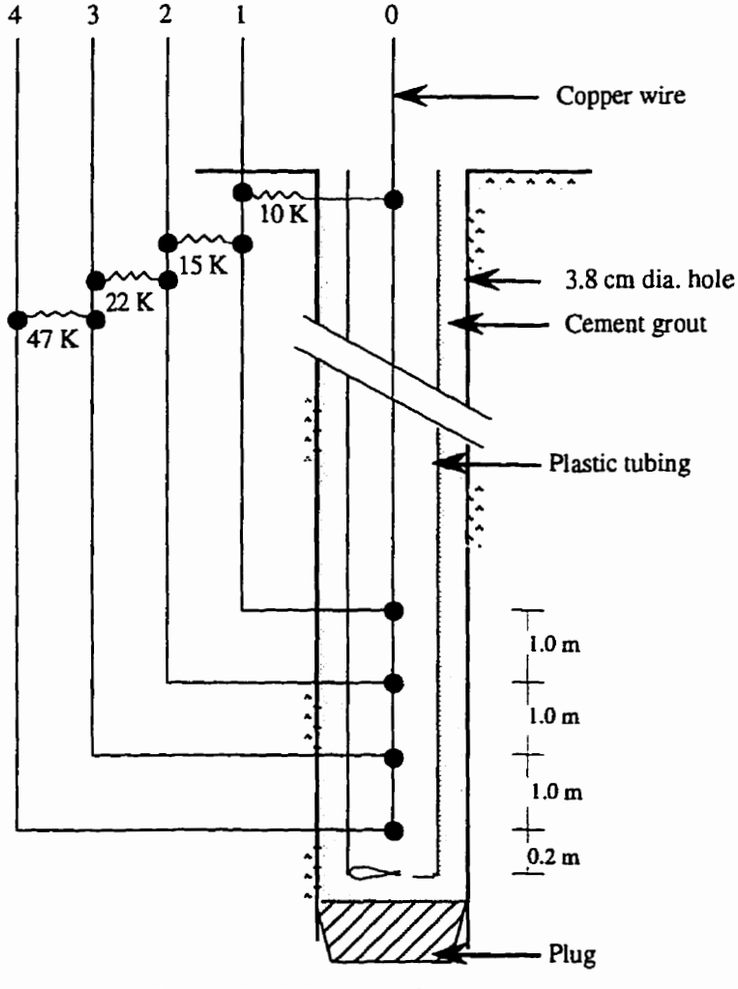

Figure 2.10 Sensor of slough meter

2.9 Microseismic monitoring

Ever since the evolution of underground mining, sound has been used to qualitatively assess the stability of rock structure. It was later discovered that as rock becomes stressed, it produces acoustic emissions whose rate and magnitude increase with the level of stress. In the 1960's, new methods and sophisticated equipment offered the possibility of accurately locating the source of acoustic emissions in three dimensions. By plotting the monitored data on maps, high-stress zones could be indicated and destressing action could be taken [53]. However, due to historic reasons, different terms have been used in various disciplines. For instance, in seismology, the term seismic activity and natural earthquake are employed to denote transient elastic waves and vibrations caused by the natural processes of fracture and frictional instabilities of the earth crust. In mining engineering, microseismic activity (MS) and rock bursts (which are also called rock noises) are the most commonly used terms used to describe elastic waves or vibrations resulting from mining-induced rock fractures and frictional motions along geostructures. In practice the term acoustic emission is reserved mostly for the field of non-destructive material testing.

2.9.1 Seismic activities

Theories of the mechanism of emission generation of seismic energy in a stressed rock body are still of a preliminary nature. The seismic activities, however, may be categorized into three levels: a micro-level, a macro-level and a mega-level [31].

The creation of a mining excavation is followed by stress transfer in the vicinity of the openings. In an experiment in 1938 to determine if the seismic velocity in mine pillars increased with pillar stress, Obert discovered by accident that the rock he tested was generating unprovoked seismic energy and that the rate and intensity of the seismic energy increased with the level of stress [48]. Since that time a number of authors have reported studies of this phenomenon.

In field work at Galena Mine in the Coeur d'Alene mining district of the USA, rock noise events were accurately plotted on maps [8]. An event is defined as seismic activity from a source

that is above a specified magnitude and is recorded on a specified minimum number of detectors. It was found that areas of high event densities delineated high-stress zones which in turn were potential rockburst sites. Similar work at White Pine Mine in Michigan shows graphically (Figure 2.11) that the rate of seismic activity increases prior to a rockfall [20].

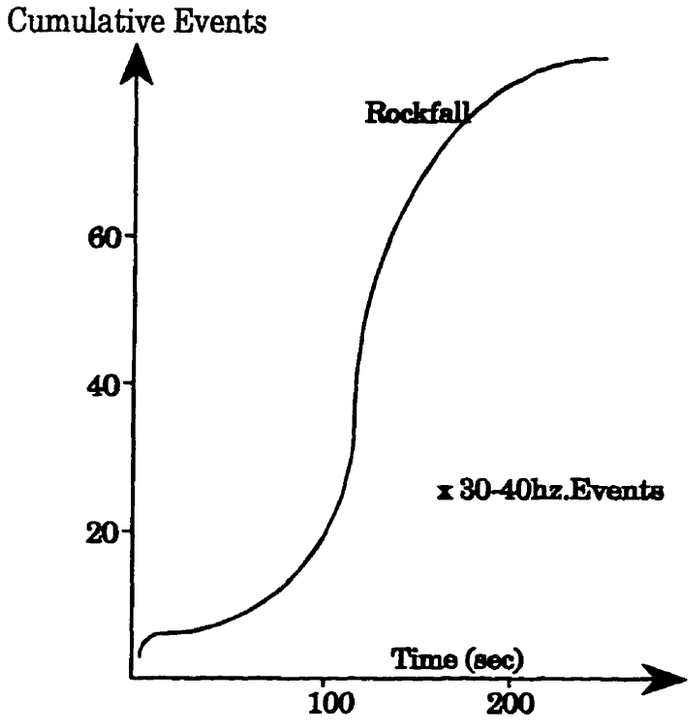

Figure 2.11 Rate of seismic activities prior to rockfall [20]

The number of cumulative events are plotted as a function time in an interval encompassing a rock fall. The graph indicates a sharp rise in the rate of cumulative events prior to a rockfall followed by a decrease after the fall. Both of these cases provide quantitative evidence that the rate of rock noise events increase prior to a rockburst or rockfall. However, the magnitude of these rate increases is not always sufficient to warrant a prediction [47].

The mining experience suggests that the majority of rate increases did not terminate in a rock fracture, which might be attributed to gradual dispersion of concentrated stress [39].

2.9.2 Seismic waves

The stress wave is made up of two separate types of waves. A compression wave, called a push pull, primary, or P-wave, moves through a rock mass, causing elastic particle motion similar to that produced by sound transmitted in a solid or fluid. This type of wave has the fastest propagation velocity and therefore arrives first at the measurement point. Particles in the path of this wave move forward and backward along the line of advance of the wave [53].

At the same time as the P-wave is generated, a second type of wave which shears or tends to change the shape of the rock medium is produced. This wave causes particle motion perpendicular to the wave front and is called a secondary, shear, shake, or S-wave. The shear wave is not capable of being transmitted in a fluid or gas.

Figure 2.12 illustrates oscillograph records of rock noises which depict both P and S-waves [8]. Both of these waves travel at different velocities and therefore tend to spread out with distance from the source. It is apparent from the diagrams that the bulk of the energy is carried in the S-wave and, in reality, studies have shown to that 60 to 70 percent of the total energy is transmitted in the S-wave.

Frequency ranges of seismic vibrations vary from 50 Hz to 10 KHz and depend on many factors; for example, the type of source mechanism, nature of the fracture formed, and the distance from the source are just a few. Frequency is rapidly attenuated as the wave moves away from the source. This situation is typical but not constant for all rock types. Cycle time varies from 0.0001 sec. for very small events to well over a minute for large earthquakes. The cycle time for a rockburst is for approximately 1sec.

For source location velocity has more significance than either frequency or cycle time [53].

2.9.3 Microseismic instruments

A recent introduction has been an automatic computer controlled microseismic monitoring system (MMS), which provides continuous current information about a rock structure and is capable of

in-situ data analyses. This system utilizes only the P-wave source location method for a minimum of five geophones. The following components of the instrumentation hardware are included [53].

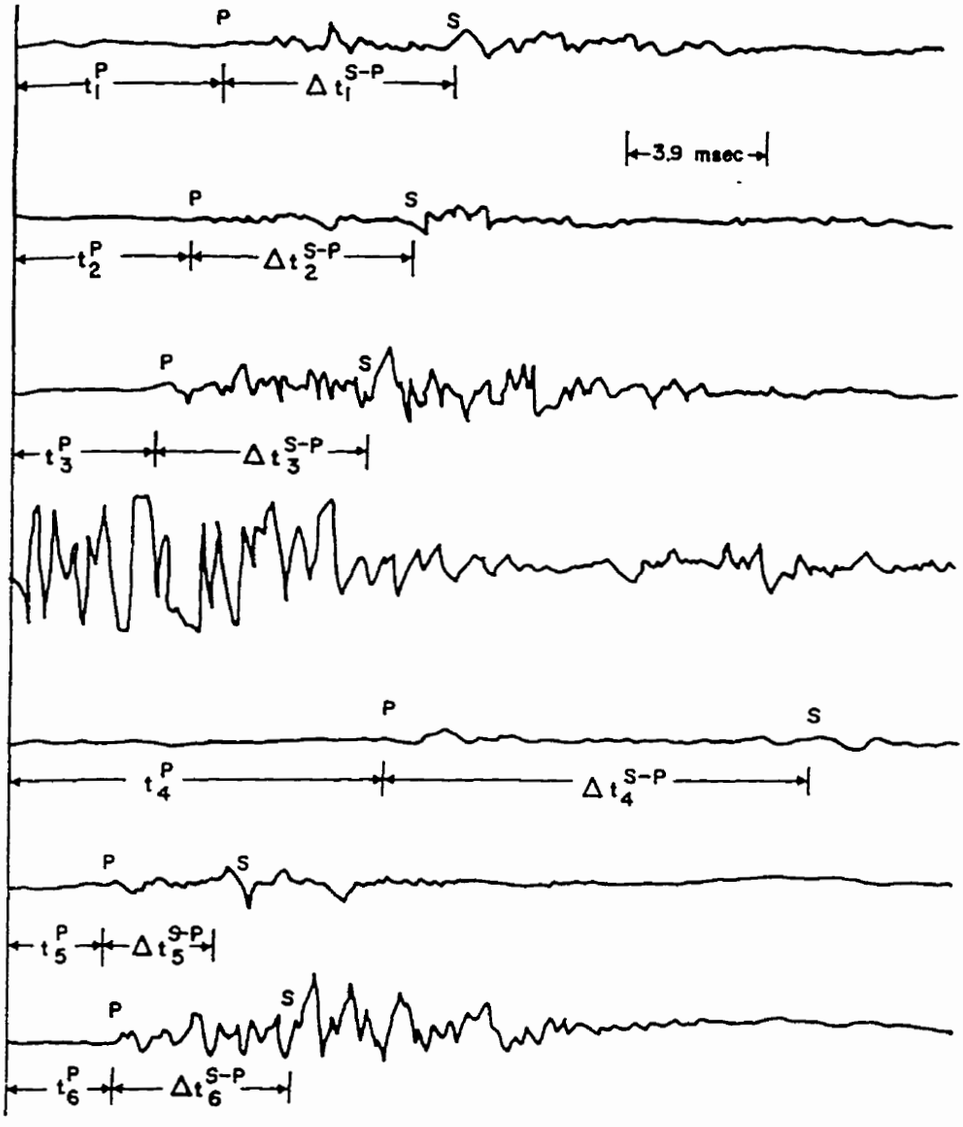

Figure 2.12 Typical seismograph of a rock noise [8]

1. Signal generators or geophones are velocity transducers and accelerometers. A velocity transducer operates on basically the same principle as an electric generator, where current is induced by ground vibration. Piezo-electric accelerometers house a group of discs. Vibration causes the mass to exert a variable force on the discs which then generate a change proportional to

the mass acceleration. The generated charge changes are then sensed and converted to a voltage. The cost of transducers is ten times less than accelerometers, which warrant the use when an accuracy of less than 3 m is required or when frequencies exceed 2 KHz.

2. Preamplifiers ensure a high signal-to-noise ratio. Amplification is measured in decibels. The preamplifier is normally housed in the same casing as the geophone.

3. Cables for MMS perform two functions. Firstly, they must transfer the signal from the geophone to the monitoring station and secondly, they must transmit power to operate the preamplifier. Each cable from the geophone to the junction box contains four wires in two individually shielded circuits, one for the signal and one for power. From the junction box to the monitoring station both circuits in each cable can be used to transmit the signal and therefore the number of cables required is cut in half.

4. Signal conditioning is usually applied at the monitoring station, primarily to improve signal-to-noise ratios.

5. Timing can be done either by hardware or software methods. Hardware timing is capable of 0.0001sec. resolution as compared to 0.0005sec for software which correspond to distance of 0.6 and 3 meters respectively for a wave traveling at 6100 m/sec. Although the resolution time favors hardware timing, other factors tend to make software timing more practical in most applications. During high data rate generation, information that can be stored and later processed in software timing is lost-with hardware timing. For this reason a software timer is more desirable than its hardware counterpart in most situations [50].

6. The computer should be capable of gathering and analyzing data and subsequently displaying the data in a form that can be used as an engineering tool. The computer should have a cycle time of less than a microsecond, and be able to do the timing [8]. The memory must be large enough to store information during periods of high microseismic activity and later process these data [53].

2.9.4 Source location

Modern technology has produced a combination of instrumentation and methods that make it possible to accurately locate the source of a rock noise. This provides quantitative evidence that is later scrutinized for the purpose of determining the stability of a rock structure. The direct method solution of source location is based on the standard distance equation:

$$d_i = \sqrt{(x-a_i)^2 + (y-b_i)^2 + (z-c_i)^2} \qquad (2\text{-}2)$$

where:

a_i, b_i, c_i = the coordinates of geophone 'i',

d_i = the distance from the source to geophone 'i',

x, y, z = the unknown coordinates of the source.

In equation (2-2) d_i x, y, z are all unknown. However, since the velocity of microseismic emission in a homogeneous rock medium is constant, d_i can be calculated by:

$$d_i = V_i\, t_i \quad \text{(P-wave method)} \qquad (2\text{-}3)$$

or:

$$d_i = \Delta t_i^{s-p}\left[\frac{1}{v_i^p} - \frac{1}{v_i^s}\right] \qquad (2\text{-}4)$$

where:

v_i^p and v_i^s = the P-wave and S-wave velocities in the direction from the source to geophone 'i'.

t_i^p = the arrival time of the P-wave at geophone 'i' relative to its arrival at the closest geophone.

Δt_i^{s-p} = the difference in arrival times of the P-wave and the S-wave.

The velocities of the P-wave and the S-wave are accurately calculated by detonating a charge at a known location and measuring the time it takes to travel a given distance. Because seismic

velocities vary due to rock anisotropy, or with changes in rock type, a velocity survey is conducted in the vicinity of each geophone and a specific velocity is assigned to the geophone.

The least squares method greatly increases the accuracy of source location outside the geophone array and minimizes the net effects of random errors and equipment limitations. Accuracy can be improved by as much as 50 percent with the addition of a single geophone above the minimum requirement and, in general, the more geophones the better the solution.

The single most important factor influencing the accuracy of a source location is the determination of arrival times [39].

2.9.5 Data analysis

Rock-noise quantity as a function of time has proven to be an effective method of delineating high-stress zones, but it does not measure the magnitude of any events.

A measure of the magnitude of the events when coupled with compiled rock-noise quantity data will provide a more quantitative assessment of the behavior of a rock structure. The magnitude of a seismic event can be calculated by considering the energy radiating from a spherical source. The energy is given by:

$$E = kr^2\bar{v}^2T \qquad (2\text{-}5)$$

where:

k = a constant dependent on the rock density and seismic velocity,

r = the distance from the source to the point of measurement,

$\bar{v}$ = the average particle velocity,

T = the duration of the event.

In practice the energy of the whole wave is calculated by combining the P-wave and S-wave portions. Both the average particle velocity, $\bar{v}$, and the event duration, T, are easily measured, as is the constant, k, which is represented by:

$$k=dc \qquad (2\text{-}6)$$

where:

d = the mass density of the rock,.

c = the average seismic velocity of the P-wave and S-wave.

After the energy released has been calculated, the volume of rock broken or destressed can be estimated by the relation [8]:

$$v = \frac{8}{3}\frac{E}{p^2}G \qquad (2\text{-}7)$$

where:

V = the volume of rock affected,

E = the seismic energy released,

G = the modulus of rigidity of the rock,

P = the applied field stress at the source.

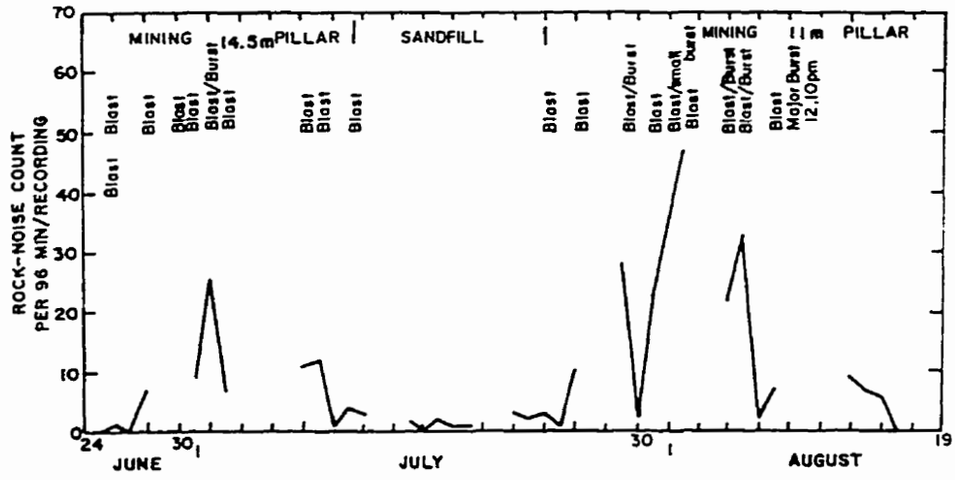

Figure 2.13 Quantity of rock noise events as a function of time [8]

This information can be used to make quantitative estimates of the consequences of seismic activity in a rock structure.

Once calculated, the energy release rate can be plotted as a function of time and correlated to the 'rock-noise versus count' plot (Figure 2.13). There are instances where energy release data may provide unique information regarding the stability of a rock structure [53].

2.10 The stress alert instrument

This is a newly developed device. It detects, measures and analyses microseismic emissions of rock providing an on-going interpretation of the magnitude and rate of stress change in the rock structure. If the detected stress changes conform with its pre-programmed signature patterns of an impending roof fall or rock burst, a 'stress alert' should give a warning signal so that defensive action may be taken.

The instrument is battery operated, readily portable and built for underground service. It can also be easily installed or removed in a few minutes [39].

CHAPTER 3

3. IN-SITU STRESS MEASUREMENTS

3.1 Introduction

It is a matter of interest that there is no instrument in existence which measures stress directly, because stress is a concept and cannot be measured directly. Actually, the stress cells measure a strain or displacement, which is used to determine stresses by the stress-strain relationship $\sigma = \varepsilon E$, where E is the Young modulus. The in situ state of stress is one of the most important items of design data and is widely used by the underground excavation engineers for validating the hypotheses of calculus and the stability study of excavations. The data in this stage are normally obtained by the instrumentation of the underground excavation before construction and include: the magnitudes and directions of the principal stresses which exist in the rock mass before the creation of an excavation.

Many methods for measuring in situ stresses in rock have been proposed and these may be grouped under the following:

3.2 Hydraulic fracture techniques

This method is suitable for the measurement of stresses at distances of more than about 50m from the point of access. This method has been used for determination of in-situ stress. The method has the advantage of being operable in highly stressed rock masses, where fracturing, limit the use of for example, the overcoring methods.

Fractures are induced in the rock by the application of a hydraulic pressure to the internal walls of a borehole and, from a knowledge of the pressure at which fracture occurs and the directions of the fractures, the in situ stresses can be estimated. Unfortunately, The method is not applicable if the vertical stress is of lower magnitude than the horizontal principal stress, and considerable judgment and experience are required in the interpretation of results [33].

3.3 Direct stress measurement using flat jacks

This method is one of the first methods of stress measurement including measurement of the pressure required to restore a set of measuring which are occupied before the slot was cut. This measurement is carried out by making a slot in the wall of the opening with sufficient area to partially relieve strain in the proximity of eight gauges. A cut is then made between the eight gauges and a flatjack grouted into a slot. Flatjacks are fabricated by forming two identical halves out of malleable sheet metal and welding the halves together (Figure 3.1). Panek and Stock constructed the flatjack, which is often used for the measurement of pressure in the rock. For their procedure it is necessary to cut two slots in the rock wall. In the upper slot the small hydraulic cells should be installed, which are grouted in the slots. In the lower slot the flatjack should be installed and grouted in the slot.

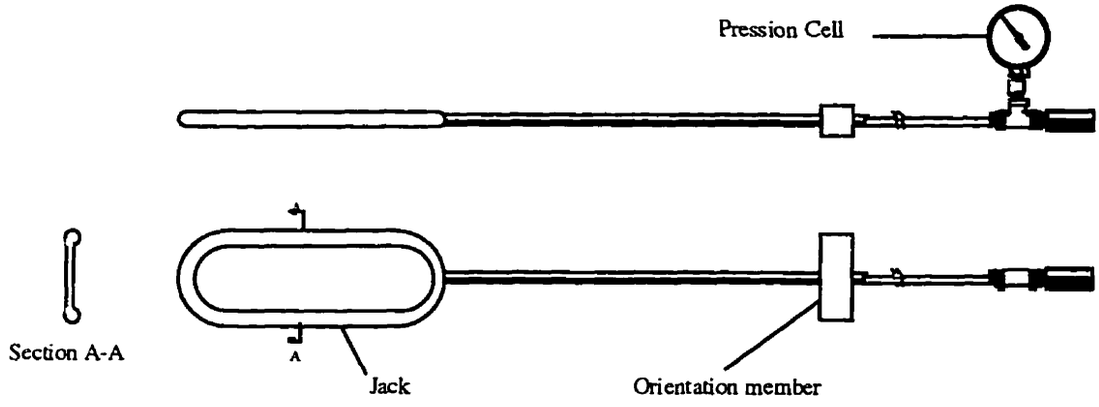

Figure 3.1 Stress measurements by flat-jack cell

Obviously this method can only be used where access is available in an exploration adit or pilot tunnel. This method for measurement of the absolute stress is convenient for the inelastic rock mass, because it is not necessary to know the elastic behavior of the rock [49]. The technique is not suitable for heavily jointed rock or rock which has been severely damaged by blasting. Recently a flatjack cell for installation in drill holes has been developed.

3.4 Biaxial strain CSIR cell (doorstoper)

One method of measuring stresses in rock is to apply a strain gauge to the surface of the rock in-situ, take a reading, and then remove the portion of rock to which the gauge is attached by cutting a groove around it and breaking off the core. During removal, the rock core is relieved of stresses and the readings of the strain gauge before and after removal give a measure of the stresses in the rock. If a large strain gauge is used, cumbersome equipment is required for removing the rock core because of the large diameter of the core This method has the disadvantage that particularly in hard rock, measurements may have to be confined to rock close to the surface.

A hole is drilled into the rock to the depth at which the stress is to be determined The end of the hole is ground flat and smooth and electrical-resistance strain gauges are glued to it. When the glue has hardened, strain readings are taken from each of the gauges. The maximum depth of drill holes is up to 50 m.

An annular groove is then drilled around the strain gauges at the end of the borehole, leaving them on a central core relieved of stress. The core is broken off at the end and withdrawn from the borehole. Strain readings are then taken from the a gauges. The difference between the strain readings before and after freeing the rock core is a measure of the stress in the rock surrounding the end of the borehole.

One difficulty experienced with electrical-resistance strain gauges used for this purpose is their sensitivity to water. A waterproof strain cell incorporating the strain gauges has therefore been developed. This cell makes it possible to use the tree-spanning stress-relieving technique with wet or dry drilling at almost any distance from the rock face.

The strain cell is comprised of a rectangular strain gauge rosette of three strain gauges measuring in the:

0°-horizontal, 45° - inclined, 90° - vertical

or

0° horizontal, 135° - inclined, 90° - vertical

It is molded into a rubber casting which fills a plastic shell. Four gold plated connectors are also molded in the plastic shell, so that when plugged into the inserting tool they affect the electrical contact between the strain gauges and the strain-indicating instrument.

A key way in the plug section of the plastic shell ensures that the cell can be plugged into the installing tool with only one possible orientation. The cell can be used in a standard BX diamond-drilled borehole.

When installed on the end of a BX borehole, changes in strain on the surface of the rock resulting from the overcoring operation are transmitted to the strain-indicating instrument via the strain gauges which are glued on the rock. The rubber and plastic shell protects the strain gauge from damage and from water during the over-coring operation.

Strains in the cell are measured directly by means of a strain indicator (essentially a Wheatstone bridge circuit) in micro strain units. The measured strains are then used to calculate stresses.

The instrument known as a 'doorstoper' was developed by the South African Council for Scientific and Industrial Research (CSIR). A new developed model of CSIR is able to measure the stresses in three directions [49].

3.5 Borehole deformation gauge (USBM)

It monitors deformations along three diameters of a single plane, normal to the axis. This device consists of three pairs of strain gauged cantilevers, each pair oriented at 120° to the next. These cantilevers are held within a sealed, stainless-steel housing, and their tips are deflected by means of tungsten carbide faced plungers.

The overcoring technique is as follows: the borehole gauge is inserted inside an EX diamond drill hole so that the plungers are depressed and the initial deflection of the cantilevers is measured by connecting the signal cable to a conventional strain indicator read-out box (e.g. Vishay Model P350A) equipped with the necessary switch and terminals.

With the gauge still in the EX borehole, a 15cm concentric hole is drilled around the gauge so that it is eventually isolated from the stressed rock mass inside a 14cm diameter core about 30cm long.

As this core is liberated from the stress field, it expands, and the resultant change in the diameter of the EX is measured by the strain gauged cantilevers. During this time the signal cable is located down the middle of the drill rods and issues from the back end through a special water swivel incorporating a water-tight gland.

After each overcore, the core is removed from the hole and placed inside a biaxial modulus chamber. This chamber incorporates a neoprene membrane which permits hydraulic pressure to be exerted radially on the rock core while the resultant change in the EX borehole diameter is once again measured by means of the borehole gauge. The stress/strain relationship so measured is used to calculate the elastic modulus of the rock which then permits the rock stress to be computed from the measured strains during overcoring.

This procedure, repeated in three differently oriented boreholes, permits the magnitude and direction of the three principal stresses of the three-dimensional state of stress to be calculated, using an appropriate computer program.

In rock which tends to fracture easily, that is 'disc' or 'poker chip' during overcoring, the borehole gauge can be modified by replacing the standard housing with a reverse casein which allows the cantilever plungers to be positioned very close to the start of the EX hole.

A calibration jig is available for periodic checks on the stability of the gauge calibration. Other essential accessories include setting rods for placing and orienting the gauge; also, it is advisable to have on hand spare cables, plungers and biaxial modulus chamber membranes [39].

3.6 Triaxial strain cell (CSIRO)

This instrument was developed in Australia by the Commonwealth Scientific and Industrial Research Organization. It would be most suitable for triaxial stress determination. It is widely used for the determination of rock stresses in many underground operations, including Canada and in near surface boreholes for geotectonic studies. The principal characteristics of this instrument are:

1. Construction: The hollow inclusion (HI) cell is a fully encapsulated array of nine strain gauges, which is grouted in an EX diamond drill hole and monitored while being overcored. Strain

response registered during this process is analyzed to determine the principal stresses and their orientation. The HI cell consists of three strain rosettes, each of three gauges, precisely oriented at 120° along the circumference of an epoxy pipe. Full encapsulation and epoxy grouting mean that the instrument is unaffected by moisture. Each gauge is 10mm long, minimizing the influence of rock grain size. Gauge orientation produces a statistically powerful result of high sensitivity when strain response is analyzed to determine the stress tensor.

2. Installation: The cell is grouted in the EX hole by filling the epoxy tube with epoxy cement, then extruding the cement by displacement with a piston at target depth. A trip wire within the cell registers completion of extrusion. Piston activation is either by forcing a protruding rod against the end of the borehole or by manually pulling the piston into the epoxy shell. Multiple seals confine grout flow around the cell. The strain gauges are thus fully bonded 1.5mm from the borehole wall: allowance for this geometry is made in the data reduction program.

3. Overcoring: This is the final stage of instrumentation. Monitoring of strain response (and the trip-wire) is via a twelve-core cable from the HI cell through the overcoring rods and out of the diamond drill through a modified water swivel. A 9-channel switch box and quarter bridge strain indicator are connected to the cable and strain response is monitored during overcoring. When plotted graphically, this response is invaluable in indicating overcore conditions such as the onset of core cracking or inelastic response [39].

3.7 Photo-elastic biaxial cell

Sometimes known as the photo-elastic disc or the photo-elastic stress concentration disc, this transducer takes the form of a small plastic disc with an axial hole which is bonded to the test surface through a thin annulus with one face adjacent to the edge of the disc. The firm, famous for production of the photo-elastic disc, is Horstman Ltd. [39].

The adhesive for the photo-elastic disc is generally two-part, fast setting adhesive and it enables an efficient bond to be achieved with most surfaces at normal temperatures in a matter of minutes.

The photo-elastic discs are interpreted by use of the Horstman precision hand viewer, which was originally designed for use with photo-elastic transducers in rock mechanics investigations.

When the compensator is set to zero, an isochromatic fringe pattern in the photo elastic gauge may be observed. The colored pattern will show two axes of symmetry through the center point of the disc. The axes of symmetry show the direction of the underlying principal strains. The principal strain and stress directions in the plane of measurements are thus determined in relation to the black detour line already on the disc.

The major principal strain is then obtained by multiplying the total fringe order , by the gauge factor. The minor principal strain is obtained by referring the observed pattern to profiles considered in the basic calibration procedures, or more accurately by simple computation from the isotropic point spacing. This method is discussed by Hawkes & Moxon [33].

Calculation of the stress from the photo-elastic disc is simple compared to the doorstoper technique. For example, direction of major (σ_1) and minor (σ_2) principal stresses is read directly from the overcored disc. The major principal stress is calculated very simply; for example, if the fringe order is 1.86 (in white light), strain is determined when this value is multiplied by the factor 440 (i.e. ε_1 is 818μ) Minor strain (ε_2) is determined from reading the distance between isotropic points on the ε_2 diagram. Positive or negative signs for the stresses are given from disc readings.

3.8 Glass stress plug

A photo-elastic glass plug is similar to a photo-elastic disc, but a stress plug meter is sometimes difficult to read in deep boreholes.

The behavior of a glass stress plug in rock is the same as a photo-elastic disc. Usually the obtained results are in terms of stress, and strictly speaking the plugs should be calibrated in the rock. Stress plugs should be glued on the end of the borehole. The photo-elastic set-up for reading is illustrated schematically in Figure 3.2.

The glass stress plug is 3.75cm long, 3.12cm in diameter and is usually glued into a 3.43cm diameter hole. The front polarizer and quarter wavelength filter are combined and attached to the glass plug.

The precision hand viewer consists of a quarter wavelength retardation plate and a linear polarizing screen held in a circular frame which is graduated from 0.0 to 1.0 in 0.01 increments. The optical axis of the quarter-wave plate is aligned at 45° axis of the linear polarizing screen which is aligned with the viewer handle, when the index of the semi-circular scale reads zero. Rotation of the linear polarizer relative to the fixed quarter-wave plate, with the viewer handle held in a fixed position, moves the index of the viewer over the scale. This rotation alters the effective line of the system by the process of goniometric compensation and changes the viewed fringe pattern optically by one complete fringe order or unit for 180° rotation on the scale.

A glass stress plug is a permanent installation at the end of the borehole and is overcored only when the reading installation is completed and disassembled. It is difficult to make a daily stress reading in the long borehole. This system is usually used for determining the changes in stress underground.

Calculation of stress in rock can be on the basis of the principal stress differences (σ_1-σ_2) at any point (r,θ) in a hollow cylindrical inclusion in an elastic host material.

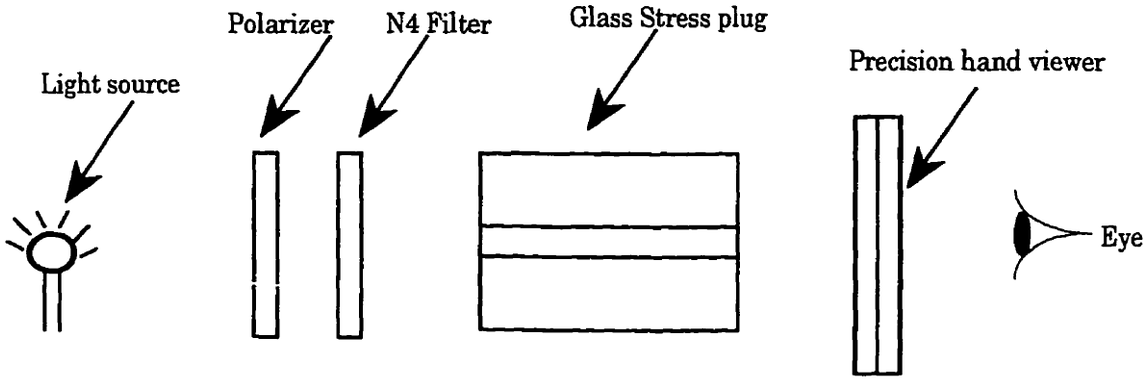

Figure 3.2 Set-up for photo-elastic stress plug

3.9 Vibrating wire stress meter

This device offers an alternative to the glass plug for measurements of change of stress with the advantage that it is easier to read and can be pre-stressed so that tensile as well as compressive stress changes can be measured.

The vibrating wire stress meter can be used to determine the relative change of strain in the surrounding rock of mine excavations. The instrument consists of a hollow steel cylinder containing a pre-tensioned steel wire oriented diametrically across the cylinder. The stress meter is anchored in a 3.75cm borehole using a sliding wedge and plate with a hydraulic installation tool. A portable read-out unit is used to vibrate the steel wire and its resonant frequency can be converted to the relative stress value along the axis of the wire [66].

There are principally two types of stress meters: VWS, developed by Hawkes & Hooker [46], and IRAD, which has been used at Kidd Creek Mine, for measurements of highly concentrated abutment stress, which was found at a distance equal to one half of the width of the opening from the excavation boundary. The measured results were used in designing effective cable bolting and destressing of the highly stressed ground [66].

The disadvantage of this instrument is that stress changes are determined only across one diameter but a more sophisticated version has been made in Germany (Maihak) which measures strains across three diameters in one cell [46].

3.10 Prop load cell

The measurement of pressure in the back and floor of a mine opening is an important element in ground control. There are several kinds of prop cells for measuring the load applied by or to a prop. Generally speaking, there are two principal types of prop load cells and these are described below [39]:

l. The photo-elastic load cell is a simple, rugged device for insertion between the prop and the roof of the mine excavation in order to measure the load applied to the prop.

The basic principle of the prop load cell is that the deformation of a lateral hole through a body subjected to an axially applied load can be directly related to the magnitude of the load. The deformation transducer is a cylinder of optical glass aligned so that it is diametrically loaded by deformation of the hole. The glass cylinder is strained by application of load to the cell body, illuminated with polarized light and observed through a hand viewer. Photo-elastic interference

fringe where fracturing patterns are visible in the glass cylinder. The observed fringe pattern provides a direct indication of the load applied to the cell body. The load cell light polarizer should be in position in the prop load cell as illustrated in Figure 3.3. The cell will accommodate a maximum eccentricity of 10° in loading, if it is set in line with the axis of the prop and perpendicular to the roof bar, to allow for subsequent shifts in direction caused by differential lateral roof and floor movements.

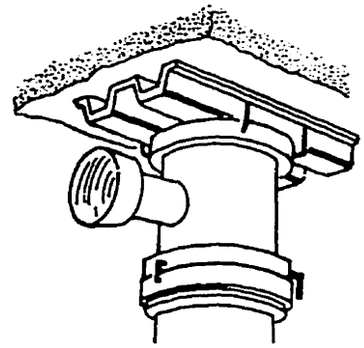

Figure 3.3 Photo-elastic load cell positioned for reading of light polarizer

2. Mechanical load cells have much wider application than the photo-elastic type. There are several types of pressure cells produced on the market, but generally speaking two of them are most common:

(a) Dowty hydraulic dynamometer up to 25 metric ton load, with automatic registration of the changes of the load. They have been widely used in the coal mines for closure measurements.

(b) Wohlbieau-Ambatiello dynamometer with automatic registration of the pressure. It can be used for measurement up to 40 metric ton load.

Some companies have fabricated load cells using a resistance-strain gauge, as the transducing element, mounted on a metal annular ring. By securing end plates to the annular ring, this transducing element is converted into a load cell suitable for use in measuring prop loads.

CHAPTER 4

4. INSTRUMENTED CYLINDER OF THE UNIVERSITÉ DE SHERBROOKE (CIUS)

4.1 Introduction

Nowadays, along with the improvement in the construction techniques, the structures (mines, dams, bridges,.....) have become more and more complicated. In addition, monitoring of the variation of stresses and deformations over a long period of time has become an essential way for understanding the state of stability in these structures. In underground mines, especially, the need for an instrument for monitoring the effects of changes in ground stress conditions, resulting from mining activities (blasting, excavations extension, ...) has existed for a long time.

Such an instrument must have characteristics as follows:

- long term reliability

- resistance to the harsh environments (blasting, corrosion, humidity,.....)

- precision of measurements in different host mediums

- possibility of arriving at conclusions regarding the future stability state of structures, using presently recorded data. For example, to have ability to reach a conclusion about the stability of mining stopes and pillars by measuring the variation of stresses and deformations.

To meet these needs, the Rock Mechanics Laboratory of the Université de Sherbrooke has developed a new instrument called CIUS (Cylindre Instrumenté de l'Université de Sherbrooke) to monitor the behavior of civil and mining structures by measuring the variation of stresses and deformations.

4.2. Principle of CIUS

The principle of CIUS is simple. It is a cylindrical concrete inclusion, instrumented with vibrating wires (Figure 4.1). To meet the principal requirements of a measuring instrument which can be used in the different environments, the following requirements are taken care of during the development of CIUS:

- the gages which are used in CIUS are suitable for long term operation (more than 50 years)

- the recorded data (deformations) are independent of the deformation of the casted concrete in CIUS (creep)

- the effect of rigidity difference between the concrete and gages is considered in the measurements

- the cement grout used for injection the bore hole has enough resistance against tension

- after knowing the stress concentration factor, resulting from the difference between the elastic properties of the host medium and those of the inclusion, and after determining the stress variations of concrete, we are able to determine the stress variations of the host medium (rock mass, concrete) [59].

The behavior of CIUS has been simulated in the laboratory and its precision and its reliability have been demonstrated [2].

Once CIUS has been installed, it can be considered as a permanent device, because the materials and instruments remain stable over time. The data can be read using a portable frequency measurement device or by an automated aquisition system (Figure 4.1).

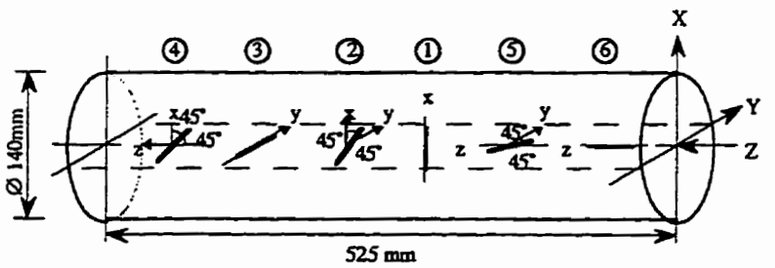

Figure 4.1 Instrumented cylinder, directions of extensometers

Figure 4.2 CIUS and dummy cylinder, ready for installation at Niobec

Calculation of the variations of stresses in the host medium is realized by application of the equations of the transfer of deformation and stress in a cylindrical inclusion which has been sealed by a grout. These equations are developed in three dimensions. They consider the cylinder, the grout of inclusion and the host medium, all of which are elastic, homogeneous and isotropic but with the different properties.

4.3 Extensometers

For instrumentation of CIUS the extensometers with vibrating wires have been chosen. The main advantages of these extensometers are summarized as follows:

- the transmission of signals is carried out in the form of frequency, rather than voltage and it is not affected by the variations of resistance in the transmission wires;

- the vibrating wires are protected against the humidity, so they can be used for any environment

- It is demonstrated that the vibrating wires operate during a long period of time (50 years) [18].

4.3.1 Principle of vibrating wires

The vibrating wires operate on the following physical phenomena:

a) the frequency of vibrating wires changes with the applied tension along its length according to the following expression:

$$f_n = \frac{1}{2L}\sqrt{\frac{\sigma}{\rho}} \qquad (4\text{-}1)$$

Where:

f_n : harmonic frequency (Hz);

L : length of wire (m);

σ : tension of wire (Pa);

ρ : density of wire's materials

n : number of harmonic

The tension of wire changes according to deformation and the Hook's law:

$$\varepsilon = \frac{\Delta L}{L} = \frac{\sigma}{E} \qquad (4\text{-}2)$$

Considering (4-1), we have:

$$\varepsilon = \frac{\Delta L}{L} = \frac{4L^2 \rho f_n^2}{E} = K \times f_n^2 \qquad (4\text{-}3)$$

As it can be seen the deformation has a direct relation to the square of frequency. So if we take an initial frequency, changing the tension of wire, the frequency of wire will change. By this means we are able to determine the applied deformation on the wire using the following relation:

$$\varepsilon = \frac{\Delta L}{L} = K \times \left(f_n^2 - f_{n_0}^2 \right) \qquad (4\text{-}4)$$

Where:

k : extensometric coefficient

f_{n0} : initial frequency (Hz)

f_n : final frequency (Hz)

The extensometers (vibrating wires) of TELEMAC C90 are used for the instrumentation of CIUS (Figure 4.2). These vibrating wires are made of a tight steel tube between two heads which are also made of steel. The two round heads define the base of measurement. The small lateral block at the half of the length includes the bobbins for listening and excitation. The lead out for the wires is at the middle of the device for limiting as much as possible the disturbance of load distribution.

4.4 Fabrication of CIUS

Preparation and installation of CIUS include a series of operations as follows:

- mold making and arrangement of extensometers
- preparation of concrete, the elastic parameters of concrete in CIUS are chosen according to those of the host medium
- preparation of sealing grout
- casting of concrete

-frequency calibration of extensometers

-thermal calibration of extensometers

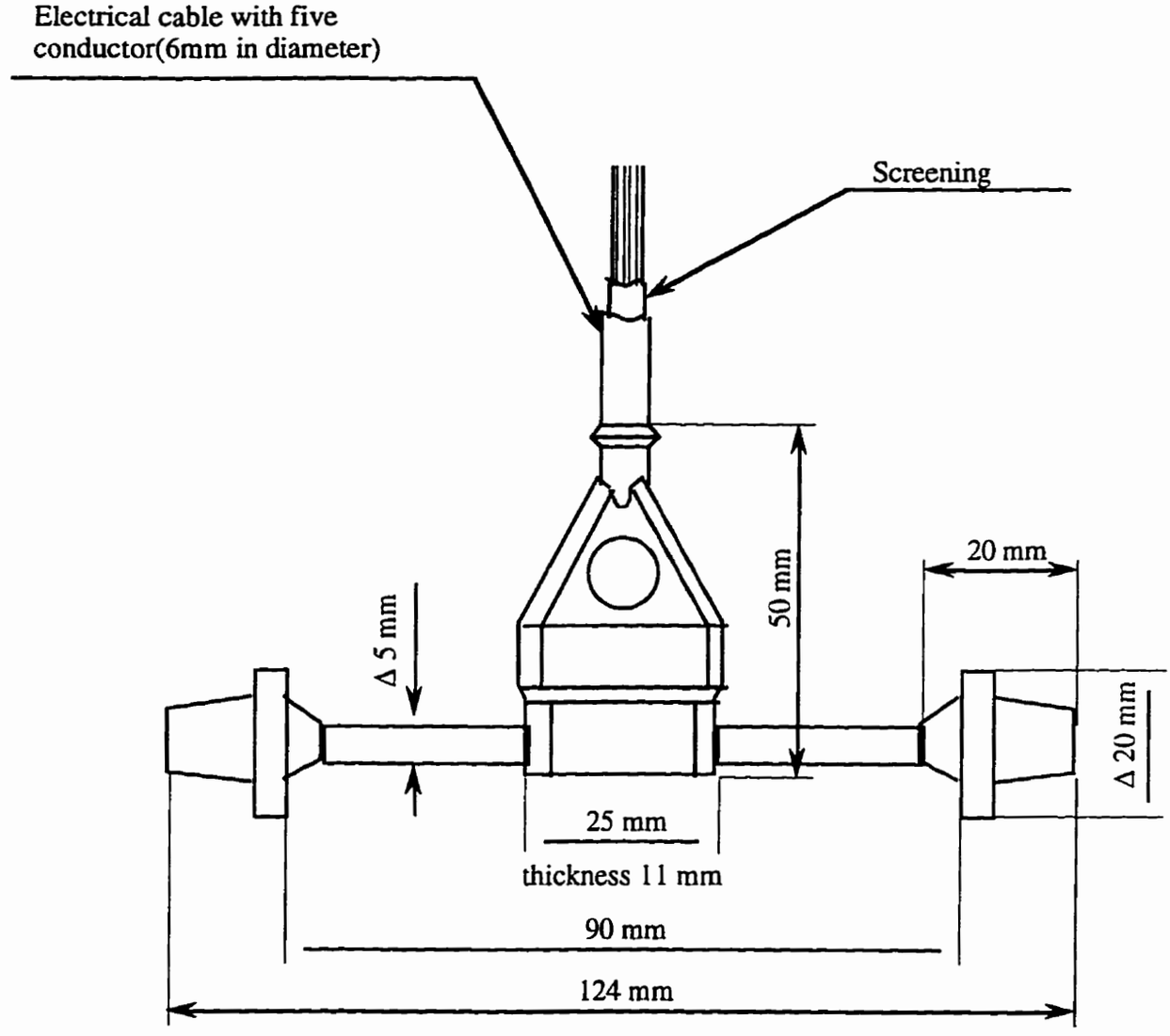

Figure 4.3 Vibrating wire extensometer

4.4.1 Mold making and arrangement of the extensometers

The extensometers are temporarily fixed with the help of thin brass wires in a mold which is made of PVC (Figure 4.4).

Three or six extensometers will be installed in CIUS to measure the variations of stresses and deformations in the host medium in two or three dimensions respectively (Figure 4.5, 4.6).

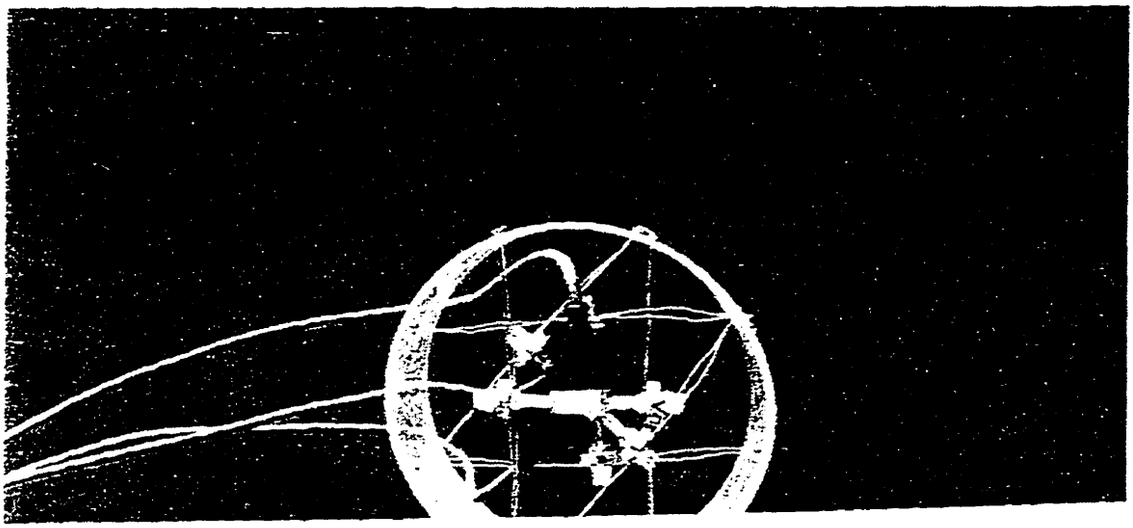

Figure 4.4 Picture of mold and the arranged extensometers

4.4.2 Fabrication of the CIUS' concrete

Development in the concrete technology allows us to make a concrete with different mechanical properties, (with experience of making the high performance concrete at the Université de Sherbrooke, it is possible to prepare a concrete with mechanical properties, such as elasticity modulus, Poisson ratio as close as possible equal to that of the rocks, Table 4.1). So it has been

possible to prepare a concrete with the desired properties for each site, which minimizes the stress concentration around the inclusion.

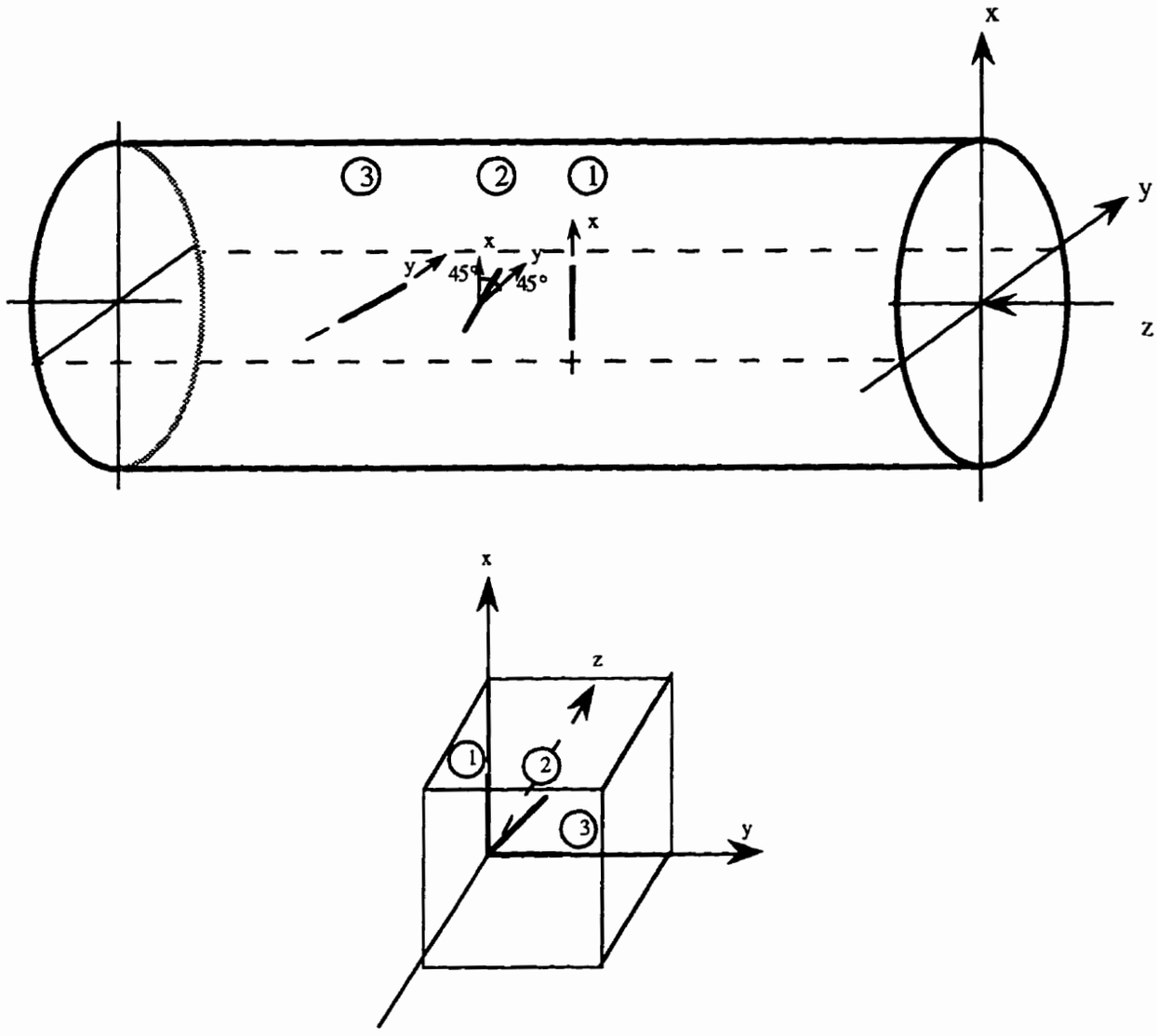

Figure 4.5 Instrumented cylinder for 2D measurements

4.4.3 Fabrication of the sealing grout

In order to have a good stress transmission between rock mass and inclusion, a sealing grout must perfectly join the two parts (Figure 4.6). To ensure this, a sealing grout has been prepared with an

elasticity modulus equal to 5-25 GPa and the Poisson's ratio equal to 0.2 (Table 4.1). The grout is made up of Portland cement containing an expansive agent to inhibit separation and to assure that all voids are filled.

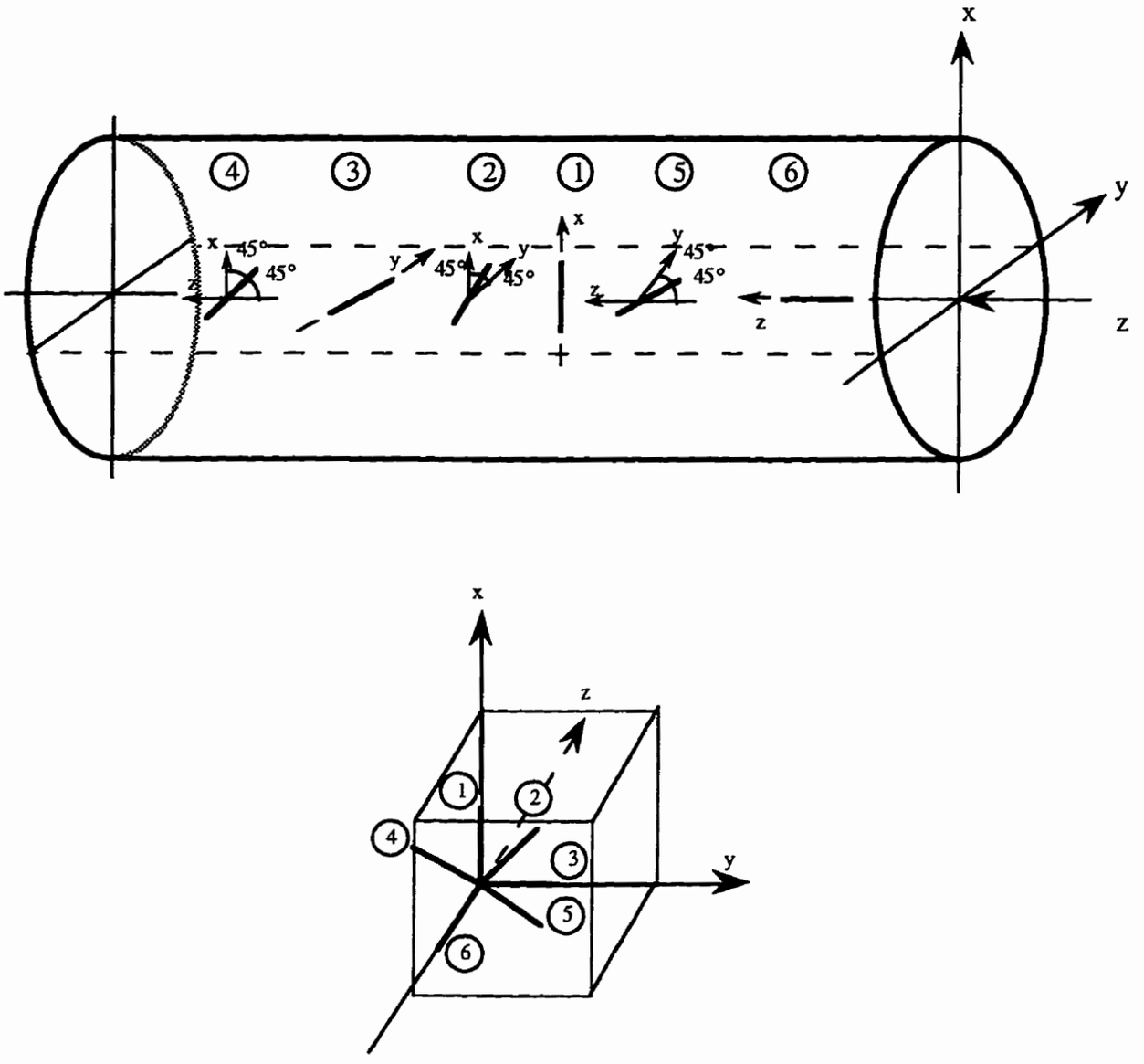

Figure 4.6 Instrumented cylinder for 3D measurements

Table 4.1 Mechanical properties of materials

	Simple Resistance in Compression (MPa)	Young Modulus (GPa)	Poisson's Ratio
Concrete	15-150	10-60	0.2
Cement Grout	10-60	5-25	0.2

4.4.4 Casting of the concrete

After preparing the concrete, it is casted in the mold in which the extensometers have been already installed. The casting of concrete in the designed mold will embed the extensometers. After removing the concrete cylinders and before being calibrated by a biaxial confining cell, the CIUS are placed in a saturated atmosphere for a period during which the frequencies of extensometers are read daily. If the extensometers show stability in frequency we conclude that the casting of concrete is complete. For CIUS the period during which the extensometers reach the frequency stability, is at least 28 days.

4.4.5 Frequency calibration of the extensometers

The extensometers must be calibrated to consider the effects of the heterogeneity of concrete, the sensitivity of wires and the rigidity difference between concrete and extensometers. The calibration of extensometers allows one to relate frequencies of extensometers to the deformation of the CIUS' concrete. It is carried out by a biaxial confining cell which provides a homogeneous stress distribution in CIUS. The relation (4-5) is used to relate the frequencies of extensometers to the radial deformations in two dimensional measuring CIUS [59].

$$\varepsilon_r = -\frac{(1-\nu)\rho}{E} = K_1 \times \left(f_n^2 - f_{n_0}^2\right) \times 625 \times 10^{-5} \qquad (4\text{-}5)$$

$$\begin{aligned}
\varepsilon_1 &= -\frac{(1-\nu)\rho}{E} = K_1 \times \left(f_n^2 - f_{n_0}^2\right) \times 625 \times 10^{-5} \\
\varepsilon_2 &= -\frac{(1-\nu)\rho}{E} = K_1 \times \left(f_n^2 - f_{n_0}^2\right) \times 625 \times 10^{-5} \\
\varepsilon_3 &= -\frac{(1-\nu)\rho}{E} = K_1 \times \left(f_n^2 - f_{n_0}^2\right) \times 625 \times 10^{-5} \\
\varepsilon_4 &= -\frac{(1-3\nu)\rho}{2E} = K_1 \times \left(f_n^2 - f_{n_0}^2\right) \times 625 \times 10^{-5} \\
\varepsilon_5 &= -\frac{(1-3\nu)\rho}{2E} = K_1 \times \left(f_n^2 - f_{n_0}^2\right) \times 625 \times 10^{-5} \\
\varepsilon_6 &= -\frac{2\nu\rho}{E} = K_1 \times \left(f_n^2 - f_{n_0}^2\right) \times 625 \times 10^{-5}
\end{aligned} \qquad (4\text{-}6)$$

In the case of three dimensional measurements, the frequency of each extensometer is related to the deformation of CIUS in the corresponding direction of the extensometer, by the relations (4-6) in which the frequencies are first related to the applied pressure and then to the deformation of CIUS.

4.4.6 Thermal calibration of the extensometers

The extensometers, which are used in CIUS, are able to measure the temperature in the host medium based on the ohmique resistance of the bobbins. The practical sensitivity of these measurements is $1\,^{C}$ to $2\,^{C}$. The thermal calibration of extensometers is done by temperature reading of each extensometer with the help of the listening bobbin and considering the temperature of the room in which they are placed. Having the difference between two measurements, the average deviation of measurements gives the correction factor for the temperature of each extensometer [56].

4.5 Installation of the CIUS

The dimensions of CIUS are 14 cm in diameter and 52-60 cm in length (Table 4.2). It is installed in a borehole, 15.2 cm (6 in) in diameter. However, a version of CIUS which can be installed in a borehole 9 cm in diameter (HQ Caliber), has also been developed and used in the underground laboratory of Atomic Energy of Canada Limited (AECL) [4]. The sealing is carried out by an grout made of Portland cement grout containing an expansive agent to inhibit separation. CIUS can be connected to a dummy cylinder whose role is to detect all forms of environmental phenomena. This cylinder is equipped with one vibrating wire extensometer and is placed in a hollow cylinder closed at both ends (Figures 4.2, 4.7, 4.8).

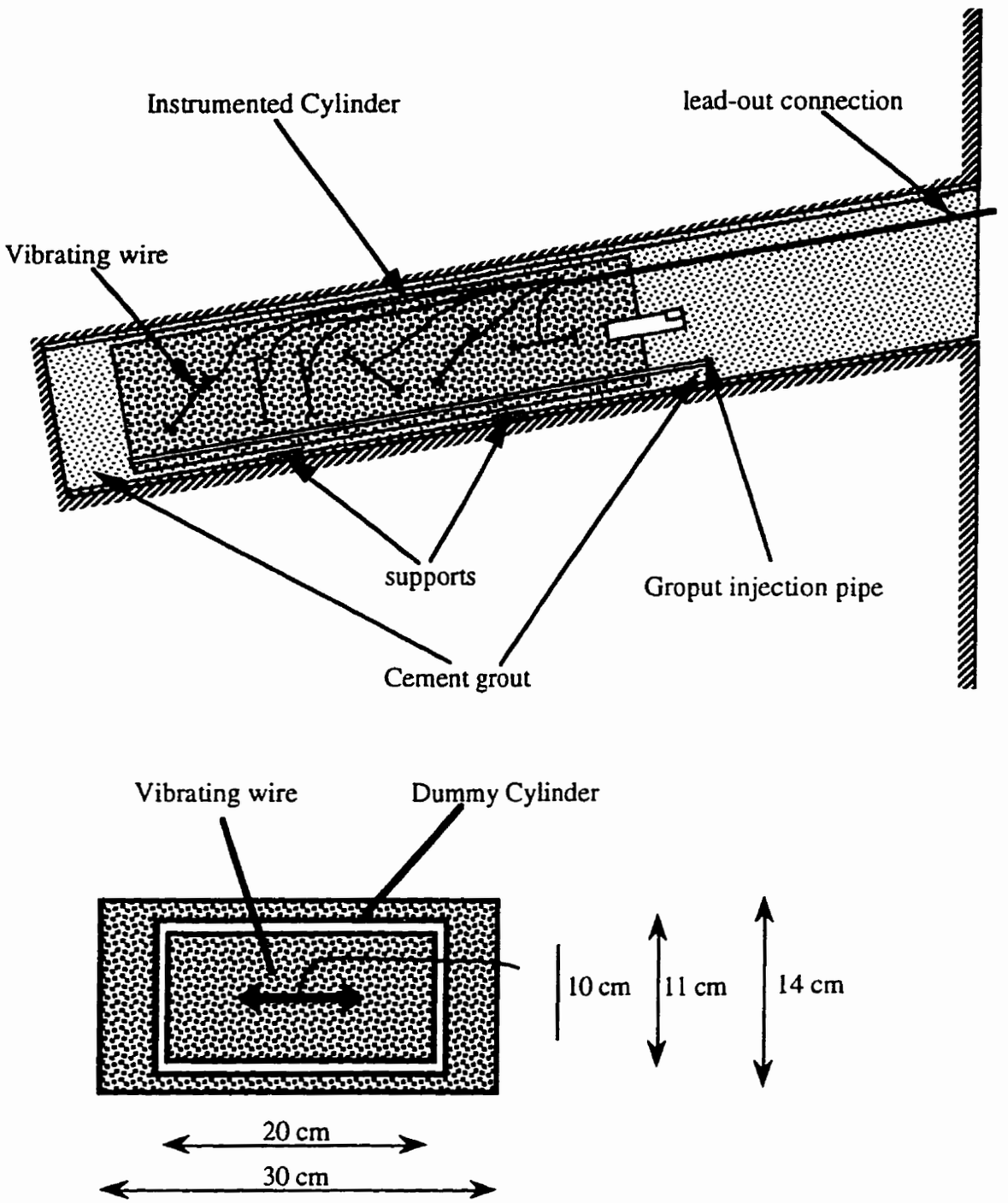

Figure 4.7 Instrumented cylinder of the université de Sherbrooke, CIUS (3D) and dummy cylinder

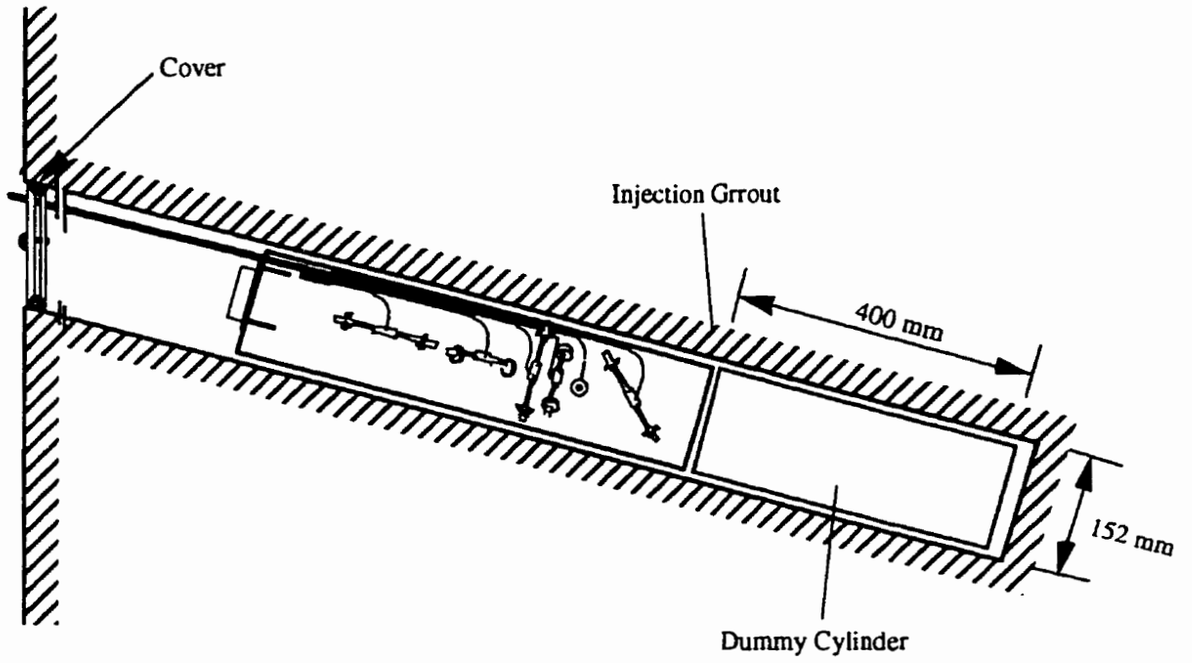

Figure 4.8 Installation of the CIUS

Table 4.2 Dimensions of the CIUS

	Borehole Diameter (mm)	CIUS' Diameter (mm)	CIUS' Length (mm)
2D	152	140	400
3D	152	140	525

Data can be read using any device which can be adapted with the vibrating wires. So far it has been done by a portable device for frequency measurement which operates with the help of a computer PC IBM (Figure 4.9). It can be done by an electronic data acquisition system for signal processing (CAIUS) developed at the Université de Sherbrooke [3].

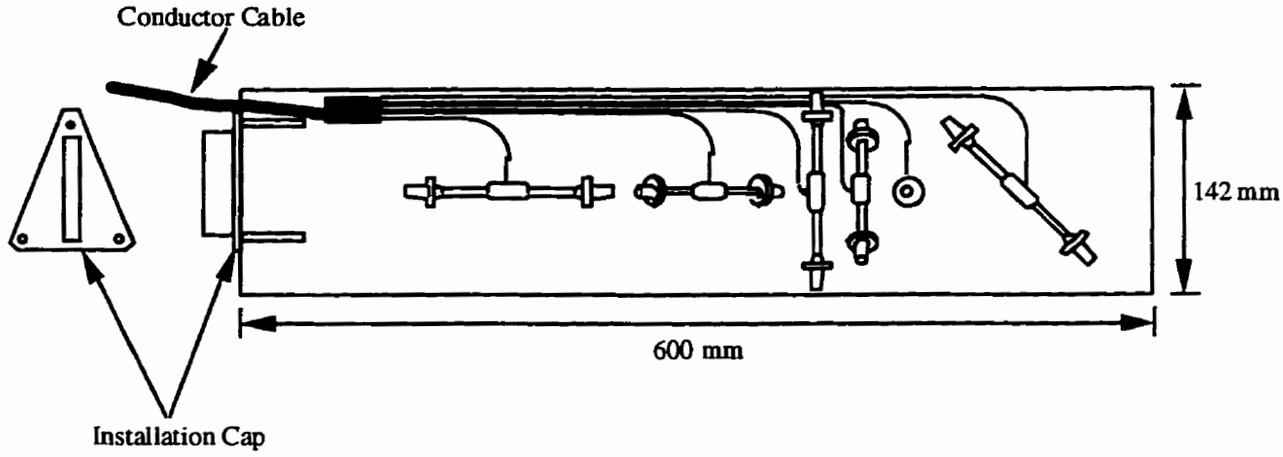

Figure 4.9 Lead out connection in the CIUS

4.6 Data analysis

4.6.1 Calculation of the total tensor of deformations

Using the relations (4-5) and (4-6) one can calculate the deformations. The complete tensor of deformations is shown as follows:

$$\varepsilon_1=\varepsilon_{zz}$$

$$\varepsilon_2=1/2(\varepsilon_{xx}+\varepsilon_{zz}+\gamma_{xz})$$

$$\varepsilon_3=\varepsilon_{xx}$$

$$\varepsilon_4=1/2(\varepsilon_{yy}+\varepsilon_{zz}+\gamma_{zy})$$

$$\varepsilon_5=1/2(\varepsilon_{xx}+\varepsilon_{yy}+\gamma_{xy})$$

$$\varepsilon_6=\varepsilon_{yy}$$

and we have:

$$\varepsilon_{xx}=\varepsilon_3$$

$$\varepsilon_{yy}=\varepsilon_6$$

$$\varepsilon_{zz}=\varepsilon_1$$

$$\gamma_{xy}=2\varepsilon_5-(\varepsilon_3+\varepsilon_6)$$

$$\gamma_{xz}=2\varepsilon_2-(\varepsilon_1+\varepsilon_3)$$

$$\gamma_{zy}=2\varepsilon_4-(\varepsilon_1+\varepsilon_6)$$

The complete tensor of deformations is represented by a 3×3 matrix as follows:

$$|M_1|=\begin{vmatrix}\varepsilon_x & \gamma_{xy} & \gamma_{xz}\\ \gamma_{yx} & \varepsilon_{yy} & \gamma_{yz}\\ \gamma_{zx} & \gamma_{zy} & \varepsilon_{zz}\end{vmatrix} \qquad (4\text{-}7)$$

4.6.2 Calculation of the corrected tensor of deformations

The total measured deformations by the extensometers inside CIUS are the sum of the elastic and thermal deformations and the deformations due to humidity, creep and other environmental phenomena.

$$\varepsilon_{total} = \varepsilon_{elastic} + \varepsilon_{thermic} + \varepsilon_{creep} + \ldots\ldots \qquad (4\text{-}8)$$

For obtaining the tensor of elastic deformations, the measured deformation by the dummy cylinder must be subtracted from the total deformation.

$$\varepsilon_{ij}(\text{elastic}) = \varepsilon_{ij}(\text{total}) - \begin{vmatrix}\varepsilon_{\text{dummy cius}} & \text{if } i=j & \text{(Normal Deformation)}\\ 0 & \text{if } i\neq j & \text{(Tangential Deformation)}\end{vmatrix}$$

The corrected tensor of deformations inside the inclusion will be represented as follows:

$$|M_2|=\begin{vmatrix}\varepsilon_{xx}-\varepsilon_d & \gamma_{xy} & \gamma_{xz}\\ \gamma_{yx} & \varepsilon_{yy}-\varepsilon_d & \gamma_{yz}\\ \gamma_{zx} & \gamma_{zy} & \varepsilon_{zz}-\varepsilon_d\end{vmatrix} \qquad (4\text{-}9)$$

For the initial state of deformations which is equal to zero, the diagonalization of the above matrix allows one to determine the principal deformations inside the inclusion (ε_1, ε_2, ε_3). By solving the following third degree equation one can obtain the values of principal deformations [1].

$$\varepsilon_i^3-\left(\varepsilon_{xx}+\varepsilon_{yy}+\varepsilon_{zz}\right)\varepsilon_i^2+\left(\varepsilon_{xx}\varepsilon_{yy}+\varepsilon_{xx}\varepsilon_{zz}+\varepsilon_{yy}\varepsilon_{zz}-\frac{\gamma_{xy}^2}{4}-\frac{\gamma_{xz}^2}{4}-\frac{\gamma_{yz}^2}{4}\right)\varepsilon_i$$
$$-\left(\varepsilon_{xx}\varepsilon_{yy}\varepsilon_{zz}-\varepsilon_{xx}\frac{\gamma_{yz}^2}{4}-\varepsilon_{yy}\frac{\gamma_{xz}^2}{4}-\varepsilon_{zz}\frac{\gamma_{xy}^2}{4}+\frac{\gamma_{xy}\gamma_{xz}\gamma_{yz}}{4}\right)=0 \qquad (4\text{-}10)$$

4.6.3 Determination of the state of the stresses inside the host medium

Supposing that the elastic constants for the three different materials are the same, one can suppose that the medium is homogeneous and isotropic, so the variation of stresses may be calculated by the equations of stress-deformation in an elastic medium. Finite element and boundary element methods are the other methods for solving this problem.

$$\sigma_{xx}=\frac{E}{1+\nu}\left[\varepsilon_{xx}+\frac{\nu}{1-2\nu}\left(\varepsilon_{xx}+\varepsilon_{yy}+\varepsilon_{zz}\right)\right]$$
$$\sigma_{yy}=\frac{E}{1+\nu}\left[\varepsilon_{yy}+\frac{\nu}{1-2\nu}\left(\varepsilon_{xx}+\varepsilon_{yy}+\varepsilon_{zz}\right)\right]$$
$$\sigma_{zz}=\frac{E}{1+\nu}\left[\varepsilon_{zz}+\frac{\nu}{1-2\nu}\left(\varepsilon_{xx}+\varepsilon_{yy}+\varepsilon_{zz}\right)\right]$$
$$\tau_{xy}=\frac{E}{2(1+\nu)}\gamma_{xy} \qquad (4\text{-}11)$$
$$\tau_{xz}=\frac{E}{2(1+\nu)}\gamma_{xz}$$
$$\tau_{yz}=\frac{E}{2(1+\nu)}\gamma_{yz}$$

4.6.4 Back analysis method

For determining the variations of stresses inside the mine pillars, one can use the Homogeneous Medium Method. In the case of CIUS, the elastic constants are smaller than those of rock mass, but the difference between CIUS' characteristics and those of rock mass are within the acceptable limits. Using the relations (4-11) one can determine the variation of stress. Knowing the initial state of stresses inside the medium, one can determine the final stresses tensor by the following relations.

$$\left[\underline{\sigma}_{ij}\right]_{Final} = \left[\underline{\sigma}_{ij}\right]_{Initial} + \left[\underline{\sigma}_{ij}\right]_{Variation} \tag{4-12}$$

The principal stresses as well as their directions in the rock mass are obtained by solving the following equation [34].

$$\begin{aligned}\sigma_i^3 - \left(\sigma_{xx}+\sigma_{yy}+\sigma_{zz}\right)\sigma_i^2 + \left(\sigma_{xx}\sigma_{yy}+\sigma_{yy}\sigma_{zz}+\sigma_{zz}\sigma_{xx}-\tau_{xy}^2-\tau_{yz}^2-\tau_{zx}^2\right)\sigma_i \\ -\left(\sigma_{xx}\sigma_{yy}\sigma_{zz}-\sigma_{yy}\tau_{yz}^2-\sigma_{zz}\tau_{xy}^2+2\tau_{xy}\tau_{yz}\tau_{zx}\right)=0\end{aligned} \tag{4-13}$$

The three roots of this equation are the principal stresses (σ_1-maximum principal compressive stress, σ_2-intermediate principal compressive stress, σ_3-minimum principal compressive stress). Calculation of the direction cosines for the principal stresses is based on the following simultaneous equations:

$$\begin{aligned} l(\sigma_{xx}-\sigma_n)+m\tau_{yx}+n\tau_{zx}&=0 \\ l\tau_{xy}+m\left(\sigma_{yy}-\sigma_n\right)+n\tau_{zy}&=0 \\ l\tau_{xz}+m\tau_{yz}+n(\sigma_{zz}-\sigma_n)&=0 \end{aligned} \tag{4-14}$$

$$l^2+m^2+n^2=1 \tag{4-15}$$

where l, m, n the direction cosines of the principal stress (σ_n) to the axes x, y, z [35].

CHAPTER 5

5. PRINCIPLES OF PROGRAMMING IN A ROCK FAILURE WARNING SYSTEM

5.1 Introduction

The most desirable goal in underground mining is the control of the ground motion, deformations and loads in the rock surrounding the underground openings. It is necessary to predict excessive movement or stresses as these can endanger the stability of excavations.

Rock mechanics instrumentation is indispensable for detecting potential ground instability and for providing warnings of potential problems. With such an arrangement remedial measures can be implemented before the problems reach a stage where remedial measures become either very expensive or impossible to execute.

One of the most important objectives of instrumentation at Niobec is to detect the instabilities which may endanger safety of underground openings, such an instrumentation trigger the warning signals when any instability is anticipated. The programming of a warning system using the CIUS' data (deformation) can be achieved according to different procedures and using several algorithms and methods.

The evaluation of a remote monitoring system, consists of measuring instruments, acquisition system and a warning system. Several parameters have to be considered. They are listed as follows:

- number of sensors installed in the monitored zone;
- precision of sensors which must be high enough for being capable of detecting the instabilities;
- resistance of instruments which must resist mechanical stresses, corrosion, blasting, temperature variations and humidity in the rugged environments such as in an underground mine.
- variations of measurements of each sensor;
- rate of acquisition;

- position of the sensors so that the detection of instability is carried out as soon as possible without devices damaging;
- time between triggering of warning signals and collapse of structure which must be long enough so that the necessary verifications can be done;
- time interval between two successive tests for triggering or not the warning signals;
- possibility of having several triggering levels;
- precision of monitoring system in forecasting the time of collapse;
- monitoring system capability to detect defects in the materials and instruments and to switch on automatically after each power failure;
- the time needed to restart the system after each stop. For example in the underground mines the monitoring system must be shut down during blasting operations to prevent triggering of warning signals, but must be reactivated immediately after blasting operations before the mine's personnel arrive;
- facility with which software can be used and their capability to visualize the data after recording and at the time of treatment and storing;
- memory of the system;
- capability of the system to forecast system's memory saturating point;
- capability of the system to pick out actual variations of rock masses from those of the instruments;
- accepted risk of failure in releasing the warning signals at the commencement of instability;
- accepted risk of having an unjustified warning;

5.2 The hypothesis of warning system programming

5.2.1 Introduction

Considering all above mentioned parameters and phenomena which are supposed to be measured by measuring instruments (deformation) and the nature of data which will be used as the input of

the warning system for detecting the instabilities in the underground rocky structures, one can apply three principal methods:

- threshold method
- precursory events method
- gradient method

Advantages and disadvantages of each method are discussed in the followings sections.

5.2.2. Threshold Method

In this method the warning signals are triggered as soon as the threshold is reached. The threshold can be programmed for frequencies, deformations, stresses and other variables (Figure 5.1).

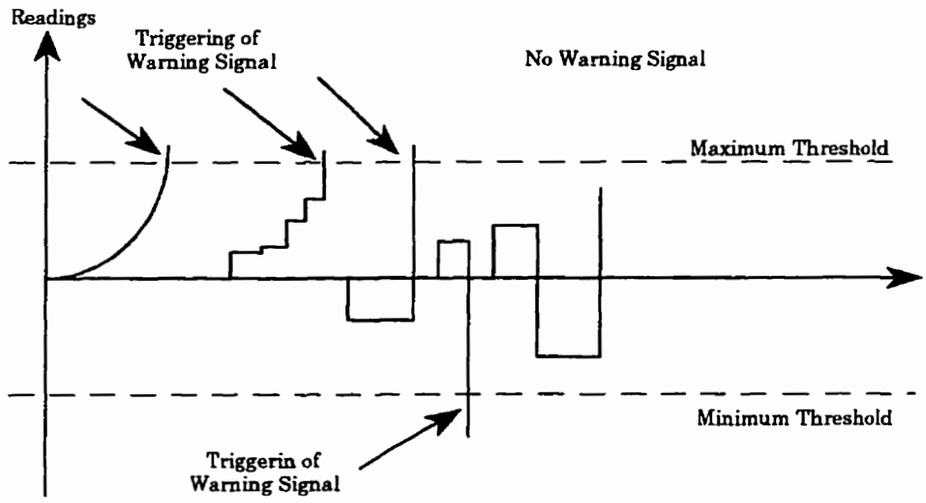

Figure 5.1 Release of warning signals in threshold method

It is necessary to define two thresholds, maximum threshold and minimum threshold. Although the programming of a warning system by this method is simple, there are many disadvantages that limit its application in the underground mines. Disadvantages are summarized as follows:

- It is necessary to differentiate between variations of rock mass from those of instruments (Figure 5.2).
- Before being able to define the threshold, the behavior of the monitored rock mass must be known quantitatively for a long period of time. This knowledge may be obtained by experimental, analytical or numerical modeling of the behavior of rock structures. However determinations are not normally precise enough to be used in a warning system in the underground mines.
- It is necessary to distinguish the threshold beyond which the rock mass failure will happen (S_1) from the other one, beyond which the system will warn us about the failure before it happens (S_2); the first one (S_1) is not an applicable threshold in a warning system programming; but the second threshold is useful for this purpose; however other parameters must be considered when using this method, such as the safety factor (η) $\eta = S_1 / S_2$ ($\eta \geq 1$). If $\eta=1$, we have the warnings at the failure time and if $\eta=\infty$, the warning signals are triggered all the time.

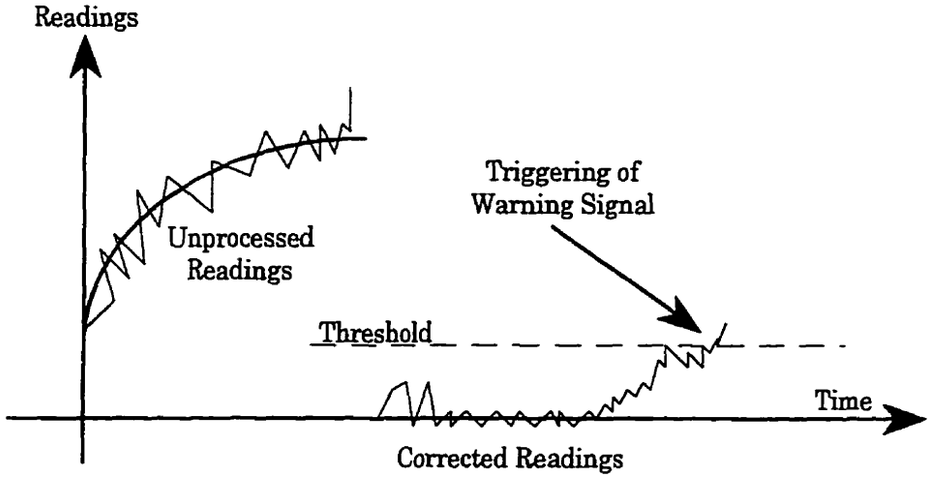

Figure 5.2 Unprocessed variations and real variation of readings

5.2.3 Method of precursory events

In this method, the warnings are triggered, upon the presence of precursory events. Like an earthquake, which is preceded by minor earthquakes, a mine collapse can be preceded by minor readjustments, which are indications of an imminent destruction of structure (Figure 5.3). These

movements can be detected by the sensors in the form of a jump or light oscillations (earthquake case and rock burst prediction).

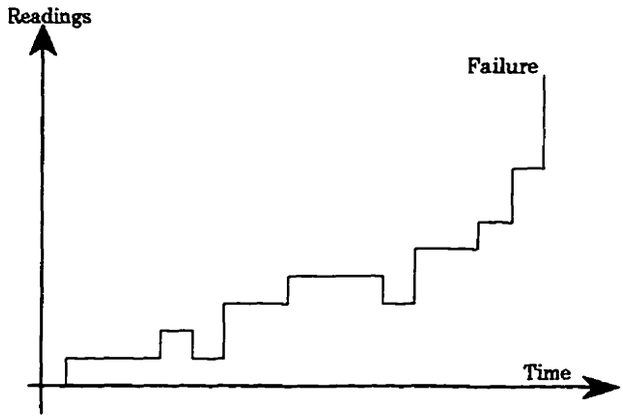

Figure 5.3 Triggering of warning signal in the precursory events method

Figure 5.4 shows the precursory events which were recorded before the earthquake in the sea of Japan on May 26, 1983 [42]. In the beginning of March 1983, there was an increase in the number of precursory events leading up to the time of the earthquake.

The programming of a warning system by this method, similar to the threshold method, is easy, but due to some limitations, it can not be applied to the programming of a warning system in the underground structures. These limitations are summarized as follows:

- This method is capable of indicating the increase of the accident risk, but it can not precisely predict the time of collapse. It can be seen, in Figure 5.4 that the first warning signal was released in March and the second in April for the collapse that happened in May. So, along with this method another reliable technique has to be used.
- On the other hand, there may not be always precursory events before a collapse even if they are, it will be difficult to detect them. Figure 5.5 shows the measured deformation variations before, during, and after the earthquake of Loma Prieta on October 17, 1989 by using a deformation measuring cell [28]. Since the precursory events have a weak amplitude, this programming method can be of interest to program with the emission acoustic sensors.

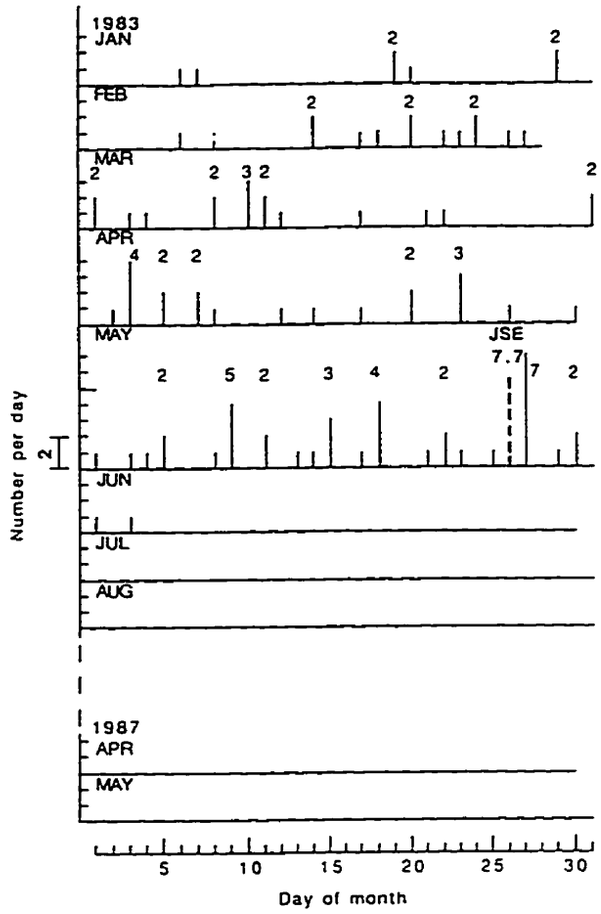

Figure 5.4 The number of precursory events in terms of time: before, during and after the earthquake in the sea of Japan [42]

5.2.4 Method of gradient

After having been disturbed the ground's equilibrium by an excavation, the ground conditions evolve to a new state of equilibrium expressed by the subsiding deformation when there is no active effect of this disturbance; on the contrary, all non-subsiding evolution can end with the structure's collapse in the long run (Figure 5.6), and detection of an abnormal evolution (acceleration) on the deformation rate is a sign of near failure [5, 16, 17, 27, 40, 54, 55, 56].

In addition, modern technology has made it possible to investigate the effect of prolonged loading or time dependent loading behavior of in-situ rock mass until rupture (creep rupture) by means of microseismic monitoring.

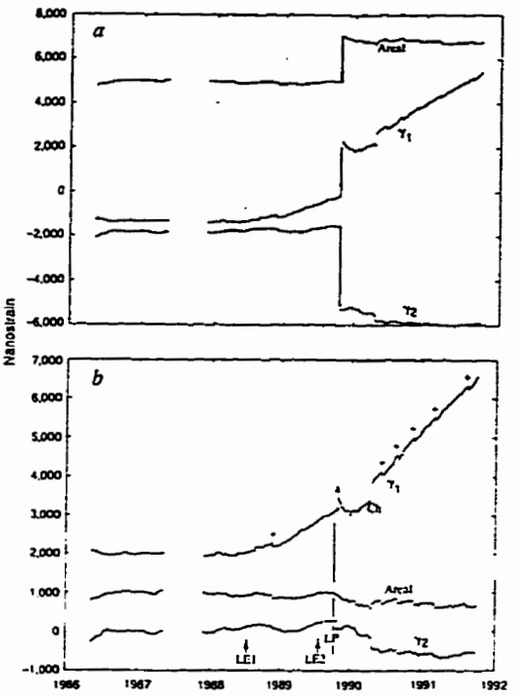

Figure 5.5 Measured deformations during the earthquake of Loma prieta (USA); a) Unprocessed data, b) Processed data [28]

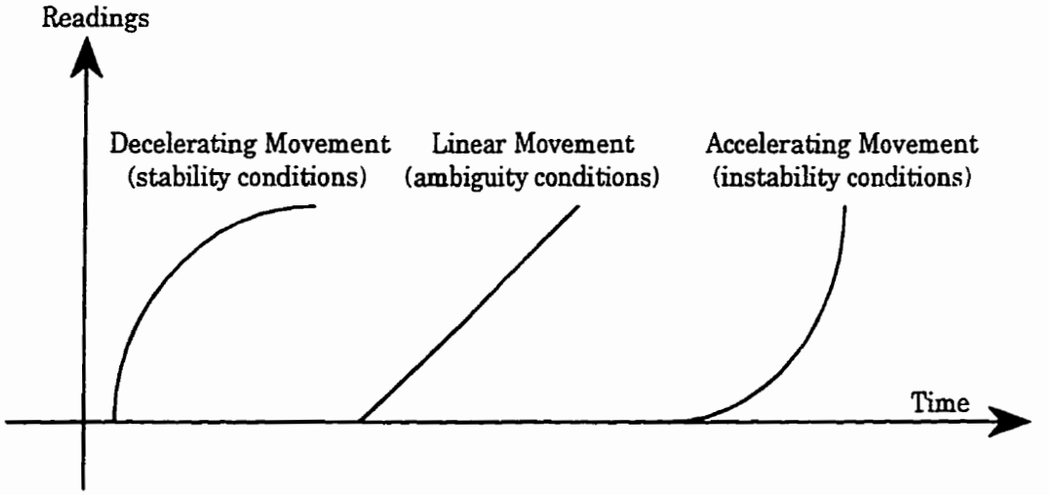

Figure 5.6 Triggering of warning signal upon the gradient method

These studies indicate that there is a period of accelerated movement in in-situ rock preceding failure. This shows that there is in fact a tertiary creep phase (accelerating strain increment) that is much longer than the lab studies indicate. Microseismic disturbance periods range from a few hours for a rock fall of several tons to several weeks for a large body of rock, such as a 250-ton roof fall or the failure of a mine pillar. From this we can infer that in-situ rock also exhibits transient, steady state and tertiary creep [49]. The creep behavior of rock mass will be discussed in chapter 7.

It must be mentioned that having a decelerating evolution in rock mass deformation can not assure the stability of the monitored zone because the deformation tendency can be inverted (Figure 5.7), and this change will be detected by finding an accelerating rate of deformation [40].

Therefore, in the CIUS' case by using the gradient method, the warning signals can be triggered by finding the anomalies in the rates of frequencies, stresses or deformations. This method of programming is more complicated than the two above described methods. In this method the monitoring system must consider the previous recorded deformation rates and their changes in the past periods. In addition, the variability of phenomenon and those of instruments must be kept in the memory system. It must be considered that a continuous phenomenon is often constituted of a sudden change upon the applied scale of time [40] (Figure 5.8, 5.9).

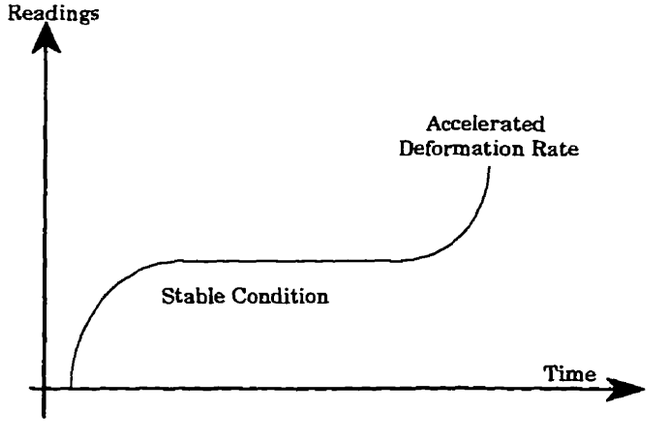

Figure 5.7 Presentation of a sudden accelerated rate after a stable tendency

The gradient method can be applied for three types of programming [54]. The first one (Figure 5.10) is based on seeking a linear adjustment of movements with respect to time during a control period and comparing the tendency of this adjustment to the average tendency during the

previous periods as a reference period [54]. So, it is possible to make the decision to trigger the warning signals only at the end of each control period.

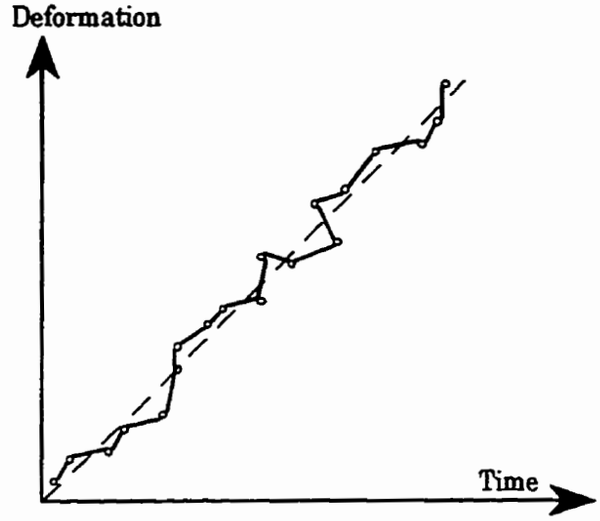

Figure 5.8 Measured deformation by convergence meter at an Iron ore mine in France [40]

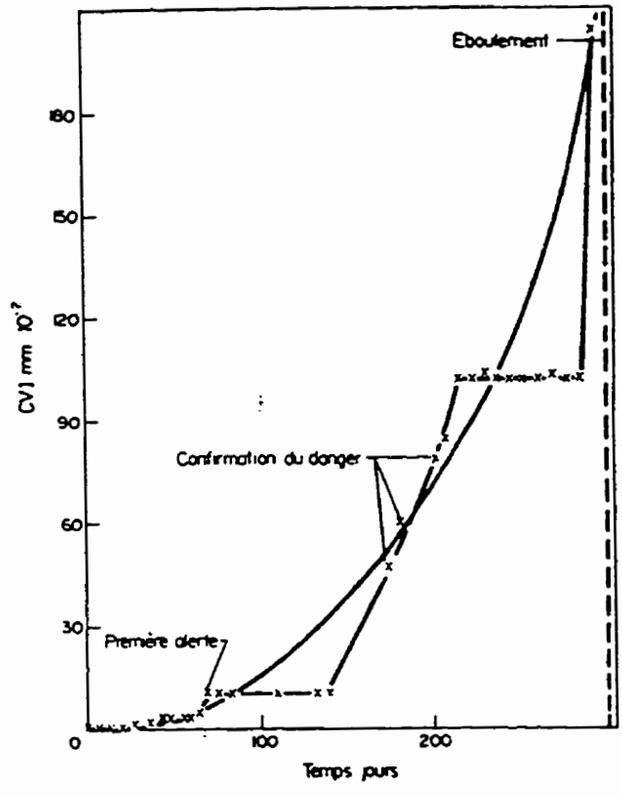

Figure 5.9 Measured deformation by convergence meter at the Saint-Sauve mine in France [27]

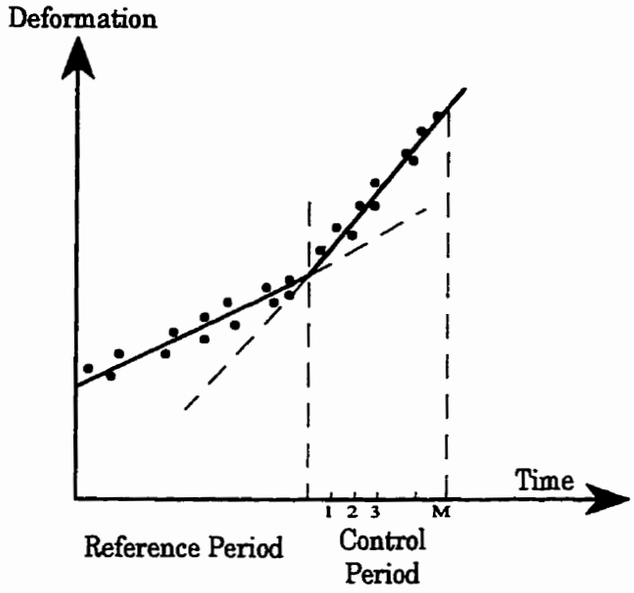

Figure 5.10 Detection of an accelerating rate in deformation by comparing the tendencies with a linear adjustment

If the difference between two tendencies is greater than a determinable confidence interval, we can conclude that there is an abnormal evolution of deformation (slope warning); otherwise, there is stability.

The second method (Figure. 5.11) is based on detecting all points which depart from the reference line defined in the first method. This warning is punctual and the test is realized after each reading.

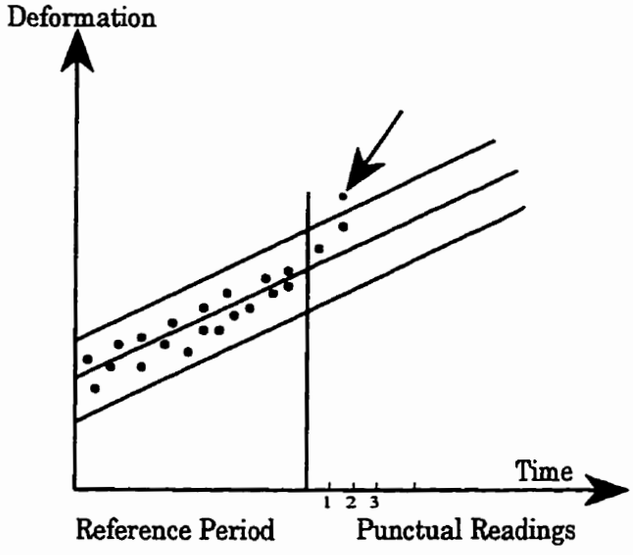

Figure 5.11 Punctually finding an accelerating rate in deformation

The third way consists of evaluating the parameters of adjustment in the curves $Y=f(t)=b+at+ct^2$ (Figure 5.12).

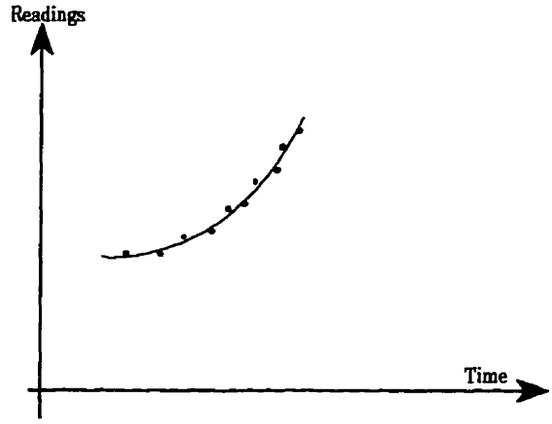

Figure 5.12 Finding an accelerated deformation rate by a parabolic adjustment

So, in this method the system will warn us if the parameter of acceleration (c) is significant or greater than zero.

These three methods call for statistical calculations, which take into account two risks in making a wrong decision: these are α (risk of triggering an unjustified warning) and β (risk of concluding a stability while an instability is starting) [16].

The process of decision making in a warning system will be discussed in detail in the next chapter.

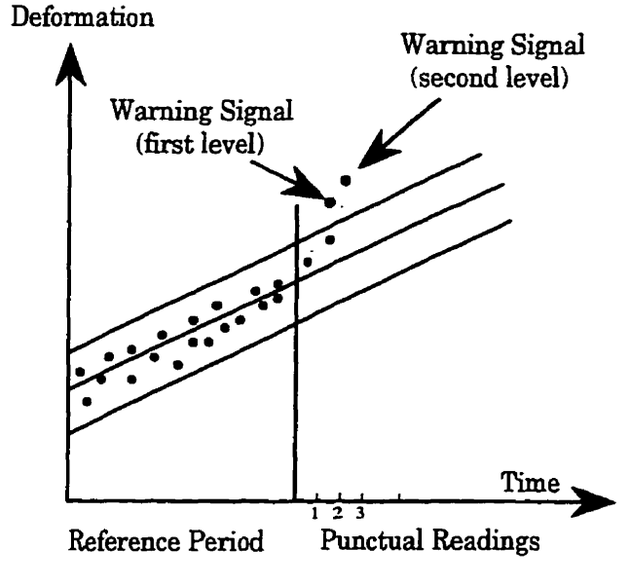

Figure 5.13 Punctual warning levels

They can be programmed for a group of sensors and it is generally supposed that the measurements deviation is the same for all the sensors and the triggering level depends on the duration of abnormal evolution (acceleration) at the time [16]. So It is possible to consider several levels of triggering (Figure 5.13).

In the CIUS' case, the gradient method consists of the detection of an accelerated rate on the read frequencies or calculated deformations.

The programming of a warning system by this method is more complicated than by the other methods, in which the history of monitored zone must be considered and be stored in the system's memory. The effectiveness of such warning systems depends on the period between the structure's collapse and the tripping of the warning signal, which may be nearly zero or several weeks [4].

CHAPTER 6

6. PROBABILISTIC ANALYSIS OF MAKING DECISION IN A ROCK FAILURE WARNING SYSTEM (PREVENTION AND PREDICTION OF FAILURE)

6.1 Introduction

According to the gradient method, a rock failure warning system should detect the anomalies in the rate of deformation and provide warnings of potential instabilities in order that necessary verifications can be done before the problems developed to a stage where there is no chance of having control over an imminent danger. It is shown that when deformation is the measured variable, then in that case, the gradient method is the most reliable method for a warning system to be programmed.

Throughout this chapter an algorithm is developed based on the gradient method for an instability preventive model. The two important risks (α, β) associated with the decision making process in a warning system as well as the statistical parameters of measurements are considered. The theories, presented in this chapter may be applied to other programmable systems which are concerned with the decision making process by using the random measurements.

6.2 General definition of an instability preventive model upon the gradient method

So far it has been proven and shown that an instability in rock mass can be predicted by recognizing an accelerated deformation rate which may be detected by comparing the average tendency of deformations during a specified period (characterized by a regression line) with the previous evolution of deformations (Figure.6.1).

There is actually variability in the measurements of deformation; first due to the precision of measurements and secondly, due to the variability of the phenomenon (sudden changes in the

strain's rate). This variability can be represented by a standard deviation (σ_R) around the regression line *.

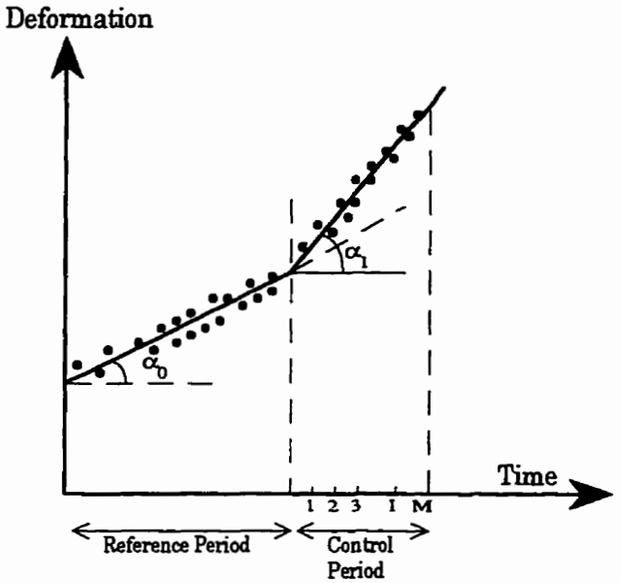

Figure 6.1 Detection of an accelerating rate by comparing the tendencies

According to the gradient method the recognition of an accelerated rate in the deformation of rock mass is carried out at the end of the periods which, in this study, are called the control periods (T), each period contains (M) measurements (e.g. deformation measurement). If a series of sensors, which monitor the rate of strain or any other variable (stress,...) in the monitored zone show an abnormal rate of deformation (acceleration) we may expect an abnormal behavior of rock mass which in the long run can end to a failure in structure.

In this condition, there must be a significant difference between the rate of deformation recorded during the control period (T) and that during the previous period, called reference period. This comparison will be called tendency or slope test. As it has been already mentioned, this test is carried out at the end of each control period on the recorded deformations' rate.

---

* σ_R is usually unknown and must be estimated from the sample data, the statistic uses an estimated σ_R, and is called the Residual Standard Deviation denoted by S_e and defined by :

$$S_e = \sqrt{\frac{SSE}{n-2}} \text{ where } SSE = \sum_{i=1}^{n}\left(Y - \hat{Y}\right)^2$$

SSE is the total squared error, and n is the total number of data, Y=observed value, $\hat{Y}$=predicted value.

In other words the difference between two rates of deformation must be greater than a determinable confidence interval whose value depends on the statistical parameters of measurements as well as on the associated risks in making decision on the stability state of the monitored zone. In order to examine the decision making process of a rock failure warning system for triggering the warning signals, two parameters may be considered at this stage, as follows:

- Number of readings (measurements); M
- Time left between two readings; Δt

Where;

$$T = M \times \Delta t; \text{ is Control Period}$$

Since a reliable stability monitoring is carried out by several sensors, read at the same time, the number of sensors which must detect an anomaly has an indispensable effect on the decision making process of the monitoring system, as well as on the values of the associated risks. So this parameter is considered by the number of sensors (represented by r) which show an abnormal rate in the deformation regime of structure. Therefore, the second series of parameters is entered into the model.

- Number of sensors; N
- Number of sensors which show an abnormal deformation rate in the monitored zone; r

According to the second method of programming in the gradient method, during a control period we may be warned if some measurements are apart from a specified interval whose value depends on the deviation of measurements and the accepted risks of α, and β. This warning is punctual and will be discussed in paragraph 4.

6.3 Probabilistic analysis of a single sensor

Considering a zone which has been monitored with a measuring sensor during a period at the end of which the tendency test is realized. Arriving at a decision on the stability of the zone is associated with two risks.

1 - α: the risk of concluding an abnormal deformation rate, while in fact there is no abnormal behavior of deformation in the monitored zone.

2 - β: the risk of concluding a normal rate where there is an anomaly in the rate of deformation in the considered zone.

For each incorrect conclusion we actually pay a price, for α, there is a worthless intervention and for β, no reaction to an abnormal deformation rate.

According to the described hypothesis for the gradient method and considering the random characteristic of the measurements (readings) by a number of installed sensors, one can represent these data by a Gaussian probability law in which the average of data depends linearly on time and whose deviation remains constant and equal to σ_R. This can be represented by the following relationship.

$$Y = \beta_1 + \beta_0 I + \varepsilon, \quad \varepsilon \approx N(0, \sigma_R) \qquad (6\text{-}1)$$

Where:

Y is the observed deformation.(deformation function)

In this study the duration of a control period is divided into equal intervals (Δt) with increments during a period is represented by I, (number of readings since the beginning of the control period).

- $I = \dfrac{\text{passed time since commencement of period}}{\text{time between readings}}$

- β_1: strain rate, during the control period

- β_0: intercept of the line (linear adjustment)

One can consider the random characteristic of readings by instruments (sensors), the actual value deformation's rate ($\beta_1 \times I + \beta_0$) is unknown and we consider ($b_1 \times I + b_0$) as an estimation of the actual rate which is calculated by M readings, so b_1 is an estimation of the actual rate of

deformation or β_1, the deviation of the second value from the first one depends on the following parameters:

- Residual standard deviation of readings; σ_R
- Number of readings during the control period; M

We show that b_1 is a realization of a Gaussian random with an average equal to β_1, and a standard deviation equal to σ.*

$$\text{Where } \sigma = \sqrt{\frac{12\sigma_R}{M\left(M^2-1\right)}} \tag{6-2}$$

$$\text{VAR}(b_1) = \frac{12\sigma_R^2}{M\left(M^2-1\right)} \tag{6-3}$$

$$b_1 = E\left(\beta_1, \sigma_R\sqrt{\frac{12}{M\left(M^2-1\right)}}\right) \tag{6-4}$$

According to the gradient hypothesis, the slope test carried out by the system, consists of determination of the difference between β_1 and β_{1ref}, where β_{1ref} is the strain rate during the past periods or reference period and β_1 is the strain rate during the control period.

$$*\sigma^2 = \text{VAR}(b_1) = \frac{\sigma_R^2}{\sum\left(x_i-\bar{x}\right)^2} \text{ and : } \sum_1^M\left(x_i-\bar{x}\right)^2 = \sum_1^M x_i^2 - M\bar{x}^2$$

$$\bar{x} = \frac{1}{M}(1+2+3+.....+M) = \frac{M(M+1)}{2M} = \frac{M+1}{2}$$

$$\sum_1^M x_i^2 = 1^2+2^2+3^2+.....M^2 = \frac{M(M+1)(2M+1)}{6}$$

$$\sum_1^M (x_i-x)^2 = \frac{M(M+1)(2M+1)}{6} - M\times\frac{M(M+1)^2}{4} = \frac{M(M+1)(M-1)}{12} = \frac{M\left(M^2-1\right)}{12}$$

Since the actual values of β_1 and β_{1ref} are unknown, the slope test is carried out with their estimations b_1 and b_{1ref}.

If the deviation of the readings during the control period (contains M readings) remains constant and equal to σ_R (readings deviation during the reference period), we can assume that the relation between b_{1ref} and β_{1ref} is the same as that between b_1 and β_1. When the reference period is longer than the control period, "this means that there has not been an anomaly during the previous periods" the number of readings by which we have calculated β_{1ref} is greater than M, so deviation of β_{1ref} is smaller than that of β_1, which decreases the associated risks of α and β.

The value of b_1- b_{1ref} is also a Gaussian random with an average equal to β_1 -β_{1ref} and whose variance is determined as follows:

$$VAR(b_1 - b_{1ref}) = 2 \times \frac{24\sigma_R^{\,2}}{M(M^2-1)} = \frac{24\sigma_R^2}{M\left(M^2-1\right)} \qquad (6\text{-}5)$$

Considering the deviation of this random variable, we conclude that there is an anomaly in the rate of deformation, if the value of b_1- b_{1ref} is sufficiently great.

The risk of α can be represented as follows;

α = Prob. (wrong warning),

$$\alpha = \text{Prob. } \left\{ |b_1 - b_{1ref}| \rangle B,\ \beta_1 - \beta_{1ref} = 0 \right\} \qquad (6\text{-}6)$$

With the help of the following Gaussian relationship one can specify the risk of α by the value of B, over which we conclude that there is an abnormal behavior in rock mass (Figure 6.2);

$$t_\alpha \le \frac{|B|}{\sigma_R \sqrt{\frac{24}{M\left(M^2-1\right)}}} \qquad (6\text{-}7)$$

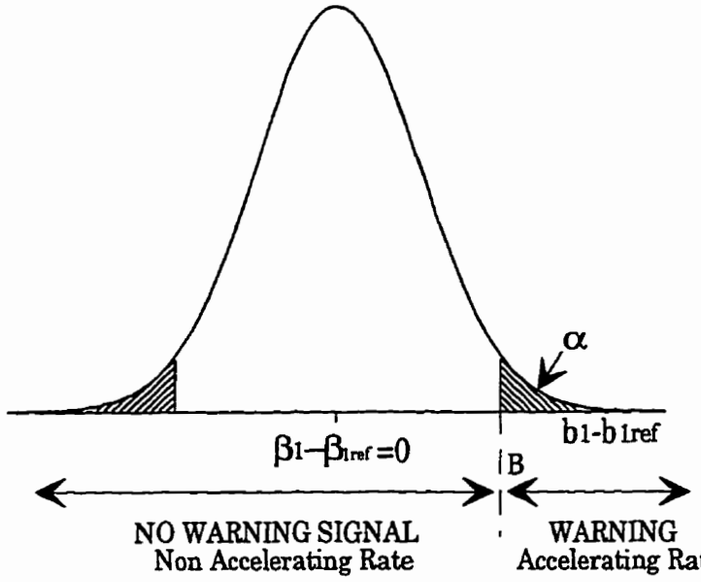

Figure 6.2 Probability of having a wrong warning signal (α)

For example from Table 6.1:

for probability of $\alpha = 0.05$ $t_\alpha = 1.645$

for probability of $\alpha = 0.010$ $t_\alpha = 1.28$

for probability of $\alpha = 0.20$ $t_\alpha = 0.85$

The risk of β, as has already been mentioned, is the probability of coming to a conclusion that there is not an abnormal evolution while an instability is starting. Indeed, it is the probability of finding the value of b_1-b_{1ref} to be less than B (Figure 6.3).

β = Prob. (failure in detection of an accelerating rate)

$$\beta = \text{Prob.}\left\{|b_1 - b_{1ref}| \langle B,\ \beta_1 - \beta_{1ref} \neq 0\right\} \qquad (6\text{-}8)$$

The value of β depends on the δ (changes in the rate of deformation or acceleration of deformation) which is shown by $\delta = |\beta_1 - \beta_{1ref}|$, the value of δ is unknown and the greater it is, the smaller β we have, with a constant δ the warning system (tendency test) will be more reliable when β is smaller.

β is related to B by (6-9):

$$\int_{t_\alpha}^{\infty} \frac{1}{\sqrt{2\pi}} e^{-x^2/2}\, dx = \alpha$$

t_α	.00	.01	.02	.03	.04	.05	.06	.07	.08	.09
0.0	.5000	.4960	.4920	.4880	.4840	.4801	.4761	.4721	.4681	.4641
0.1	.4602	.4562	.4522	.4483	.4443	.4404	.4364	.4325	.4286	.4247
0.2	.4207	.4163	.4129	.4090	.4052	.4013	.3974	.3936	.3897	.3859
0.3	.3821	.3783	.3745	.3707	.3669	.3632	.3594	.3557	.3520	.3483
0.4	.3446	.3409	.3372	.3336	.3300	.3264	.3228	.3192	.3156	.3121
0.5	.3085	.3050	.3015	.2981	.2946	.2912	.2877	.2843	.2810	.2776
0.6	.2743	.2709	.2676	.2643	.2611	.2578	.2546	.2514	.2483	.2451
0.7	.2420	.2389	.2358	.2327	.2296	.2266	.2236	.2206	.2177	.2148
0.8	.2119	.2090	.2061	.2033	.2005	.1977	.1949	.1922	.1894	.1867
0.9	.1841	.1814	.1788	.1762	.1736	.1711	.1685	.1660	.1635	.1611
1.0	.1587	.1562	.1539	.1515	.1492	.1469	.1446	.1423	.1401	.1379
1.1	.1357	.1335	.1314	.1292	.1271	.1251	.1230	.1210	.1190	.1170
1.2	.1151	.1131	.1112	.1093	.1075	.1056	.1038	.1020	.1003	.0985
1.3	.0968	.0951	.0934	.0918	.0901	.0885	.0869	.0853	.0838	.0823
1.4	.0808	.0793	.0778	.0764	.0749	.0735	.0721	.0708	.694	.0681
1.5	.0668	.0655	.0643	.0630	.0618	.0606	.0594	.0582	.0571	.0559
1.6	.0548	.0537	.0526	.0516	.0505	.0495	.0485	.0475	.0465	.0455
1.7	.0446	.0436	.0427	.0418	.0409	.0401	.0392	.0384	.0375	.0367
1.8	.0359	.0351	.0344	.0336	.0329	.0322	.0314	.0307	.0301	.0294
1.9	.0287	.0281	.0274	.0268	.0262	.0256	.0250	.0244	.0239	.0233
2.0	.0228	.0222	.0217	.0212	.0207	.0202	.0197	.0192	.0188	.0183
2.1	.0179	.0174	.0170	.0166	.0162	.0158	.0154	.0150	.0146	.0143
2.2	.0139	.0136	.0132	.0129	.0125	.0122	.0119	.0116	.0113	.0110
2.3	.0107	.0104	.0102	.00900	.00964	.00939	.00914	.00889	.00866	.00842
2.4	.00820	.00798	.00776	.00755	.00734	.00714	.00695	.00676	.00657	.00639
2.5	.00621	.00604	.00587	.00570	.00554	.00539	.00523	.00508	.00494	.00480
2.6	.00466	.00453	.00440	.00427	.00415	.00402	.00391	.00379	.00368	.00357
2.7	.00347	.00336	.00326	.00317	.00307	.00298	.00289	.00280	.00272	.00264
2.8	.00256	.00248	.00240	.00233	.00226	.00219	.00212	.00205	.00199	.00193
2.9	.00187	.00181	.00175	.00169	.00164	.00159	.00154	.00149	.00144	.00139

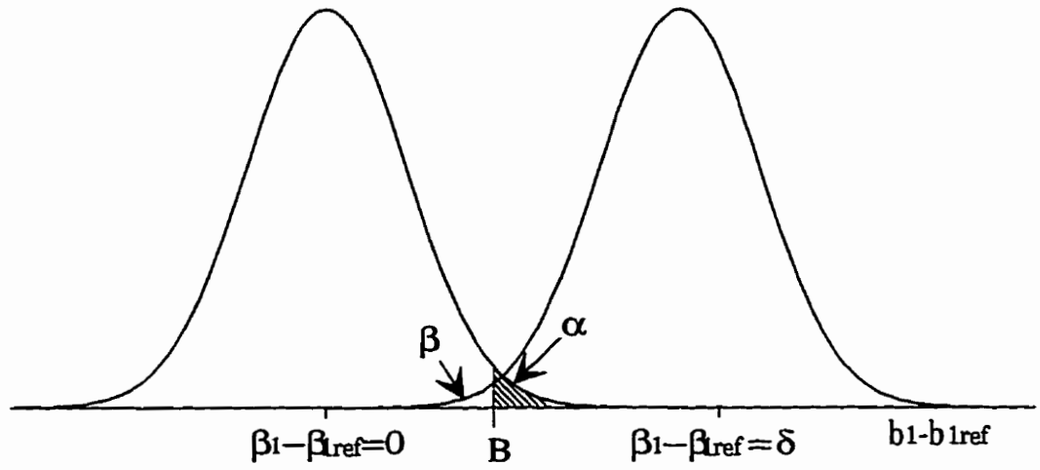

Figure 6.3 Probability of failure in detection of an accelerating rate (β)

$$t_\beta = \frac{B-\delta}{\sigma_R\sqrt{\frac{24}{M\left(M^2-1\right)}}} \tag{6-9}$$

with:

$$\beta = \text{Prob.}\left\{E(0,1) \rangle t_\beta\right\} \tag{6-10}$$

by showing B in terms of α:

we obtain:

$$t_\beta = \frac{t_\alpha \cdot \sigma_R\sqrt{\frac{24}{M(M^2-1)}} - \delta}{\sigma_R\sqrt{\frac{24}{M(M^2-1)}}} = t_\alpha - \frac{\delta}{\sigma_R\sqrt{\frac{24}{M(M^2-1)}}} \tag{6-11}$$

By choosing an accepted risk of α and using this formula one can calculate the value of β (risk of concluding that there is normal behavior in rock mass deformation's regime while an anomalous rate is beginning). In other words, we can calculate the minimum detectable value of the tendency test with a good probability.

For showing the relationship between δ and σ_R (readings deviation) we will take the value of δ as a reference such that the average deviation of readings in the end of a period will be equal to

the standard deviation of the readings. Since the average deviation of readings is in the form of $(\beta_1-\beta_{1ref})\times I$ in each instant of the control period, one can conclude that at the end of the control period T, the average deviation is equal to $(\beta_1-\beta_{1ref})\times M$ where:

$$\delta_{ref}=\frac{\sigma_R}{M} \tag{6-12}$$

δ or the difference between two tendencies, can be shown in terms of σ_R, M and a new parameter which is represented by Q:

$$\delta=\frac{\delta_{ref}}{Q}=\frac{\sigma_R}{Q\times M} \tag{6-13}$$

in other words:

$$Q=\frac{\text{Standard Deviation of Measurments}(\sigma_R)}{\text{Deformation Rates Deviation}\left(\frac{\delta}{\Delta t}\right)\times\text{Duration of Period}(M\Delta t)} \tag{6-14}$$

With Q = 1 we will have a deviation at the end of the control period equal to σ_R (Figure 6.4), and with Q = 0.5, the deviation will be equal to $2\sigma_R$. In other words we have a non negligible chance of having a reading which is separated from the zone of readings during the reference period. In these conditions t_β can be shown as follows:

$$t_\beta=t_\alpha-\frac{\frac{\sigma_R}{QM}}{\sigma_R\sqrt{\frac{24}{M\left(M^2-1\right)}}}=t_\alpha-\frac{1}{Q}\sqrt{\frac{M^2-1}{24M}} \tag{6-15}$$

where:

$$Q=\frac{1}{t_\alpha-t_\beta}\sqrt{\frac{M^2-1}{24M}} \tag{6-16}$$

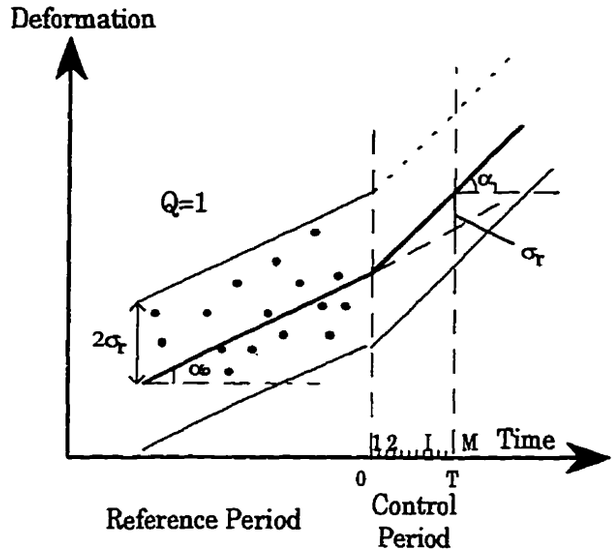

Figure 6.4 Deviation of measurements (Q=1)

So, it is possible to calculate the reliability of the warning system or the detectable tendency difference (δ), related to σ_R (readings deviation) in terms of α (risk of having a wrong warning), and M (number of readings), with a specified β (risk of failure in instability detection). Table 6.2 gives the values of Q in terms of M for the different values of α and β; and these values are brought on the Figure 6.5, 6.6 and 6.7.

6.4 Interchange effects of the parameters of model

- By decreasing α, the reliability of system in the process of making decision on the stability state of structure decreases, for example with α=0.20, our warning system is able to detect a tendency difference (slope test result) which is equal to $3.45\times\sigma_R$,when β=0.01 (one chance per 100 of failing in anomaly detection) and this means Q = 0.29. While with α=0.1 the detectable value of strain acceleration increases to $4\times\sigma_R$, and it will be $4.35\times\sigma_R$ when α=0.05 and in this case Q=0.23.

Table 6.2 The values of Q in terms of M, α and β

		$\alpha = 0.05$ $t_\alpha = 1.645$			$\alpha = 0.10$ $t_\alpha = 1.285$			$\alpha = 0.2$ $t_\alpha = 0.85$			
M	$\sqrt{\frac{M^2-1}{24M}}$	**β= 0.10 t_β= -1.280**	**β=0.01 t_β= -2.330**	**β= 0.05 t_β= -1.645**	**β= 0.1 t_β= -1.280**	**β= 0.05 t_β= -1.645**	**β= 0.01 t_β= -2.330**	**M**	**β= 0.1**	**β= 0.05**	**β= 0.01**
4	0.40	0.14	0.10	0.12	0.15	0.14	0.11	**4**	0.19	0.16	0.12
8	0.57	0.20	0.14	0.17	0.22	0.20	0.16	**8**	0.27	0.23	0.18
12	0.70	0.24	0.18	0.21	0.28	0.24	0.20	**12**	0.33	0.28	0.22
15	0.81	0.28	0.21	0.25	0.32	0.28	0.23	**16**	0.38	0.33	0.26
20	0.91	0.31	0.23	0.28	0.36	0.31	0.25	**20**	0.43	0.37	0.29
24	1.00	0.34	0.25	0.30	0.39	0.34	0.28	**24**	0.47	0.40	0.31
28	1.08	0.37	0.27	0.33	0.42	0.37	0.30	**28**	0.51	0.43	0.34
32	1.15	0.39	0.29	0.35	0.45	0.39	0.32	**32**	0.54	0.46	0.36
50	1.44	0.49	0.36	0.44	0.56	0.49	0.40	**50**	0.68	0.58	0.45
100	2.04	0.70	0.51	0.62	0.80	0.70	0.57	**100**	0.96	0.82	0.64
150	2.50	0.85	0.63	0.76	0.98	0.85	0.69	**150**	1.17	1.00	0.79

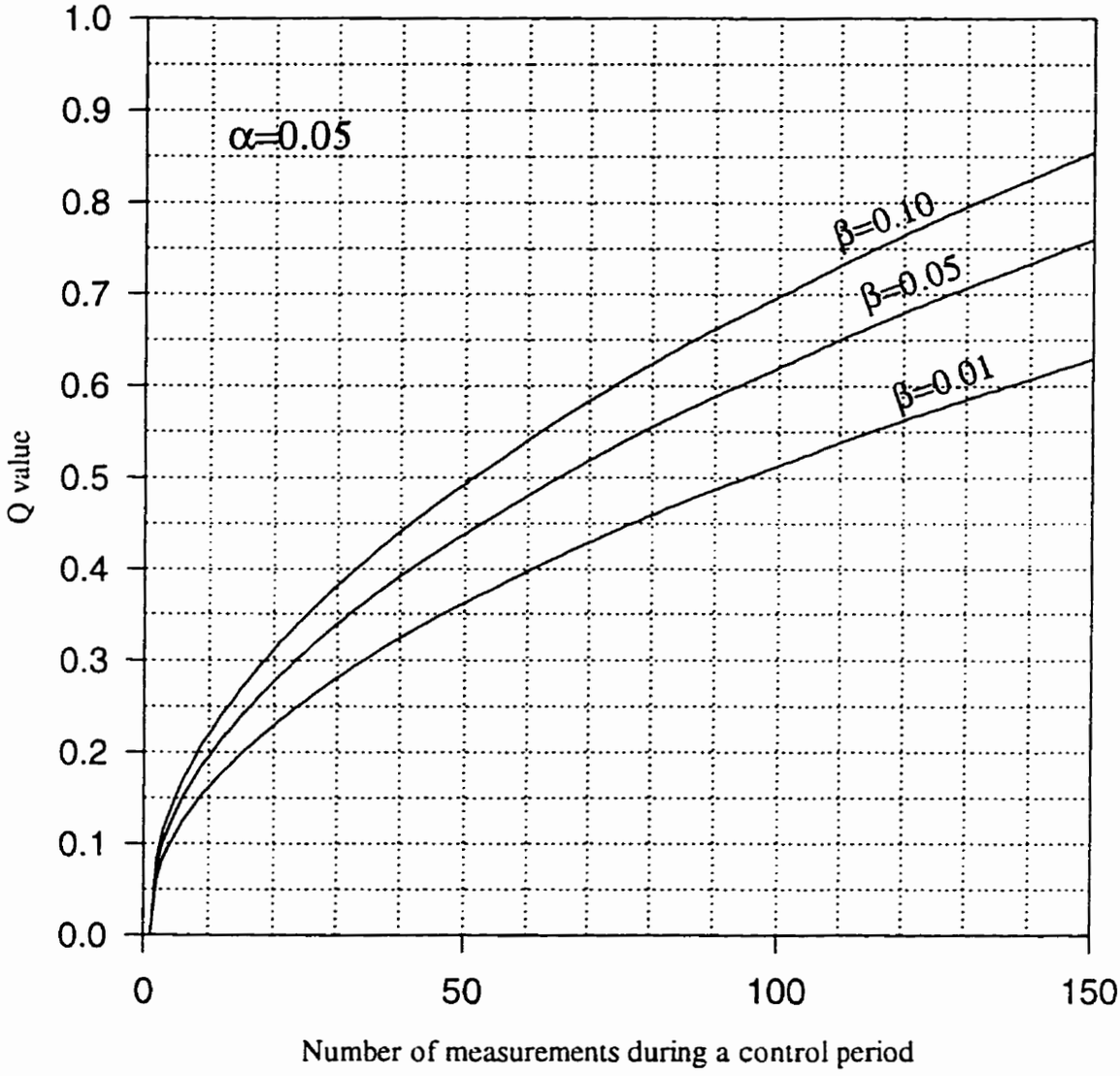

Figure 6.5 The detectable value of Q in terms of the risks α and β and the number of readings during the control periods (α=0.05)

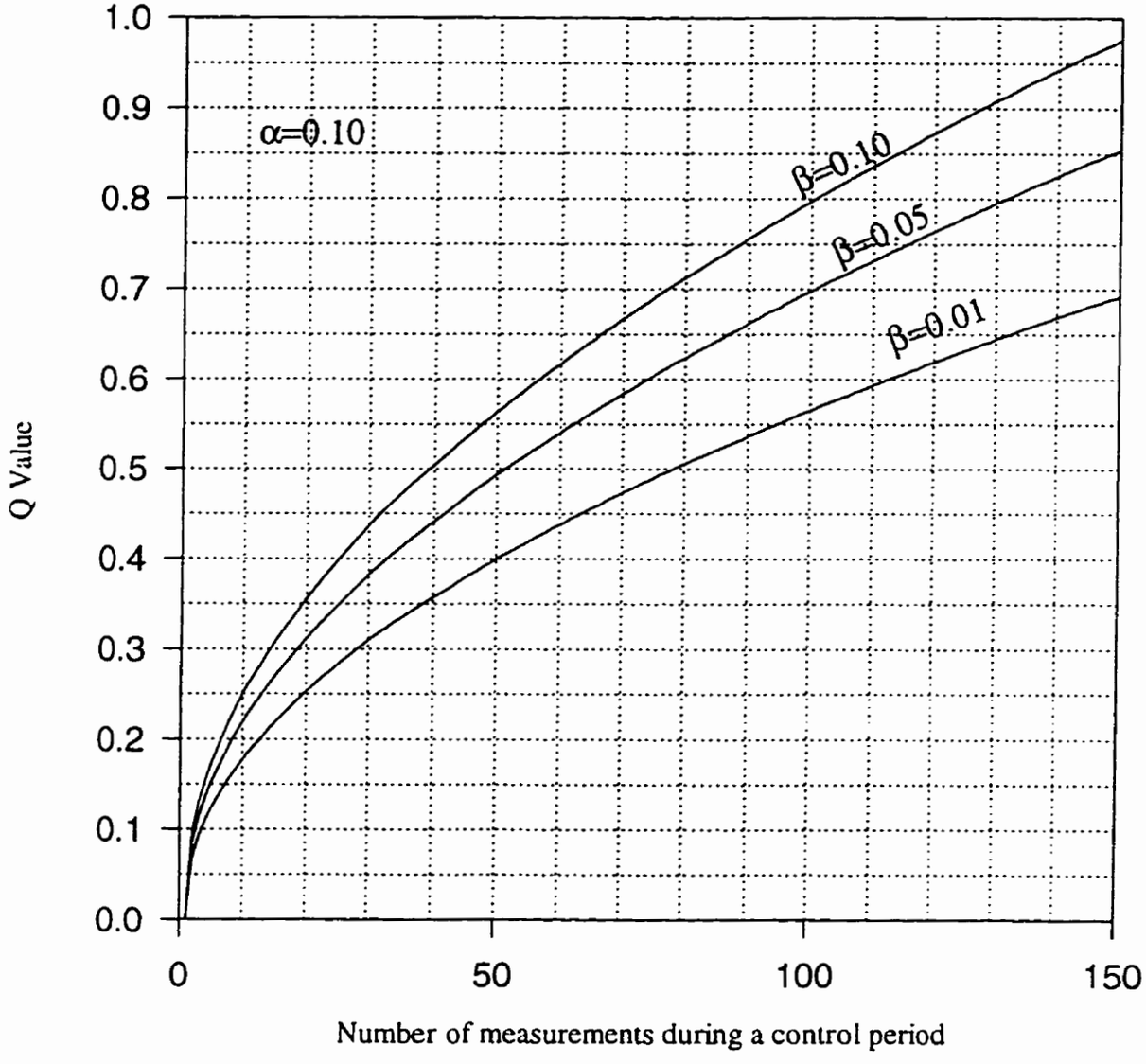

Figure 6.6 The detectable value of Q in terms of the risks α and β and the number of readings during the control periods (α=0.1)

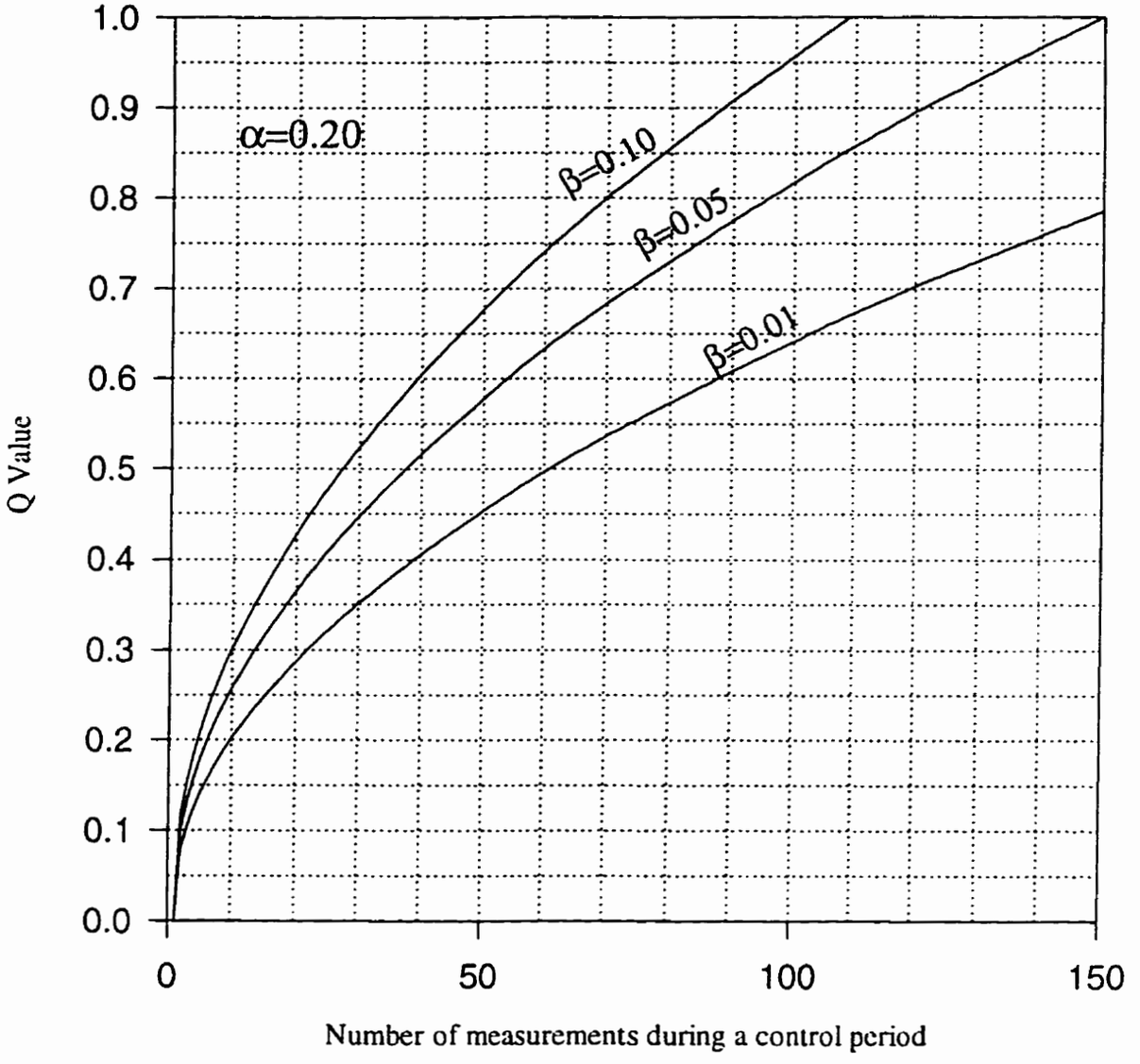

Figure 6.7 The detectable value of Q in terms of the risks α and β and the number of readings during the control periods (α=0.2)

- M; by increasing M, the expression of Q tends to $K\sqrt{M}$, in which K is expressed in terms of α and β, so it is possible to have a desired reliability in our monitoring system with the specified values for α, β and M, when M increases the value of Q changes in the form of $\sqrt{M}$, so to double the monitoring reliability, it is necessary to multiply M by 4.

It is possible to increase M in the two following ways:

1- by lengthening the control period and comparing the tendencies at the end of each period. By this way, the test is repeated less often before hand. One should recall the fact that, the repetition of the test is determined by the time between the start of the abnormal rate in rock mass and its collapse.

2- by increasing the number of readings during the control periods. Figure 6.8 shows the variation of the detectable anomaly (stain rate's change over time) in terms of α and M for $\beta = 0.01$ and $\beta=0.005$.

6.5 Probabilistic analysis of a series of sensors

Considering a system in which N sensors monitor the strain's rates in an underground structure such a system may be programmed to trigger the warning signals if at least r sensors among N detect an anomaly in the rate of deformation which has been continuing during a relatively long period of time.

For being able to evaluate the associated risks of α and β in such a system, we introduce two risks of $\alpha(n)$ and $\beta(n)$ as follows:

- $\alpha(n)$: the risk of having a wrong warning with N sensors
- $\beta(n)$: the risk of failure in instability detection with N sensors

We show that the new risks are associated to α and β, (associated risks of the decision making process in a system with only one sensor).

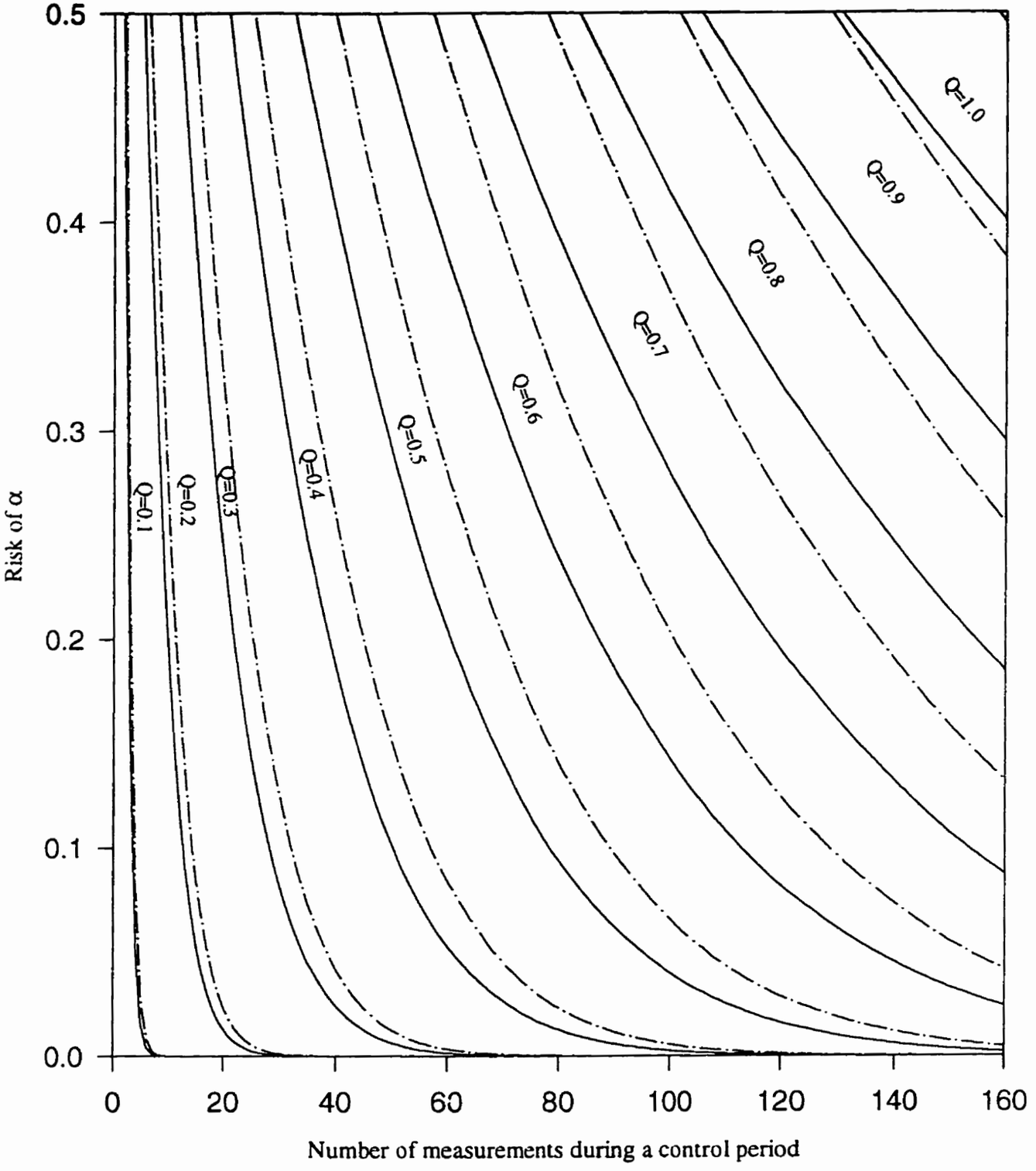

Figure 6.8 The detectable acceleration in terms of the risks α, β, and Q and the number of readings during the control periods (β=0.01, full line), (β=0.005, dotted line)

Considering a control period, at the end of which, the monitoring system performs the slope test for the total of N sensors among which K sensors have been detecting an abnormal rate, by supposing that the data in all the sensors are read at the same time and whose deviation are equal to σ_R. Regarding the tendency test (β_1-β_{1ref}), one can accept the value of (b_1-b_{1ref}) for each sensor as a sampling random value. So one can derive the risks of α and β for N sensors as follows.

6.5.1 Derivation of the risks of α and β for N Sensors

- (α_n) risk of having a wrong warning with N sensors

When there is no anomaly ($\delta = \beta_1 - \beta_{1ref} = 0$), each sensor may show an abnormal rate of deformation with a risk which is equal to $\alpha(1)$. In the case of N sensors, the number of sensors which may show an anomaly can be represented by a binomial random model which is defined by N and $\alpha(1)$.

$$k = B(N, \alpha(1)) \tag{6-17}$$

This allows one to calculate the probability of having a wrong warning with N sensors by using the following binomial random probability.

$$\alpha(n) = \text{Prob.}\{k \geq r\} \tag{6-18}$$

- (β_n) probability of failure in detection of an anomaly with N sensors

When there is an anomaly ($\delta = \beta_1 - \beta_{1ref} \neq 0$); each sensor has a risk equal to $\beta(1)$ to fail in detection of this anomaly. The number of sensors which do not show the starting of an abnormal deformation rate can be represented by a binomial random which is defined by N and $\beta(1)$.

$$N - k = B(N, \beta(1)) \qquad k = B(N, 1 - \beta(1)) \tag{6-19}$$

The warning system will not trigger the warning signals if k < r or N-k > N-r

$$\beta(n) = \text{Prob.}\{k(r\} = \text{Prob.}\{N-k)N-r\} \qquad (6\text{-}20)$$

Table 6.3 gives the values of $\alpha(n)$ and $\beta(n)$ for some usual values of α and β in terms of the sensors number (N). Looking at this table, one can understand the important role of the chosen value for r.

6.5.2 Value of r

It is clear that the lower the value of r is, the higher the value of α will be. Therefore for example, if we consider that such a system would include 3 sensors (N=3), and it is programmed to trigger the warning signals, if only one sensor shows an anomaly (r=1), in this case the risk of α (having wrong warning) is equal to 0.14, whereas when N=1 this risk is equal to 0.05.

The greater value of r, the less we can rely on the warning system. For example if we take the previous example (N = 3) and we choose to give r the equivalent of 3, then the risk of that the system, in detecting an anomaly (β) will exceed 3%. Whereas if N=1 the risk of system failure will not surpass 1%. One can clearly see on the Table 6.3 that the optimum value of r is almost always equal to N/2. In the previous example; if r=2; therefore we have $\alpha(n)$ equal to 0.07% and $\beta(n)$ = 0.003%.

Table 6.3 The probabilities of $\alpha(n)$ and $\beta(n)$

		$\alpha(n)$				$\beta(n)$			
N	r	20%	10%	5%	1%	10%	5%	1%	0.5%
2	1	36.000	19.000	9.750	1.990	1.000	0.250	0.010	0.002
	2	4.000	1.000	0.250	0.010	19.000	9.750	1.990	0.997
3	1	48.800	27.100	14.262	2.97	0.100	0.012	0.000	0.000
	2	10.400	2.800	0.725	0.030	2.800	0.725	0.030	0.007
	3	0.800	0.100	0.012	0.000	27.100	14.262	2.970	1.493
4	1	59.040	34.390	18.549	3.940	0.010	0.001	0.000	0.000
	2	18.080	5.230	1.402	0.059	0.370	0.048	0.000	0.000
	3	2.720	0.370	0.048	0.000	5.230	1.402	0.059	0.015
	4	0.160	0.010	0.001	0.000	34.390	18.549	3.940	1.985
5	1	67.232	40.951	22.622	4.901	0.001	0.000	0.000	0.000
	2	26.272	8.146	2.259	0.098	0.046	0.003	0.000	0.000
	3	5.792	0.856	0.116	0.001	0.856	0.116	0.001	0.000
	4	0.672	0.046	0.003	0.000	8.146	2.259	0.098	0.025
	5	0.032	0.001	0.000	0.000	40.951	22.622	4.901	2.475
6	1	73.786	46.856	26.491	5.852	0.000	0.000	0.000	0.000
	2	34.464	11.426	3.277	0.146	0.005	0.000	0.000	0.000
	3	9.888	1.585	0.223	0.002	0.127	0.009	0.000	0.000
	4	1.696	0.127	0.009	0.000	1.585	0.223	0.002	0.000
	5	0.160	0.005	0.000	0.000	11.426	3.277	0.146	0.037
	6	0.006	0.000	0.000	0.000	46.856	26.491	5.852	2.963
7	1	79.028	52.170	30.166	6.793	0.000	0.000	0.000	0.000
	2	42.328	14.969	4.438	0.203	0.001	0.000	0.000	0.000
	3	14.803	2.569	0.376	0.003	0.018	0.001	0.000	0.000
	4	3.334	0.273	0.019	0.000	0.273	0.019	0.000	0.000
	5	0.467	0.018	0.001	0.000	2.569	0.376	0.003	0.000
	6	0.037	0.001	0.000	0.000	14.969	4.438	0.203	0.052
	7	0.001	0.000	0.000	0.000	52.170	30.166	6.793	3.448
8	1	83.223	56.953	33.658	7.726	0.000	0.000	0.000	0.000
	2	49.668	18.690	5.724	0.269	0.000	0.000	0.000	0.000
	3	20.308	3.809	0.579	0.005	0.002	0.000	0.000	0.000
	4	5.628	0.502	0.037	0.000	0.043	0.002	0.000	0.000
	5	1.041	0.043	0.002	0.000	0.502	0.037	0.000	0.000
	6	0.123	0.002	0.000	0.000	3.809	0.579	0.005	0.001
	7	0.008	0.000	0.000	0.000	18.690	5.724	0.269	0.069
	8	0.000	0.000	0.000	0.000	56.953	33.658	7.726	3.931
9	1	86.578	61.258	36.975	8.648	0.000	0.000	0.000	0.000
	2	56.379	22.516	7.121	0.344	0.000	0.000	0.000	0.000
	3	26.180	5.297	0.836	0.008	0.000	0.000	0.000	0.000
	4	8.564	0.833	0.064	0.000	0.006	0.000	0.000	0.000
	5	1.958	0.089	0.003	0.000	0.089	0.003	0.000	0.000
	6	0.307	0.006	0.000	0.000	0.833	0.064	0.000	0.000
	7	0.031	0.000	0.000	0.000	5.297	0.836	0.008	0.001
	8	0.002	0.000	0.000	0.000	22.516	7.121	0.344	0.088
	9	0.000	0.000	0.000	0.000	61.258	36.975	8.648	4.411
10	1	89.263	65.132	40.126	9.562	0.000	0.000	0.000	0.000
	2	62.419	26.390	8.614	0.427	0.000	0.000	0.000	0.000
	3	32.220	7.019	1.150	0.011	0.000	0.000	0.000	0.000
	4	12.087	1.280	0.103	0.000	0.001	0.000	0.000	0.000
	5	3.279	0.163	0.006	0.000	0.015	0.000	0.000	0.000
	6	0.637	0.015	0.000	0.000	0.163	0.000	0.000	0.000
	7	0.086	0.001	0.000	0.000	1.280	0.006	0.000	0.000
	8	0.008	0.000	0.000	0.000	7.019	0.103	0.011	0.000
	9	0.000	0.000	0.000	0.000	26.390	1.150	0.427	0.001
	10	0.000	0.000	0.000	0.000				

6.6 Punctual warning

In this probabilistic model, and according to the second way of programming in the gradient method we may judge the stability state of a in situ rock mass after each reading, so it is not necessary to wait until the end of the control period. As soon as the control period starts, the system may be programmed to trigger the warning signals when it detects the beginning of an instability in a monitored zone by finding the readings which are not in the confidence interval, specified by the previous periods (reference period) (Figure 6.9).

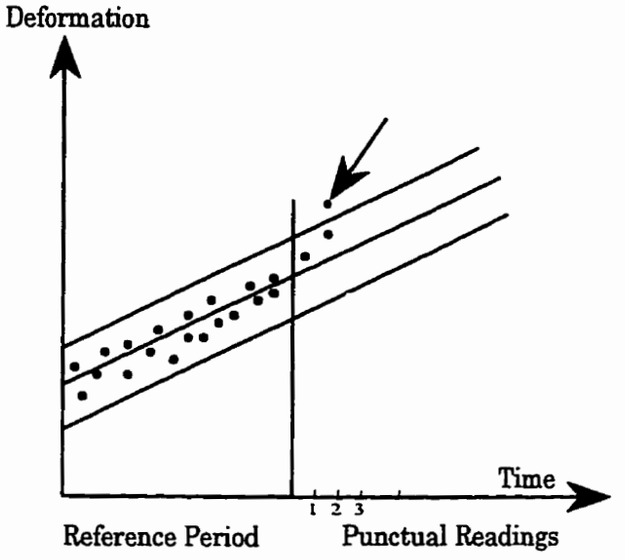

Figure 6.9 Warning signal triggering by the punctual test of readings

Considering the p^{th} reading in a control period in which P< M, P >3, an analogical reasoning can express the reliability of the slope test at that time (t_p), with the following expression.

$$t_\alpha - t_\beta = \frac{1}{Q}\sqrt{\frac{M^2-1}{12M}+\frac{P^2-1}{12P}} \qquad (6\text{-}21)$$

Since P < M the slope test at t_p is less reliable than at the end of period (t_m). This means that with a constant risk of α, the risk of β in punctual test is greater than that of in the slope test.

Since the duration of the control period is chosen so that it would be much shorter than the one during which the instability starts and terminates with the collapse of structure and having considered the fact that a destructive evolution in a rocky medium is a continuos phenomenon which is partially detected in a control period, one can conclude that the punctual test may not be considered as a powerful test in the gradient hypothesis. However it can be applied as the detection method for the sudden changes in the deformation rates in the structure. For this application it is necessary to compare the values of Y_i (read value of deformation) to the extrapolated value of the confidence interval of the reference period (predicted value of deformation).

If the predicted value for the I^{th} reading would be $\hat{Y}_i$, the dispersion of this value can be estimated using the previous model (Figure 6.10). One can understand that the observation for Y_i is distributed around a line which is characterized by β_0 and β_1 according to (6-22).

$$Y_i = E(\beta_1 + \beta_0 \times I, \sigma_R) \qquad (6\text{-}22)$$

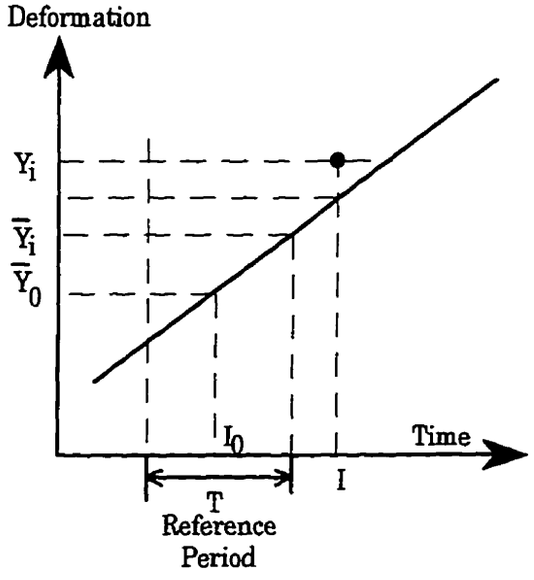

Figure 6.10 Deviation of punctual reading

We can calculate the difference between the observation of deformation Y_i and its predicted value which is defined by a regression line $\hat{Y}_i = b_1 I + b_0$. Since b_0 and b_1 are the estimation of the real values of β_0 and β_1, the value of $\hat{Y}_i$ will be a random one.

If we consider $\hat{Y}_0$ and I_0 as the coordinates of the median in the reference period (previous periods).

we have : $b_0 = \hat{Y}_0 - b_1 I_0$

$$\hat{Y}_i = b_1 I + b_0 = b_1 (I-I_0) + \hat{Y}_0 \qquad (6\text{-}23)$$

So $\hat{Y}_i$ is a Gaussian random, whose average and whose variance can be defined as follows:

$$E(\hat{Y}_i) = I\, E(b_1) + E(b_0) = \beta_1 I + \beta_0 \qquad (6\text{-}24)$$

$$VAR\left(\hat{Y}_i\right) = (I - I_0)^2 \times VAR(b_1) + VAR\left(\hat{Y}_0\right) \text{ so;}$$

$$VAR\left(\hat{Y}_i\right) = \frac{(I - I_0)^2 \times \sigma_R^2}{\sum (I - I_0)^2} + \frac{\sigma_R^2}{M} \qquad (6\text{-}25)$$

Where:
T is the previous control period

M is the number of readings in the period (T)

Considering i^{th} reading as the last reading in the (T, previous control period)

$$I - I_0 = i + \frac{M-1}{2} \qquad (6\text{-}26)$$

and $$\sum (I - I_0)^2 = \frac{M\left(M^2 - 1\right)}{12} \qquad (6\text{-}27)$$

So:

$$VAR\left(\hat{Y}_i\right) = \sigma_R^2 \left[\frac{\left(\frac{M-1}{2} + i\right)^2}{\frac{M(M^2-1)}{12}} + \frac{1}{M} \right] \qquad (6\text{-}28)$$

$$= \sigma_R^2 \left[\frac{3(M - 1 + 2i)^2 + M^2 - 1}{M(M^2 - 1)} \right]$$

Now we can have a probability law for Yi- $\hat{Y}_i$ in which the punctual test will be carried out.

Since $Y_i - \hat{Y}_i$ is a Gaussian random with an average equal to zero and whose variance is calculated by the following relation:

$$VAR\left(Yi - \hat{Y}_i\right) = \sigma_R^2 + \sigma_R^2\left[\frac{3(M-1+2i)^2 + M^2 - 1}{M\left(M^2-1\right)}\right] \qquad (6\text{-}29)$$

With the same risk for wrong warning (α) we reach the conclusion that, there is no anomaly in the rate of deformation if:

$$\frac{Yi - \hat{Y}_i}{\sigma_i} < t_\alpha$$

$$\sigma_i = \sqrt{VAR\left(Yi - \hat{Y}_i\right)} \qquad (6\text{-}30)$$

$$= \sigma_R \sqrt{\frac{3(M-1+2i)^2 + (M+1)\left(M^2-1\right)}{M\left(M^2-1\right)}}$$

The risk of α in this test will be the same as that in the slope test which is done at the end of period. So the threshold t_α will be unchanged.

Now for evaluation of this test we will consider B as a threshold above which there will be a detectable sudden change in the rate of deformation.

$B = Yi - \hat{Y}_i$ where $\qquad t_\alpha = \frac{B}{\sigma_i}$ (6-31)

with β risk of failure in instability detection and δ (minimum threshold) we have:

$$t_\beta = \frac{-\delta + B}{\sigma_i} \qquad (6\text{-}32)$$

So we will have: $\qquad t_\alpha - t_\beta = \frac{\delta}{\sigma_i}$ (6-33)

with the same value of α and β as in slope test we can have (Eq. 6.16):

$$\frac{1}{Q}\sqrt{\frac{M^2-1}{24M}}=\frac{\delta}{\sigma_i} \qquad (6\text{-}34)$$

We define $\frac{1}{Q}=\frac{\Delta}{\sigma_R}$ where Δ is the deviation of readings related to an accelerating rate in deformation, characterized by Q. The punctual test will have the same efficiency, If we can have $\delta=\Delta$ while $i = M$.

So we have:

$$\frac{\Delta}{\sigma_R}\sqrt{\frac{M^2-1}{24M}}=\frac{\delta}{\sigma_R\sqrt{\frac{3(M-1+2i)^2+(M+1)(M^2-1)}{M(M^2-1)}}}$$

So : (6-35)

$$\frac{\delta}{\Delta}=\sqrt{\frac{3(M-1+2i)^2+(M+1)(M^2-1)}{24M^2}}$$

Comparing this quantity to i /M, and having supposed an efficiency equal to that of the slope test, we are able to detect a deviation equal to δ in the i^{th} reading in the form of $\frac{i\Delta}{M}$.

So we can compare the value of (6-36) and (6-37):

$$\frac{3(M-1+2i)^2+(M+1)(M^2-1)}{24M^2} \qquad (6\text{-}36)$$

$$\frac{i^2}{M^2} \qquad (6\text{-}37)$$

Expression of (6-36) is always positive and monotonous when $M > 1$, $i \leq M$ and $M \geq 3$ what is the minimum number of readings for being able to realize the slope test.

Having the same threshold t_α for punctual testing we must verify after each reading the following inequality:

$$\frac{Yi - \hat{Y}_i}{\sigma_R \sqrt{\frac{3(M-1+2i)^2 + (M+1)(M^2-1)}{M(M^2-1)}}} \leq t_\alpha \qquad (6\text{-}38)$$

Generally speaking, the punctual test is less reliable than the slope test. However, it can be applied for a system programming which may detect the violent changes in the evolution of rock mass deformation, but for detection of an accelerated movement, the slope test is more reliable.

6.7 Principles of application

So far the algorithm of an instability preventive model which can be applied in programming a rock failure warning system has been elaborated and two associated risks in making a decision for tripping the warning signals have been defined and determined. It is essential that we know three important parameters for being able to program a warning system upon the gradient method.
These are Q, α and β.
Where:

$$Q = \frac{\text{readings standard deviation}}{\text{deviation of deformation rate to be detected} \times \text{time left between two readings}}$$

With the help of the previous analyses and for a chosen rate of acquisition we can determine the total number of sensors required for a zone and the number of sensors which must detect an anomaly for triggering the warning signals.
Knowing the essential parameters we have a simple procedure to calculate the required parameters.

The known parameters:
σ_R : standard deviation of measurements

δ_v : deviation of deformation rate to be detected

T : maximum delay for detection of an anomaly in the deformation's regime (duration of the control period)

Δ_t : minimum time between two readings

α : accepted risk for having a wrong warning

β : accepted risk of failure in anomaly detection

we are able to calculate the values of M and Q as follows:

$$M = \frac{T}{\Delta_t}$$

$$Q = \frac{\sigma_R}{\delta_v \times T}$$

$$\tau = \frac{1}{Q}\sqrt{\frac{M^2 - 1}{24M}} \qquad (6\text{-}39)$$

According to the previous calculations, if the accepted risks of α and β have been chosen so that the value of t_α-t_β fulfills (6-40), monitoring can be theoretically realized by a single sensor. So we can conclude that there is an anomaly in the deformation's regime if the difference between the deformation's rates during two consecutive control periods are equal to or greater than RD which is calculated by the following relation:

$$t_\alpha - t_\beta \leq \tau \qquad (6\text{-}40)$$

$$RD = t_\alpha \times \sigma_R \times \sqrt{\frac{24}{M(M^2 - 1)}} \qquad (6\text{-}41)$$

If τ is much greater than the value of (t_α-t_β) we can reduce the number of readings during each control period, according to the following relation.

$$t_\alpha - t_\beta = \frac{1}{Q}\sqrt{\frac{M^2 - 1}{24M}} \qquad (6\text{-}42)$$

and then;

$$M = 12(t_\alpha - t_\beta)^2 Q^2 + \sqrt{(t_\alpha - t_\beta)^4 \times 144 + 1} \qquad (6\text{-}43)$$

Figure 6.11 shows the changes of t_α and t_β in terms of α and β.

For example, considering the following parameters which are used for programming a monitoring system in a zone:

N=8

M = 400

Q = 1

$\alpha = 0.1$, t_α=1.28

$\beta = 0.01$, t_β= -2.33

$t_\alpha - t_\beta$=3.61

we obtain: $\tau = 4.08$

Since the value of $t_\alpha - t_\beta$ is less than τ the monitoring of the zone can be theoretically done by a single sensor. So the number of readings in each period may even be reduced according to the (6-43), and be equal to 313 readings per period, so the system will warn us if the result of the slope test (deformation rates difference) is greater than t_α=1.28.

Having selected r=4 (number of sensors which must show an anomaly) we have $t_\alpha = 0.70$ and $\alpha(1)$ = 24.2 %.

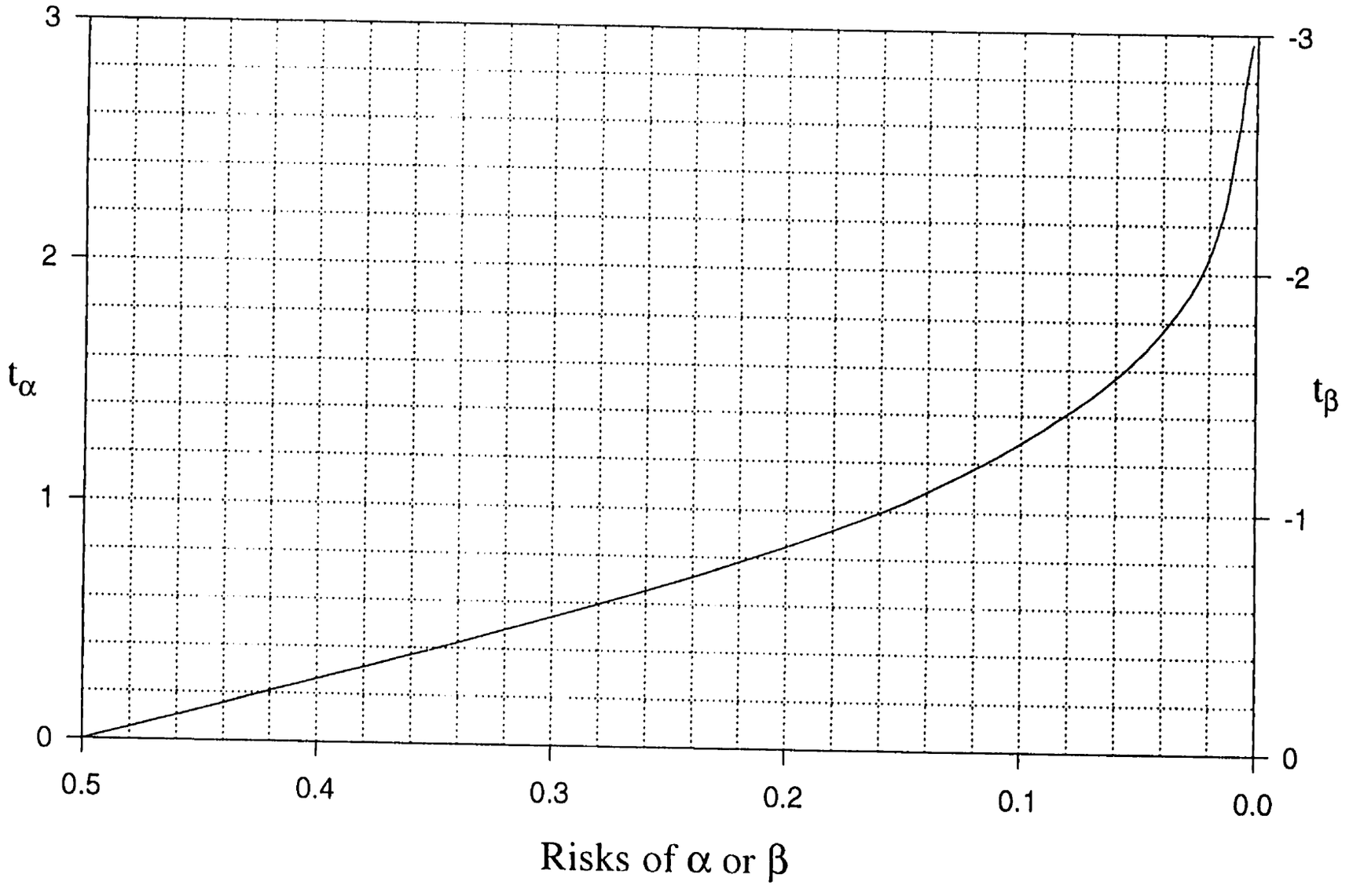

Figure 6.11 the values of tα and tβ in terms of the risks α and β

6.8 Problem of defective sensors

Among several sensors which are monitoring a site, it must be expected that a number of sensors send incorrect data or do not send any signals. In these conditions the system must decide how the data from the other sensors is interpreted. Keeping the same reliability in the monitoring system, the value of β is held constant even with the defective sensors. For reaching this objective and keeping M and Q constant, the value of α (wrong warning) must be modified.

6.8.1 Analysis of the accepted risks of α and β with the defective sensors

Two types of defect in the sensors may occur in a monitoring system. In the first type the defective sensors do not send the signals but in the second type they send incorrect data.

A probabilistic analysis of these two defects is carried out with the previous example which contains 8 sensors for monitoring the stability of an in situ rock mass.

In the first type, if one sensor among 8 becomes defective, the acquisition system receives the data from only 7 sensors. So one can consider two choices for triggering the warning signals.

1- the warnings are triggered when 3 sensors show an anomaly in the strain's rate of structure

2- the warnings are triggered when 4 sensors show an anomaly in the strain's rate of structure

With the first choice (N=7, r=3) when $\alpha(n) = 0.01$ (risk =10%), Table 6.4 gives $-t_\beta(1)=0.71$ or $\beta(1) = 23.6\%$.

Keeping the initial values of M and Q constant, we must have $t_\alpha - t_\beta = 1.61$, and we obtain $t_\alpha(1)=1.61-0.71=0.90$, this gives $\alpha(1)=18.4\%$, r =3 so $\alpha(n)=0.12$ what is approximately equal to the initial value (10%).

With the second choice (N=7, r =4) we have $-t_\beta(1) = -1.07$, that leads to $t_\alpha(1)=1.61-1.07=0.54$, so $\alpha(1) = 29.5\%$, and $\alpha(n)=0.12$ either.

It can be seen that our system has nearly the same reliability level, in spite of loosing one sensor, but it is necessary to modify the applied criteria for each sensor. This modification will give us a threshold t_α =0.54 with N=7, while t_α =0.7 with N=8.

In the second type in which we receive incorrect data, there are two conditions. In the first condition a series of sensors show constantly an anomaly, while in the second condition the defective sensors can never show the abnormal evolution deformation.

- In the first condition, with N installed sensors, in fact our zone is monitored with N-1 sensors the monitoring system will warn us when the r-1 sensors show an anomaly.
Here we choose α' for expressing the risk of having an unjustified warning and it is shown as follows:

$$\alpha' = \text{Prob.}\{K \geq r-1\} \qquad (6\text{-}44)$$

where K is a binomial random variable, defined by $\alpha(1)$, (initial accepted risk), and N-1 in the following form:

$$K = B(N-1, \alpha(1)) \qquad (6\text{-}45)$$

Again with our example (N=8, r=4) we obtain $\alpha(1)$=24.2 %. The risk of α' is equal to $\text{Prob.}\{K \geq 3\}$ where $K = B(7, 24.2)$, and we find α'=22.3%, while in the normal conditions this probability is equal to $\alpha = 10\%$.
The risk of failure in anomaly detection is expressed by β' in the following form:

$$\beta' = \text{Prob.}\{K\langle r-1\} \qquad (6\text{-}46)$$

where K is the binomial random variable, defined by $\beta(1)$ (initial accepted risk) and N-1:

$$K = B(N-1, 1-\beta(1)) \qquad (6\text{-}47)$$

Applyin in our example, - $t_\beta(1)$ = 0.81 (1.61-0.70) where $\beta(1)$ = 0.21. So the probability of β' is equal to 0.006, what is less than the initial value of β = 0.01.

- In the second case the defective sensors can never show the anomalies in the rates of deformation. In fact in this condition the monitoring is carried out by N-1 sensors, but we only receive a warning when the r sensors show an instability.

The risk of having a wrong warning is expressed by α'' and is shown by the following relation:

$$\alpha'' = \text{Prob.}\{K \geq r\} \tag{6-48}$$

$$K = B(N-1, \alpha(1)) \tag{6-49}$$

For the previous example (N= 8, r = 4) we obtain:

α'' =6.2%, what is less than the initial accepted risk α =10 %.

The risk of β is expressed by β'', and is shown by:

$$\beta'' = \text{Prob.}\{k<r\} \tag{6-50}$$

$$K = B(N-1, 1-\beta(1)) \tag{6-51}$$

So β'' = 3.9 %, what is greater than the initial accepted risk β= 1%.

This example shows that the effect of incorrect data on the reliability of system is considerable, but this negative effect is not so disastrous if there are enough installed sensors in the monitored zone.

6.9 Conclusion

Regarding the developed model based on the gradient method, there are several important points which must be considered as follows:

- the statistical analyses in the model are developed assuming the homogeneity of sensors which measure the variations of deformation or other measurable variables (stress,...). This homogeneity supposes same variation in the measurements of all sensors and also simultaneity of reading by

acquisition system. In the case of CIUS, the vibrating wires are read by the acquisition system simultaneously, but the recorded data do not give the same variation of measurements. Therefore, a statistical analysis may be carried out in order to evaluate the effect of non homogeneity on the precision of the model.

- realization of a reliable stability monitoring using this model depends mostly on the number of sensors in a considered zone and on the frequency of reading during the control period. Moreover, considering all the described parameters which affect the precision of the decision making process of the model (defective sensors, erroneous data,...) and also the fact that stability in underground mining stope or pillar or any other excavation may not be monitored with a high degree of certitude when the monitoring is carried out for example by one or two sensors or CIUS. Therefore, this fact, must be considered in the selection of the instrument which is supposed to be used at mines. It must be possible economically and technically to install several of these such instruments at a mine. This problem may also be solved by using recoverable instruments.

- It must be mentioned that this model can guarantee the detection of an anomaly in deformation or other variables (stress,...) which are real and significant of movements. The conformity of this anomaly to the failure of structure is an experimental fact which may be verified in different cases, but its risk may not be assessed by this model.

- The effectiveness of such model depends on the period between the collapse of a structure and the triggering of warning signals by the system. This may vary from nearly zero second to several weeks depending on the site condition.

CHAPTER 7

7. FAILURE TIME PREDICTION BY MEANS OF DEFORMATION MEASUREMENTS

7.1 Introduction

A general materials failure relation, $\varepsilon'' = A\varepsilon'^{\alpha}$ describes accelerating creep of materials with rate coefficients α and A, by relating rates of deformation, ε', to changes in deformation rate, ε'' (acceleration) [63]. Time of failure can be extrapolated from inverse rate versus time data, and α and A may be derived to permit one to calculate the failure time. The method is of value for quantitative hazard assessments.

It is possible to forecast the failure-time in rock mass by a monitoring system in which the changes of deformation rate can be followed (Gradient Method). A warning system as a part of this monitoring system can be programmed to trigger the warning signals as soon as the detection of an accelerated rate of deformation in the monitored zone using the monitoring data.

Since the CIUS has been considered as an instrument which can follow the rate of deformation in rock mass over time and along with the elaboration of the gradient method for detection of the accelerated movements of rock mass, the studies can be conducted in the area of failure prediction with the help of deformation measuring.

Before describing the theory of time-failure prediction in rock mass it is necessary that the behavior of rock mass during the creep deformation be known.

7.2 Creep deformation

Many materials which are virtually linearly elastic at low stress levels at room temperature or short-term loading deviate from elastic behavior at high stress levels or under prolonged loading [10]. The effect of prolonged loading or time-dependent loading is known under the general name

'creep'. This type of deformation has great importance for underground stability analysis, particularly in the case of less hard rock types.

7.3 Creep mechanics

Creep represents a complex response of strain to stress as a time-dependent movement of rock under a constant load [11]. In other words, creep is a mechanical phenomenon where the strain increases as a function of time under constant stress. Figure 7.1 shows time-dependent deformation at constant load by the idealized creep curve which exhibits four principal stages of deformations as listed below:

(a) Instantaneous elastic strain.

(b) Primary or transient creep (Region I) with rapid strain increments, decelerating strain rate.

(c) Secondary creep (Region II) at a low, or near constant strain rate.

(d) Tertiary creep (Region III) accelerating strain increment to failure (creep rupture).

It has been proven that an instability in in-situ rock mass also progress in the accelerating stage of creep [5, 16, 17, 27, 40, 49, 54, 55, 56] (region III). So far an instability warning system which can be programmed to trigger the warning signals on the basis of the gradient method was described in which the most essential tasks is to detect the evolution of deformation over time and trigger audio and/or visual warning as soon as an accelerating rate of deformation in rock mass has begun. So the possibility of failure prediction by such a system may be considered

7.4 Empirical laws of creep

It has been found out that the idealized creep curve can be expressed by a relationship of the form:

$$\varepsilon = \varepsilon_e + \varepsilon_1(t) + \varepsilon_2(t) + \varepsilon_3(t) \qquad (7\text{-}2)$$

where:

ε_e = instantaneous strain.

$\varepsilon_1(t)$ = the transient creep,

$\varepsilon_2(t)$ = steady state creep,

$\varepsilon_3(t)$ = accelerated or tertiary creep,

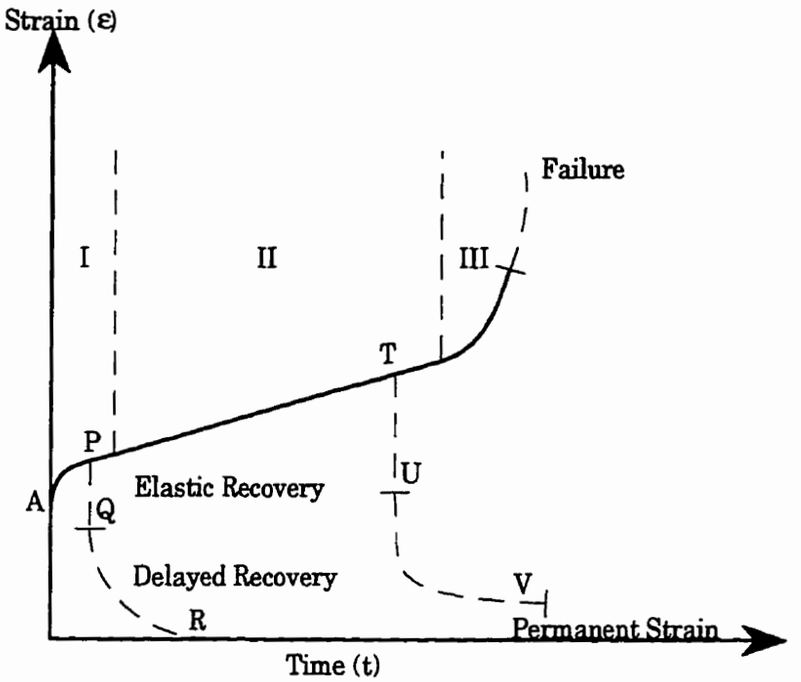

Figure 7.1 Idealized creep curve

In certain creep curves the tertiary creep usually is not included in the laboratory investigations, but in the long term stability study of mining structures this stage of creep curve must always be considered.

7.5 Accelerating creep laws

Strain (or displacement)-time relationships during accelerating creep have been divided into the following laws:

1- Saito laws [51, 52]

$$\begin{cases} \varepsilon' = \dfrac{C}{(t_f - t)^n} \end{cases} \qquad (7\text{-}3)$$

where:

ε' = strain or displacement

C: Constant

t_f = relative time of failure

t = time

n = 1, pure

$n \neq 1$, Generalized

2- Exponential laws [61]

$$\begin{cases} \varepsilon = K\left(e^{t/a} - 1\right) \\ \ln \varepsilon' = \ln \dfrac{K}{a} + \dfrac{\varepsilon}{a} \\ \varepsilon' = \dfrac{K}{a} + \dfrac{\varepsilon}{a} \end{cases} \qquad (7\text{-}4)$$

where:

ε = strain or displacement

K, a: Constant

3- Power laws [64]

$$\begin{cases} \varepsilon - \varepsilon_0 = \dfrac{\varepsilon'_1 t^{b+1}}{b+1} \\ \varepsilon' = \varepsilon'_1 t^b \\ \log \varepsilon' = \log \varepsilon'_1 + b \log t \end{cases} \qquad (7\text{-}5)$$

where:

ε_0 = strain at time zero, a constant

$\varepsilon'_1 = \varepsilon'$ at 1 minute

b: Constant

4- Zavodni and Broadbent laws [67]

$$\begin{cases} \dfrac{\varepsilon'_m}{\varepsilon'_0} \equiv K \\ \varepsilon' = Ce^{(st_f - st)} \\ \varepsilon'_f = k^2 \varepsilon'_0 \end{cases} \qquad (7\text{-}6)$$

where:

$\varepsilon'_m = \varepsilon'$ at the mid-point in the second acceleration stage

s: Constant

The above creep laws may be used to describe failure life. These relations are encompassed by a general materials failure relation (7-1) [64].

7.6 Failure-time prediction in in-situ rock mass

A materials failure relation (7-1), introduced by Voight [63], describes accelerating rate of creep under constant applied stress and temperature, and is applicable, for example, to metals and alloys, ice, concrete, polymers, rock, or soil [63]. The relation was first formulated to describe surface displacements observed during failure of large-scale slope models [21, 63]. Voight [63] demonstrated its general application, identified its constraints, and showed that the relation encompasses several widely used empirical rupture life equations. Such relationships may enable the materials failure approach to be extended to systems where loading conditions change with time.

Changing creep rate are related to rates during accelerating creep, by the materials failure relation as:

$$\varepsilon'' = A\varepsilon'^{\alpha} \qquad (7\text{-}1)$$

State variable ε is typically strain or energy release, α and A are empirical constants, and the prime superscripts represent differentiation with respect to time. This relation describes accelerating

creep of materials with rate coefficients α and A, by relating rates of deformation, ε', to changes in deformation rate, ε''.

In practical application of this relation, ε is a measurable quantity such as elongation and α and A can be derived from a given data set of rate versus time [12].

$$\varepsilon' = \left[A(1-\alpha)(t-t_*) + \varepsilon_*'^{(1-\alpha)} \right]^{1/(1-\alpha)} \tag{7-7}$$

Equation (7-7) is the solution with respect to rates for the general cases $\alpha \neq 1$, with initial time and rate t_*, ε'_*. The relationship allows one to calculate failure time t_f as

$$t_f = \frac{\varepsilon_f'^{(1-\alpha)} - \varepsilon_*'^{(1-\alpha)}}{A(1-\alpha)} + t_* \tag{7-8}$$

The constant α is dimensionless and controls the sensitivity to accelerating activity. The dimension of constant A depends on the value of α. From Eq. (7-8), $A = [T^{(\alpha-2)}L^{(1-\alpha)}]$ where T represents the dimension of time and *L* represents the dimension of ε, for example length. In the special case of α=2, A = [1/L] and, furthermore, if ε is a measure of dimensionless strain, A is dimensionless as well. A is larger than zero for increasing strain.

Voight [63] calculates from experimental results by others, $1.74<\alpha<2.01$ for metals, $1.9<\alpha<2.1$ for experimentally deformed soils, and typically $2.0<\alpha<2.2$ for slopes. However, observed values can also fall outside these narrow limits.

Time of failure can be extrapolated from inverse rate versus time data, and α and A may be derived to permit one to calculate the failure time. It has been emphasized the possibilities of a quantitative failure prediction and hazard reduction with the materials failure relation [9, 35, 41, 64], e. g., by making use of volcano eruption precursors of surface strain or seismicity [13]. In terms of practical applications the method incorporates the concept of inverse rate plots. From Eq. (7-7), the graph of inverse rate versus time is linear for a = 2. The inverse rate plot is concave

upward for $\alpha<2$ and concave downward for $\alpha>2$. Data extrapolation of inverse rate plots is done either by numerical or graphical means. For $\alpha > 1$, the equation permits the calculation of the time of singularity, that is the time at which infinite rates are expected. Alternatively, the data can be extrapolated to a certain finite rate for which failure is expected. This finite rate at time of failure can be assumed or, in some cases, may be estimated from experience. For real-time application, the interpolation of time of failure is greatly aided by a linear inverse rate trend. i. e., by assuming α to be equal or close to 2.

The application of this relation in rock mechanics can be for stability of slopes, underground excavations, ground control, rock burst and roof fall hazard mitigation, pressurized tunnels and cavities, and (potentially) earthquake prediction [64].

7.7 Conclusion

As the above law may be applied for failure-time prediction in materials such as in-situ rock mass by using deformation measurements, the law may be implanted in programming of a rock failure warning system which operates on the basis of the gradient method.

It must be mentioned that this theory has widely been applied in failure-time prediction of rock slopes and land slides [9, 35, 41, 64] and it is a matter of interest that this may be applied in forecasting of the time of failure in underground excavations by using the instruments which are able to monitor and measure the variation of deformations with time.

CHAPTER 8

8. MONITORING OF THE NIOBEC MINE

8.1 Niobec mine (Geology and Exploitation)

8.1.1 Introduction

The St-Honoré Carbonatite complex located 13 km North-East of Chicoutimi, Quebec (Figure 8.1) was discovered by SOQUEM in 1967 as a result of an airborne radiometric survey in a search of Uranium. With the exploration of the complex, a rare earth zone was first exposed followed by the discovery of two Niobium zones lying in the southern hemisphere of the Carbonatite.

Exploration of these Niobium zones was mainly carried out by 30,000 m of diamond drilling. In 1974, a joint decision was taken by SOQUEM and Copperfields Ltd. (Teck) to proceed on the exploitation of the Niobium deposit. For this purpose, the company Niobec Inc. was formed. Production started in 1976 and Niobec is now the second largest producer of Niobium oxide from the occidental world and the single underground Niobium mine in the world.

In 1979, an expansion program of 10 million dollars allowed to increase the capacity of production as much as 30%. The rate of production since February 1981 has been 2475 tons per day.

In 1989 a new formed society has become owner of 50% of Niobec's ore body, sharing with the mining group Teck.

8.1.2 General Geology-Lithology

The St-Honoré Complex has a nearly circular annular shape and covers about 25 km^2 (Figure 8.2). Carbonatite and satellite rocks are however overlaid by a capping of Ordovician Trenton limestone, with a thickness reaching up to 75m. The limestone is fossiliferous (mostly

cephalopods) mainly at its base; bedding is horizontal and the limestone lies with unconformity over the Carbonatite showing an irregular erosion surface [60].

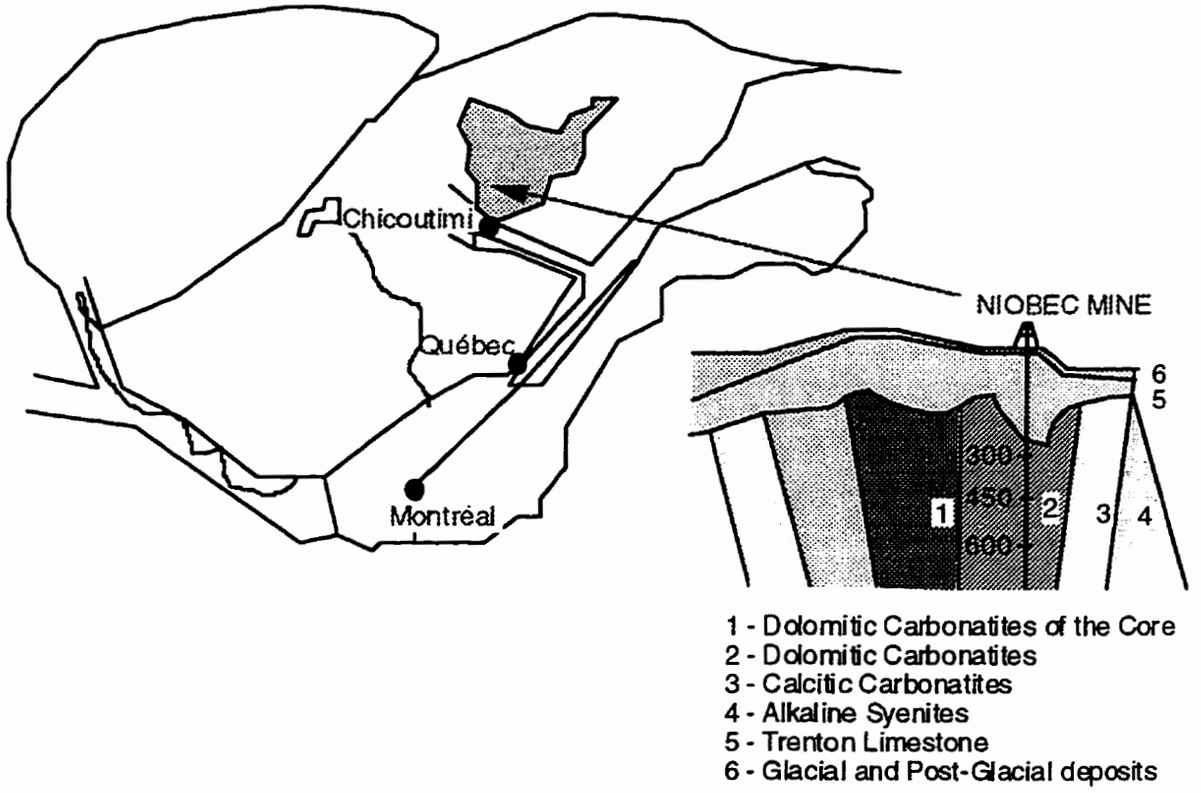

Figure: 8.1 The St-Honoré Carbonatite complex

Lithological units: The complex is constituted by the following lithological units [25]:

1. an oval Carbonatite core having the main axis in the north-south direction. From the center to the periphery (Figure 8.2).
2. a circular outer ring containing feldspathic and feldspathic alkaline rocks.
3. a triangular mass of cancrinite and garnet syenite encountered to the extreme south-east part of the complex.

The complex has a reversed conical form, slightly out of shape, revealed by the general foliation dipping towards the center.

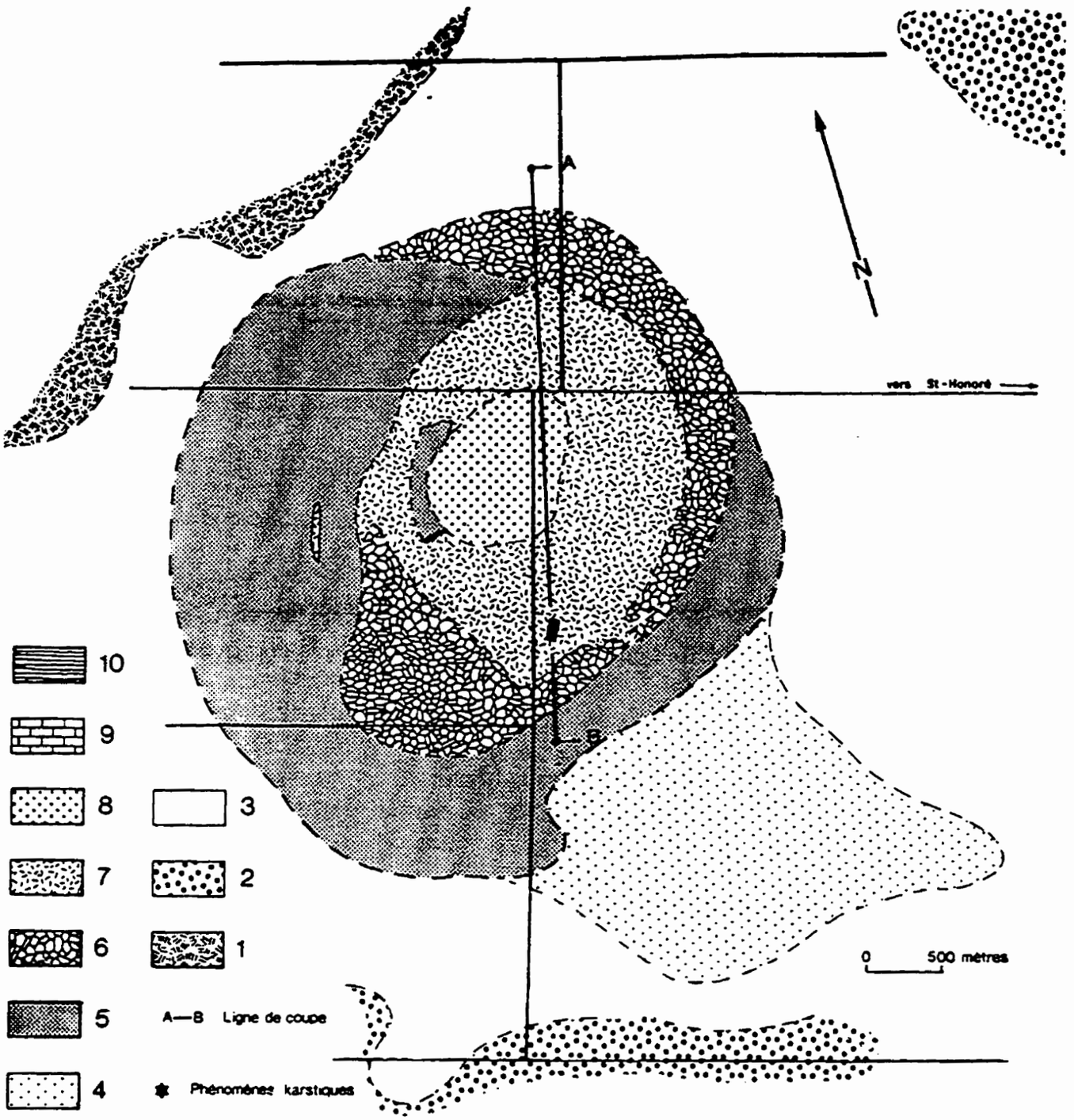

1-Anorthisite, 2-Charnockitic series, 3-Fenitisies rocks, 4-Nefeline and grenat, 5- Alkaline syenites, 6-Calcitic carbonatites, 7-Dolomitic carbonatites, 8- Dolomitic carbonatites of the core. 9-Trenton limestone, 10-Glacial and post-glacial deposites

Figure 8.2 Complex of St-Honoré (geometry)

Country rocks-alterations: Rocks immediately surrounding the complex are composed of magnetite diorite as well as hypersthene syenite. Those ones are encompassed by familiar units of the Grenville province; such as anorthosites and various gneiss affected by the amphibolite facies.

8.1.3 Origin

It is now established that core Carbonatites and their associated rocks are of magmatic origin in an inter-continental environment. Consolidation of the St-Honoré complex would be of the hypabissal plutonic type as indicated by its well developed annular structure, the presence of metamorphic surrounding rocks, a weak to medium fenitization (blue amphibole-albite) and a core Carbonatite. However the presence of feldspathic breccia (or agglomerate) in the Carbonatite itself might indicate a subvolcanic consolidation phenomenon at the limit [22].

8.1.4 Structure and Lithology

An intensive diamond drilling campaign carried out from 1970 to 1973 delineated two major Niobium zones covering a 600m by 750m area in the southern sector of the Carbonatite core (Figure 8.3). The structure is slightly curved in a general east-west trend and the dip is vertical to 70° north. The two zones are composed of lenticular bands of varying lithology with Niobium grading 0.2 to 1.00% Nb_2O_5, [23].

Dolomitites and calcitites, sometimes brecciated but usually foliated, contain concentrations of accessory minerals including the niobium-bearing pyrochlore (C3 type). This unit alternates with more massive and low niobium dolomitites, offering a more restraint mineralogical variety and containing local red brick to brown ankeritic alterations (C5 type). However, these main units frequently present inter growths probably as a result of a complex process of successive intrusions and replacements.

Finally, the niobium deposits are limited to the south by a ring-dike of massive, fine grained, gray to brick colored dolomitite containing local chlorite, pyrite and magnetite and having been

strongly affected by an hematitic alteration (C9 type). Remnants (20 to 30%) of an old fine grained feldspathic rock can also be identified from that rock unit [22].

8.1.5 Mineralogy

Table 8.1 shows the main mineralogical composition for a series of niobium of lenses. The dolomite-calcite ratio clearly indicates a dolomititic composition for the economic zone. It is also valuable to note the constant presence in the rocks of over 10% as iron oxide under the hematite, magnetite and maghemite forms. Pyrite and pyrhotite are found in disseminated traces. The complete absence of free silica (quartz) in carbonates as well as in silicates (according to other analyses and observations) indicates on the one hand a saturated environment during the formation and, on the other hand, no ulterior hydrothermal silification. Apatite represents about 10% of the total composition, is generally friable and is really present as fluorapatite [22].

Zone No. 1 extends some 550m long and contains at least six ore lenses ($Nb_2O_5 \geq 0.5\%$) of more than 20m. in thickness. The dip is vertical to subvertical. Among other aspects, this zone is characterized by the presence of colombite and the whole range of sodic to ferrian pyrochlores.

The main pyrochlore carbonatite unit (C3 type) has been divided into subtypes in order to better correlate the niobium mineralization with macroscopic features. Therefore, Zone No. 1 is mainly constituted of the C3n subtype: foliated, fine-grained, pink to brick-brown dolomitite, with apatite, and local concentrations of magnetite-maghemite hematite, pyrochlore and columbite. Other secondary minerals are present such as biotite, pyrite and pyrhotite, zircon, ilmenite, sphalerite, barite and hydrocarbon traces.

Rich pyrochlore bands of the C3a (biotite and apatite dolomitite) and C3b (magnetite, poor foliated white dolomitite) sub-types alternate with Cs type (already described) low niobium (0.10-0.0, 0.40% Nb_2O_5) dolomitite bands.

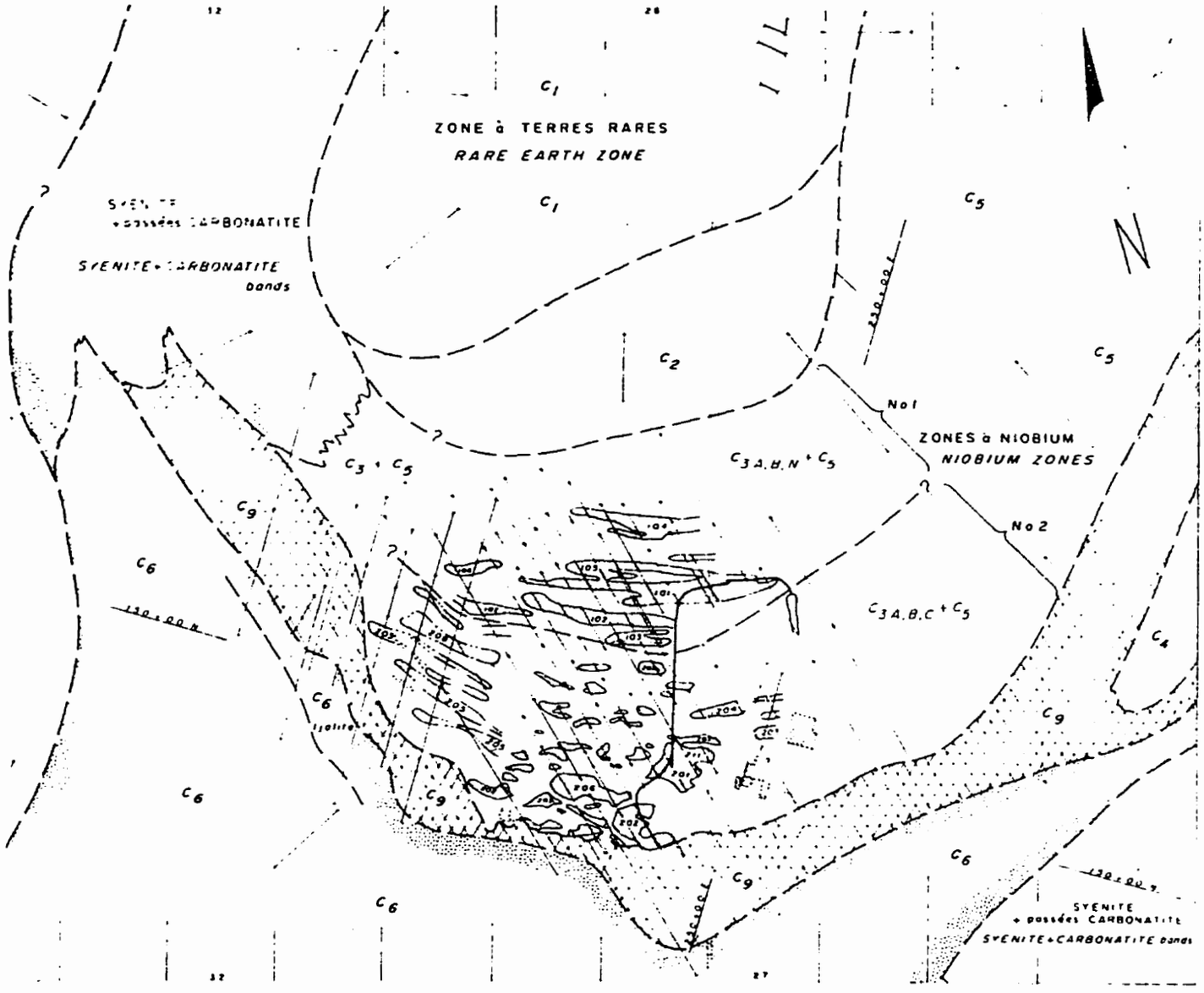

C_{3A}: Biotit Apatite and Pyrocholore dolomitite, C_{3B}: Magnetite, Apatite and Pyrocholore Dolomitite. C_{3C}; Biotite, Apatite and Pyrocholore Calcitite, C_{3N}: Apatite local Hematite+Magnetite, Pyrocholore and Columbite Dolomitite. C_5: Low Pyrocholore Dolomitite. C_9: Hematie Alteration

Figure 8.3 St-Honoré Carbonatite Niobium deposits

Percentages

Table 8.1 Major mineral composition of mineralized lenses [22]

Lot No	Pyrochlore	Columbite	Hematite+ Maghemite	Pyrite	Apatite	Calcite	Dolomie	Chlorite	Biotite	Anthraxolite	Total
											93.10
72	0.7	0.40	9.1	0.6	9	3	70			0.30	93.10
73	0.4	0.04	9.9	0.4	4	4	65			0.05	83.79
74	0.7	0.07	3.0	0.1	7	2	77			0.04	90.91
75	0.4	0.10	6.7	1.5	8	4	45	6	10	0.13	81.83
76	0.7	0.30	15.6	0.4	10	4	65			0.12	96.12
77	1.2	0.10	15.1	1.4	10	4	59	4	6	0.43	101.23
79	1.0	0.10	9.4	1.4	8	1	62		15	0.11	98.01
80	0.9	0.10	10.9	0.3	8	5	58			0.13	83.33
81	1.0	0.10	10.2	0.5	10	1	70			0.08	91.88
82	0.8	0.04	10.0	0.3	10	2	67			0.08	90.22
83	1.4	0.00	36.0	2.1	29	16	17	2		0.18	103.68
84	1.0	0.05	15.0	0.3	18	1	61	2		0.12	98.47
85	0.6	0.20	11.1	0.4	8	4	69			0.1	93.40
86	0.5	0.20	12.6	0.3	10	3	62			0.03	91.63
87	0.5	0.20	12.1	0.4	10	4	60	6	4	0.11	97.31
88	0.7	0.10	13.4	0.5	8	4	67			0.02	93.72
89	0.5	0.10	3.6	0.4	8	28	38	16	8	0.23	102.83
90	1.2	0.10	16.2	0.3	9	8	58		10	0.30	103.10
91	0.7	0.80	8.0	0.3	10	3	72			0.01	94.81
Aver.	**0.8**	**0.2**	**12**	**0.6**	**10.2**	**5.3**	**60**	**1.9**	**2.8**	**0.14**	**94.1**

Moreover, below the Trenton contact exists a strong hematitic alteration layer with local thickness up to 50m. This alteration seems to have occurred before the Trenton deposition and should be of the weathering type. Traces of hydrocarbons found in zone No. 1 are mostly associated with that upper layer of the Carbonatite.

Zone No. 2, the south ore zone presently in production, extends over 800m.long by 250m wide and includes ten ore lenses each one containing more than 0.50% Nb_2O_5. Generally, these high grade bands have a more pinch and-swell shape than zone no. 1 bands.

Zone no. 2 differs from the previous zone No. 1 by its local calcific nature (C3c subtype), the presence of niobium almost exclusively from a sodic pyrochlore, the absence of an upper ferrugineous alteration layer, the abundance of biotite and a lower content of magnetite. However, in the meridional part of zone No. 2, we can find some black fragments containing minerals such as: pyroxenes, biotite, chlorite, kaolin, calcite, with no or little potassic feldspar. Moreover, these fragments or masses locally exhibit a lamprophyre texture shown by the development of blue biotite phenocrysts (up to 3 cm) in a black matrix. This rock could therefore be the product of a complete syenite digestion or possibly originating from a lamprophyre intrusion associated with alkaline rocks of the outer ring. Values of 0.4 to 0.6% Nb_2O_5 are encountered in that rock [22].

8.1.6 Tectonic

No major faulting has been observed thus far from the Niobec mining developments. Nevertheless, there are impressive numbers of fractures and minor faults. The study of these fractures [50] allows to identify long sub-horizontal to intermediate fractures conchoidal fracture and stria. There is a relatively without any significant throw and in scattered directions. They are subdividing the intrusive into series of flat-lying plates and wedges up to several hundred meters wide and a few meters thick. Minor fractures are also associated to these decametric fractures. About 20% of the main fractures are either filled with biotite and chlorite (sometimes clay) or calcite with variable proportions of apatite. It is likely that those long major fractures be formed as the first cooling fissures of the intrusive body in response to vertical thermal contraction.

8.1.7 Ore reserves

Zone No.2 mining reserves are currently established at around 10Mt grading 0.69% Nb_2O_5. Mineralization of zone No. 1 is of the same magnitude but its nature of the mineralization locally presents some metallurgical complexities. Apatite content, estimated at 6-8% for zone No. 2 and 10% for zone No.1, offers a potential by-product as phosphate fertilizer currently under evaluation.

8.1.8 Exploitation

A typical longitudinal view of the Niobec mine is shown in Figure 8.4. The mining pattern at the Niobec mine follows the economical concentration of Niobium outlined in the interconnected vertical pods. The numerous concentrations are irregularly distributed in the main carbonatite body, therefore, an irregular open stoping method is employed.

Two tiers of operations presently exist at the mine. The upper tier is from the over-lying limestone-intrusive contact (level 250-300) to level 600. The second tier, separated from the first tier by a 33m (100 ft) sill pillar, has stopes developed to level 1000. Stopes in the lower tier follow the same pattern as stopes in the upper tier with some lateral shift due to the mineralization dip.

For economic reasons, no back fill has been used at the Niobec mine. As a result, stopes with a minimum height of 100 meters have been left open since excavation. The roofs of those stopes have been strengthened through the use of mechanical bolts, but the stopes walls (primarily pillars) are unsupported. Sloughing never exceed 3-4% of the original volume mined.

The drifts, 3m×4m in dimensions, are excavated using pre-split blasting. Drift walls are unsupported, but the backs are supported when required. In the worst areas both bolting and screening are used.

A shaft with a depth of 400 m with together a ramp allow a direct access to different levels of mine. The mine is active 24 hours in day and 5 days in week.

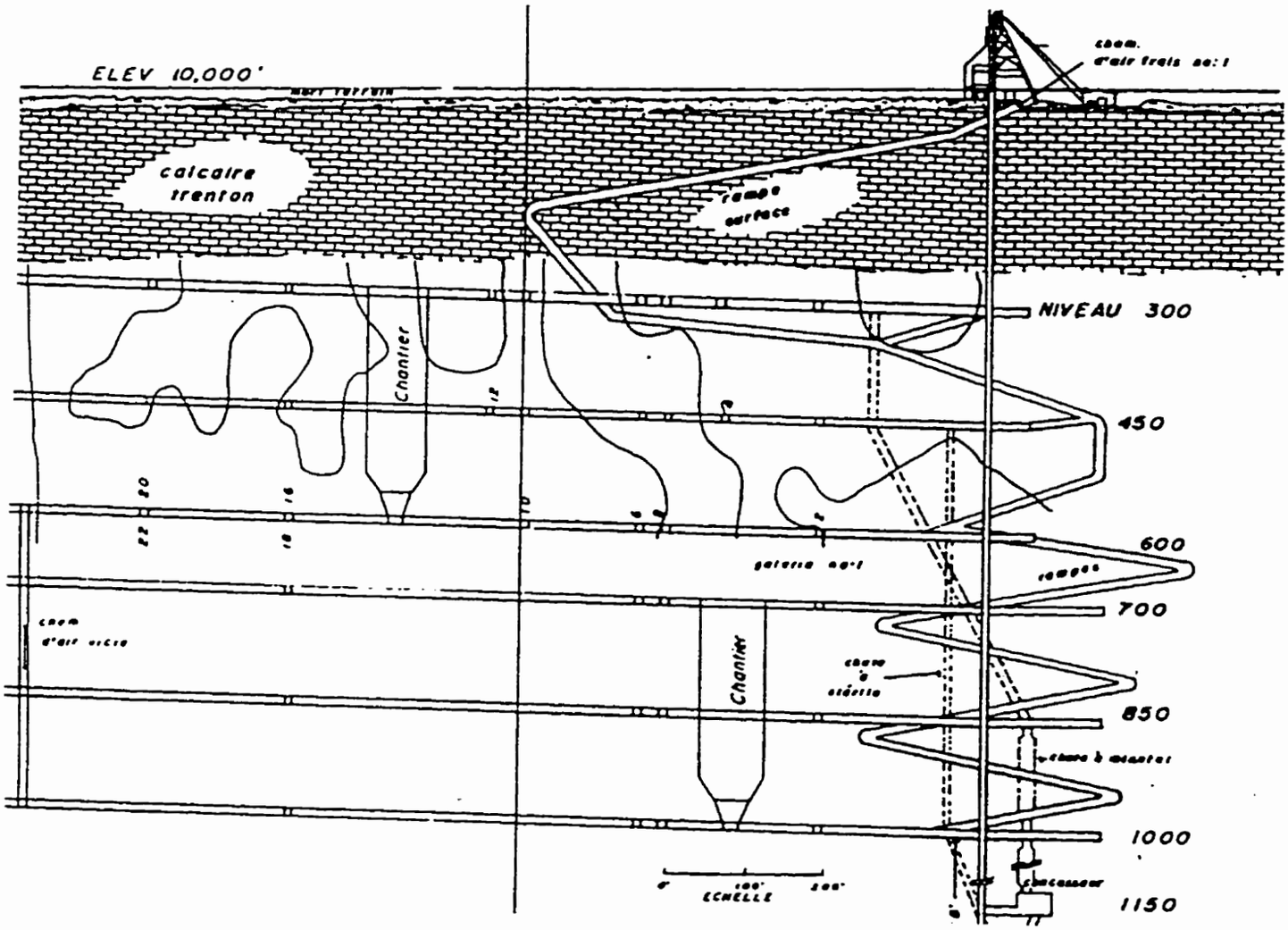

Figure 8.4 A typical cross sectional view of the Niobec mine

The blasted ore body come down by gravity to the lower levels and are transported for the primary crushing, reaching to 10cm in dimension of crushed stone and then are sent out to the surface to the mineral processing and concentration factory.

The concentration factory works 24 hours a day and 7 days a week, rate of recovery is 8lg Niobium Oxide (Nb_2O_5) from one ton of Niobium's mineral and the pyrocholore's concentrated consists of 60% Niobium Oxide (Nb_2O_5). The annual production is 7 millions LP of Nb_2O_5.

The Niobec's clients are Mitsui (Japan), Murex (England) and Metallurg (USA), They use the Niobec's product for making a Ferro-Niobium alloy which is used for making the special steel which are known for their high resistance, used in the pipeline industries, bridge construction, building and special architectures. Because of the high resistance of Niobium in comparison with its weight, the Niobium's alloys have widely been used in the car industry and in the aviation industry in the form of super alloy for making the reaction motors. The super conductivity properties of Niobium has opened a new aspect of the practical applications of this elemcnt in the super conductivity industries.

8.2 Instrumentation of the Niobec mine by the CIUS

8.2.1 Introduction

The objective of this phase of mining activities is the monitoring of rock performance which characterizes the operational response of the rock mass to mining activities. The intention is to establish a comprehension of the roles of various elements of the rock mass in the load-deformation behavior of the rock medium.

Since the stability of underground mining openings can not be ensured by the knowledge of the initial stresses field, because of high stress variations generated by mining activities, (excavations extension, blasting,...), monitoring of these openings by means of instruments which are able to monitor the variation of stresses and deformation has become necessary to provide

quantitative information (deformations and stress variations) as well as qualitative information (state of stability). These two important tasks of monitoring have been considered in the instrumentation of the Niobec mine. Consequently, two principal objectives which have been sought in the stability monitoring of this mine by CIUS are as follows:

1- Monitoring of the variation of stresses and deformations, leading to a better understanding of the stability of stopes and pillars in different levels.
2- Detection of the instabilities which may endanger the stability of underground openings by triggering the warning signals when an instability is anticipated.

Table 8.2 - CIUS Location

CIUS	Installation Date	Injection Date	Level	Pillar
NIO-300-1	11/9/89	11/9/89	300	T-202-10
NIO300	29/07/92	30/07/92	300	T-206-14
NIO600	29/07/92	30/07/92	600	T-206-14
NIO700	31/07/92	31/07/92	700	T-102-19
NIO1000	29/07/92	31/07/92	1000	T-102-19
NIO700-B	25/05/94	26/05/94	700	T-102-21

The CIUS units have been used for the instrumentation of concrete structures such as several dams, a bridge and in the underground laboratory of Atomic Energy of Canada Limited (AECL), and for the first time the CIUS was used for instrumentation of the underground excavations at the Niobec mine [2].

So far six CIUS have been installed at the different levels of this mine (Table 8.2).

8.2.2 Results

The CIUS' data are processed for obtaining the variation of stresses and deformations in the six independent directions in the form of curves (chapter 5). By the interpretation of theses curves one can detect the changes of deformations and stresses generated by great blasting operations as

well as by the extension of openings and other phenomena. These data are processed as input data for the warning system.

- Monitoring at the level 700ft by the CIUS NIO 700B

This CIUS was the last one, installed at the Niobec mine at the level 700ft in the drift's wall 7Ga-13 for monitoring the exploitation of two stopes 7-102-21 and 7-102-23 which are located between the levels 700 and 1000 (Figure 8.5). The borehole inside which the CIUS NIO700 was installed is 27.5m in length and has a slope equal to 15°. Since installation, six blasting operations have been carried out. Table 8.3.gives the dates, tonnage of blasted materials and positions of the blasting zone.

Table 8.3 Description of the blasting zones

No	Date	Day No.	Excavated Mass (ton)	Location
1	Jun. 23, 94	Day 28	37,173	Stope 7-102-21
2	Sep. 29, 94	Day 136	1,289	Upper 10-102-21
3	Oct. 7, 94	Day 144	5,405	Upper 10-102-23
4	Oct. 14, 94	Day 151	3,570	Upper 10-102-23
5	Nov.10, 94	Day 168	93,749	Stope 7-102-21
6	Apr. 13, 94	Day 323	202,000	Stope 7-102-21

The first blasting was carried out on June 23, 1994 (day 28). Figure 8.6 shows the variation of deformations generated by this operation, the generated stresses variation are as follows:

Detected induced stresses on September 29, 1994, CIUS NIO700B

Snn = 0.50 MPa Sne = 0.25 MPa

See = 0.00 MPa Sev = 0.25 MPa

Svv = 0.00 MPa Svn = 0.00 MPa

The three next blasting operations have also been detected by the CIUS NIO700B but because of a temporary period of defectivness for some of the extensometers, it was not possible to determine the variation of stresses during this period.

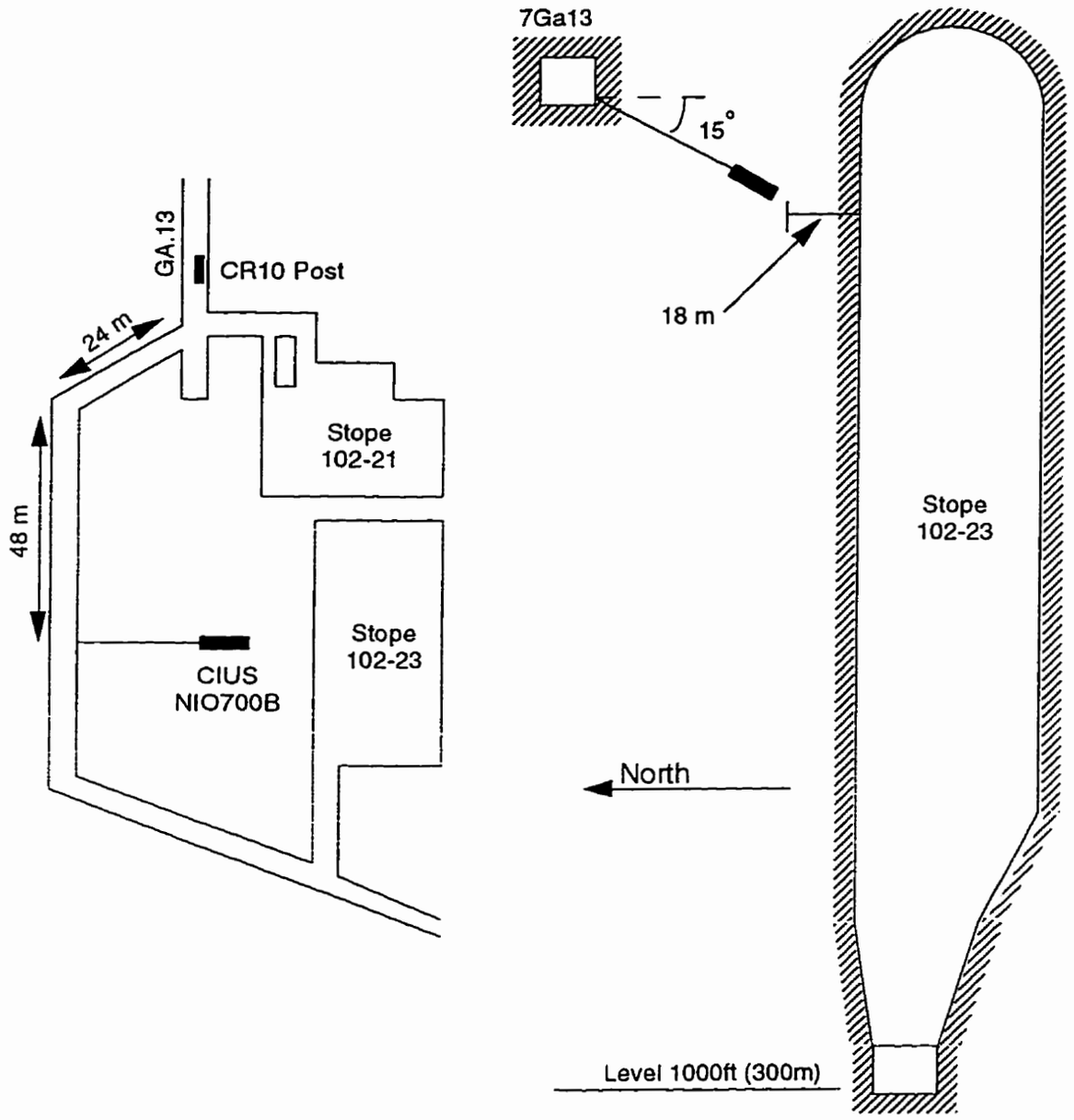

Figure 8.5 Position of the CIUS NIO700B

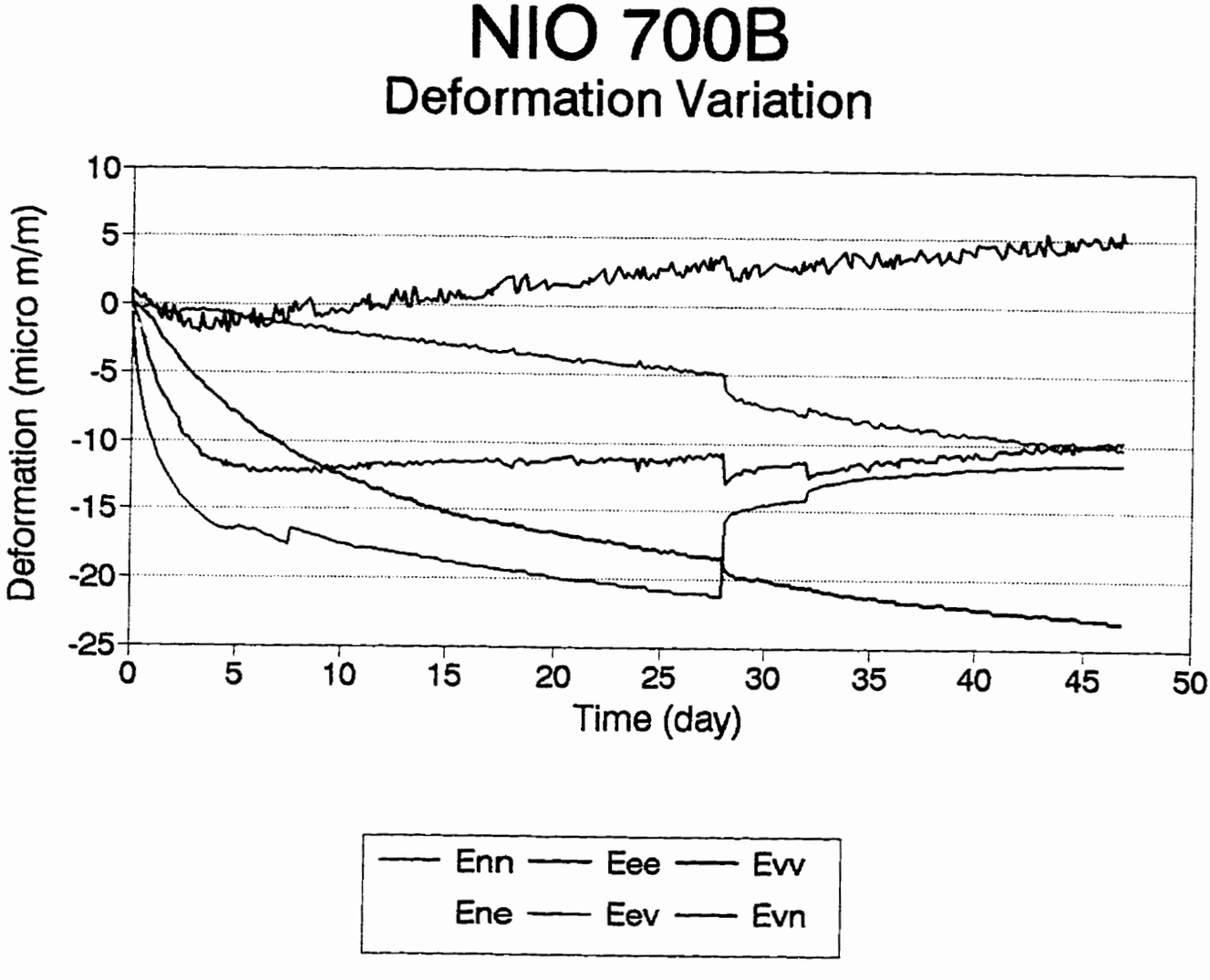

Figure 8.6 Variation of deformations after blasting on 23rd June 1994 (CIUS NIO700B)

The fifth blasting was carried out on November 10, 1994 and generated an important variation of stresses and deformations. Figure 8.7 shows the induced stresses after this blasting, the values of stresses variation can be determined as follows:

Detected induced stresses on November 10, 1994, CIUS NIO700B

Snn = 1.00 MPa Sne = 3.75.0 MPa

See = 6.25 MPa Sev = -4.25 MPa

Svv = -0.50 MPa Svn = -1.00 MPa

This blasting is the first series of blasting operations for exploitation of the stope 7-102-23 between the levels 700 and 1000. Considering the location of the blasting zone which is located just 18.2 far from CIUS 700B and nearly at the same level, the high values for the variation of stresses resulting from this operation are justified. This blasting has generated compression for the stresses in the NE, EW, NS directions, and relaxation for other directions. The largest compression stresses are in the east-west direction and the stress for the component following north-south has not dramatically changed.

The detection of these variations resulting from blasting by the CIUS NIO700B proves the ability of the CIUS in detecting the anomalous response of in-situ rock mass to the blasting and extension of excavations in mine structures, which is the final goal of a stability remote monitoring system in the mines.

The last blasting which was detected by the CIUS NIO700B was carried out on April 13, 1995. This blasting was the most important blasting in this zone with 202,000 tons of crushed materials. This blasting has had a great influence on the stability of this zone (stope 7-102-23). After this operation a violent roof failure (35ft in height) occurred in the stope 7-102-23.

This phenomenon can be explained either by a sudden change in the direction of principal stresses or by a rock burst phenomenon. The CIUS NIO700B was disconnected after this operation. The roof collapse took place 45 minutes after the blasting during which the variation of stresses and deformation certainly have not been normal and should have been detected by the CIUS. However the disconnection of the instrument, immediately after blasting must trigger a special warning signal which must be considered in the programming of the warning system.

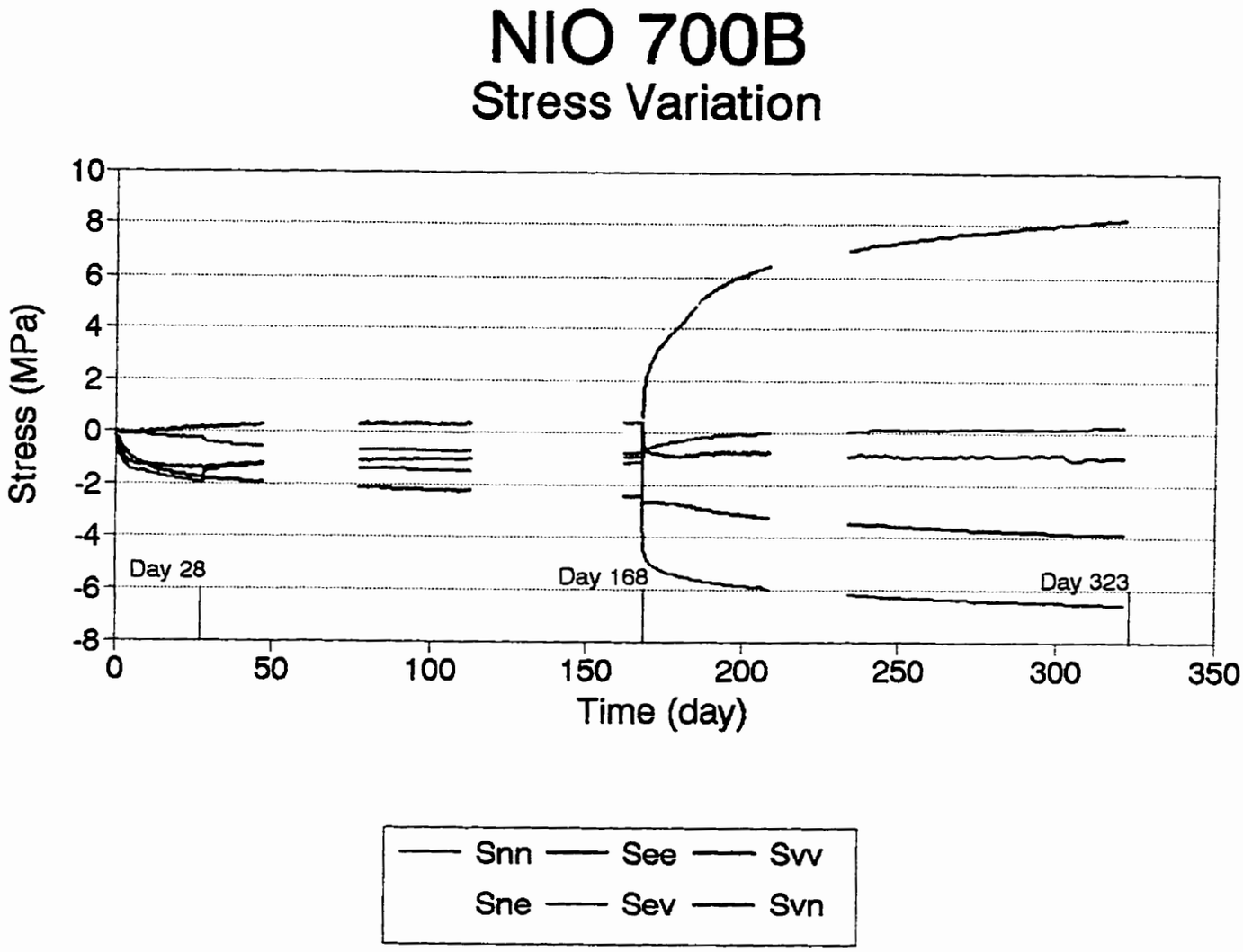

Figure 8.7 Induced stresses after blasting on 10th November 1994 (CIUS NIO700B)

Finally, the detection of abnormal changes of stresses or deformation resulting from blasting operations by the CIUS NIO700B shows the possibility of linking a warning system and an acquisition system to the CIUS' units which all together provide the means by which it is possible to record, and visualize the CIUS' data and to trigger the warning signals in the case of instability. One should remind that in programming of a warning system which is supposed to be used in the mines, during the period of blasting the monitoring system must be stopped and restarted after the operation and before the mine's personnel arrive. Appendix 1 shows the variations of the measured stresses and deformation by the CIUS NIO700B.

- Monitoring at the levels 300ft and 600ft by the CIUS NIO300 and CIUS NIO600

Figures 8.8 shows the variation of stresses, measured by the CIUS NIO300 at the level 300ft. Having evaluated the rate of deformation in the pillar (T-206-14) in which the two CIUS have been installed we observed that since March 25, 1993 the following deformation law may be adapted for explaining their behaviors.

$$\varepsilon = A\left(e^{\frac{-(t-t_0)}{\tau}} - 1\right) \qquad (8\text{-}1)$$

where:

A; is the maximum amplitude of deformation in extensometers (μm/m)

τ; is the constant parameter of time (days)

t_0; is the phase change which is related to the measured deformation during the blasting operations before March 25, 1993

Table 8.4 Parameters of deformation law since March 25, 1993

Extensometer	NIO300			NIO600		
No.	A(μm/m)	τ (Day)	t_0 (Day)	A(μm/m)	τ (Day)	t_0 (Day)
1	136.6	320.0	-61.1	80.0	325.9	92.7
2	124.9	302.1	-42.4	125.6	360.0	-80.0
3	133.5	321.0	-59.8	131.6	301.1	-125.7
4	129.8	287.6	-60.5	130.6	270.1	-51.7
5	138.5	320.5	-70.6	105.5	210.7	4.9
6	135.6	386.4	-115.4	51.5	345.2	256.6

The comparison of these functions with the readings before March 25, 1993 show that they are valid since October 14, 1992. Table 8.4 shows the parameters of this law for the CIUS NIO300 and CIUS NIO600. These CIUS have been installed for monitoring of the pillar (T-206-14).

We have used the variation of these cylinders between the interval of March 25 and November 18, 1993 for determining the constant parameters A, t_0 and τ. These values are used as the starting points in the minimization algorithm of non-linear parameters, using iterative least-square method for determining the best fitting parameters of the experimental curves (measured deformation by the CIUS).

Meanwhile, two blasting operations carried out for exploitation of the stope 206-14 (Figure 8.9). The first one was carried out on September 4, 1992 (28^{th} day) and the second one on January 27, 1993 (173^{rd} day). The first blasting was detected by both of the CIUS NIO300 and the CIUS NIO600 but the second one was only detected by NIO600.

One of the reasons for detection of the first blasting by the two CIUS is the stope's dimension which in the south-north direction is definitely greater than that of the stope 204-14 between the levels of 300ft and 600ft (Figure 8.9). Furthermore, this stope has not been able to conceal the new stope from the CIUS. The stress variations, measured by the CIUS are as follows:

Detected induced stresses on September 4, 1993, CIUS NIO300

Snn = -1.2 MPa Sne = -0.3 MPa

See = -0.5 MPa Sev = 0.1 MPa

Svv = -1.5 MPa Svn = -0.2 MPa

Detected induced stresses on September 4, 1993, CIUS NIO600

Snn = -0.8 MPa Sne = 0.1 MPa

See = -0.1 MPa Sev = 0.1 MPa

Svv = 0.1 MPa Svn = -0.7 MPa

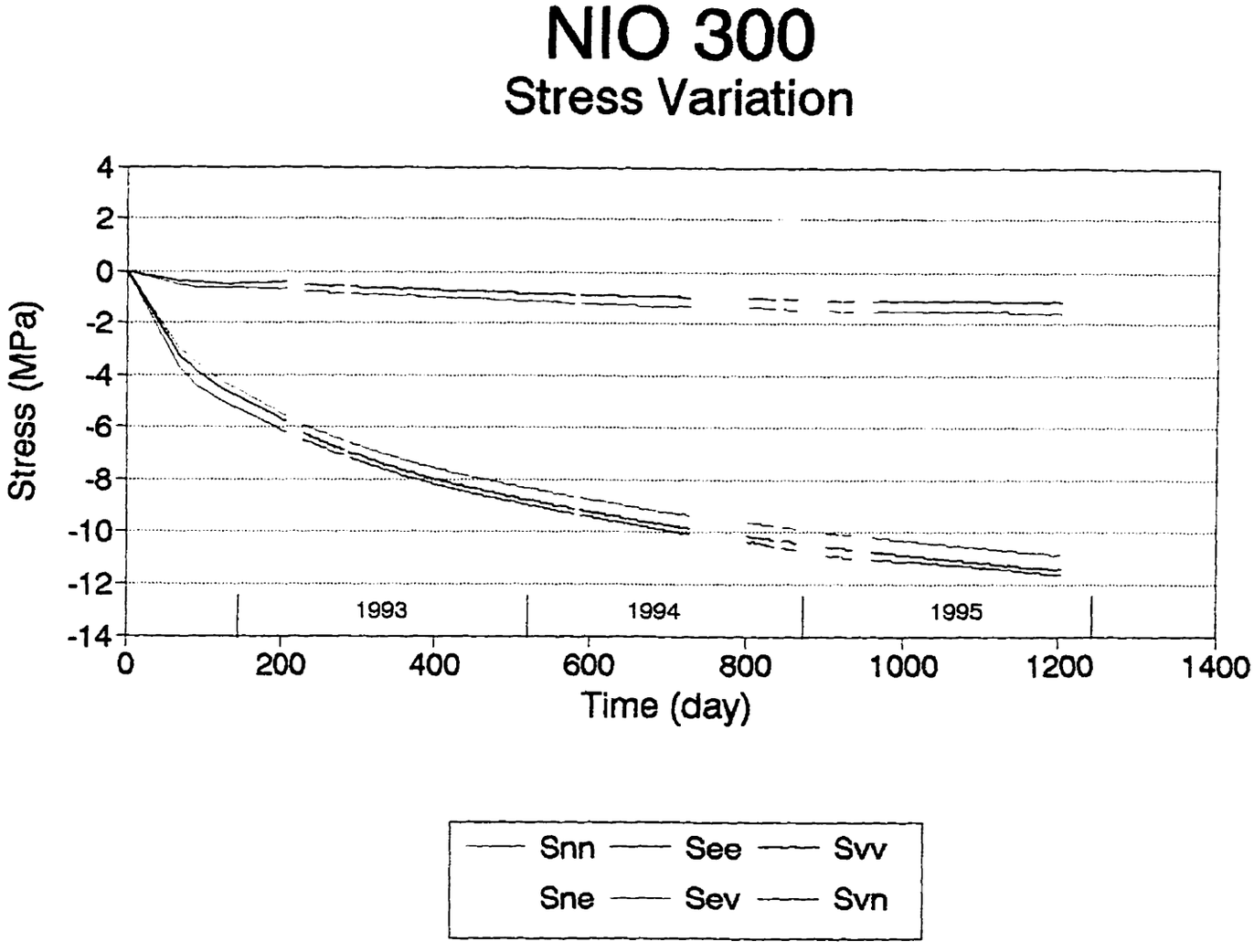

Figure 8.8 Variation of stresses (CIUS NIO300)

The CIUS NIO300 is located on top of the stope and has measured the relaxation, the stress fields going away from this zone. The greatest quantities of relaxation are in the vertical direction as well as in the south-north direction and that is because of the pillar which is located between the open stopes 206-12 and 206-14.

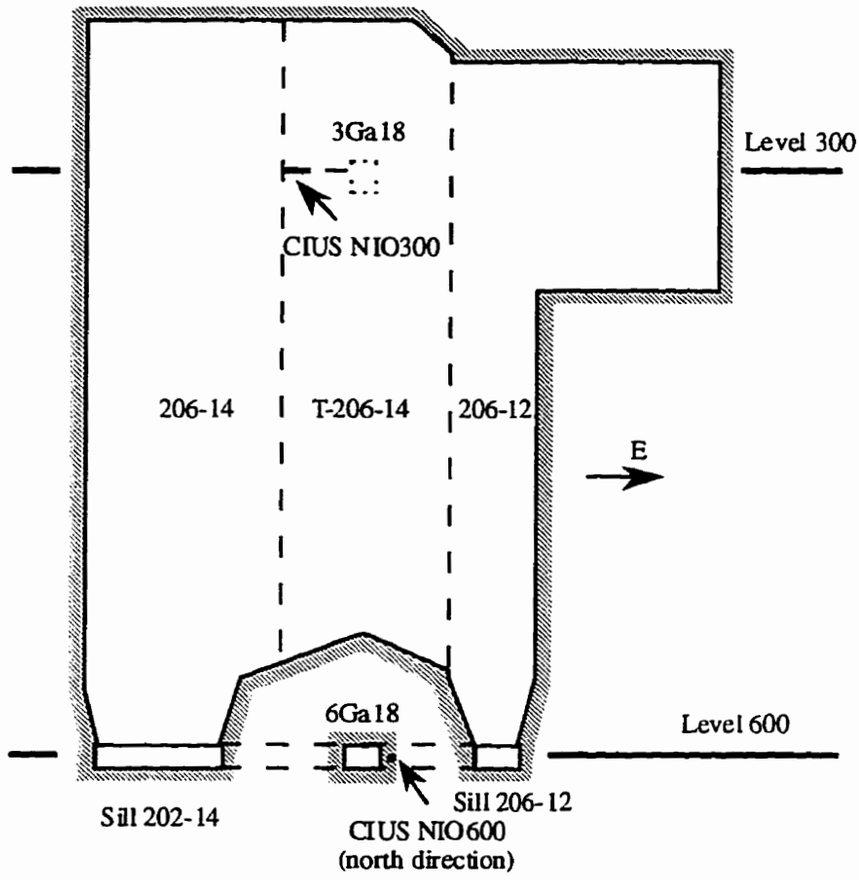

Figure 8.9 The Section of pillar and stope (206-14)

The CIUS NIO600 has been located a little on the stope's side and has measured an increase for the vertical stress and a decrease for the south-north stress. The stress fields are subjected to two effects the vertical stress has been pushed back toward this CIUS, but the south-north stress has been affected by the presence of the stopes 206-12 and 206-14.

The second blasting took place on January 27, 1993 (178, 124 tons). This blasting operation was carried out as a general blasting operation for exploitation of the stope 206-14 between the

levels 300 and 600. This blasting has been only detected by the CIUS NIO600. The measured variation of stresses are as follows:

Detected induced stresses on January 27,1993, CIUS NIO300

Snn = -0.1 MPa Sne = 0.0 MPa

See = 0.0 MPa Sev = -0.1 MPa

Svv = 0.0 MPa Svn = 0.1 MPa

Detected induced stresses on January 27,1993, CIUS NIO60

Snn = 0.8 MPa Sne = 0.1 MPa

See = 0.1 MPa Sev = 0.1 MPa

Svv = -0.2 MPa Svn = -0.2 MPa

The CIUS NIO300 detected no stress variation, the reasons may be summarized as follows:

1. The pillar was located between the open stopes 206-12 and 206-14 and it was not able to induce any perturbation in the west-east direction.
2. The stope 206-14 between the levels 700 and 1000 had already relaxed the stresses in the vertical direction.
3. The presence of many open stopes in its boundary had already relaxed this zone, it was particularly important for the south-north direction.

The CIUS NIO600 principally measured a relaxation in the south-north direction and nothing in other directions, because of the following reasons.
1. The pillar is cornered between the open stopes 206-12 and 206-14, and it has not been able to induce any stress perturbation in the west-east direction.
2. The stope 206-14 between the levels 700 and 1000 had already perturbed the stress fields in the vertical direction.
3. The excavation of the pillar had well blocked the stress field passing in the south-north direction between two open stopes 206-12 and 206-14.

8.3 Rock failure warning system at the Niobec mine

8.3.1 Introduction

In spite of the recent progress in the calculation methods in rock mechanics, the stability of mining excavations can not be predicted with great accuracy. So the monitoring of these excavations and installation of the preventive systems are indispensable for assuring the personnel's safety and the stability of excavations.

The warning system at the Niobec mine consists of measuring instruments (CIUS) and the acquisition system and a series of data treatment software which have been developed and further must be developed to accomplish the final objectives of monitoring at this mine. At the Niobec mine the objectives of monitoring have been as follows:

- ability of forecasting the stability of excavations and examining whether or not they evolve toward a rupture process by means of instrumentation
- the second objective which is operational, consists of installation of a warning system which triggers the warning signals when an instability is anticipated.
- the third step will complete the two first steps and it is the failure-time prediction, has not yet been elaborated fully.

8.3.2 Data Acquisition

The second important part of the monitoring system consists of a series of devices for data acquisition which are measured by the measuring instruments (CIUS). At present, according to the site distance, seriousness of risk, installation size and available funds, three principal systems are being used in the field of mining instrumentation.

1- Simple remote-monitoring system: In this system the measuring instrument has been installed in place and the data are manually read and in the fixed intervals from communication cables which

exit from the instrument at the borehole head, in a wiring terminal. After reading, the data processing also will be manually carried out at the processing center. This method was the first way of data acquisition and data processing used at the Niobec mine.

2- Restricted remote-monitoring system: In this system the acquisition is carried out automatically with a constant frequency by a read out device and the data are saved in a file. The frequency of acquisition may be for example one measurement every two hours. The file which may contain for example the data recorded during two weeks will be transferred to the processing center to be processed manually. This is the present method which is being used for the acquisition and processing of the installed CIUS at the Niobec mine. The acquisition of data is carried out with the help of the time-division multiplexers and two CR10 acquisition systems.

3- Automatic remote monitoring system: In this method the data are automatically read in the fixed intervals and transferred by passing through a programmable controller. Data processing and data management are locally carried out at the source. In this method only the useful data will be transferred to the outside and in the real time. The process of decision making for triggering the warning signals can be done at the processing center using the received data.

The final installation of the warning system at Niobec will be done using the last method which will provide the means by which it will make possible a reliable remote monitoring of different zones. At the Université de Sherbrooke an electronic data acquisition system (CAIUS) has been developed for signal processing at the source [3]. This system will be described in detail in the next chapter.

8.3.3 Warning system programming

As it was already mentioned, at the Niobec mine, the gradient method will be used for programming an instability warning system. This method is based on the consideration of the rate of deformation, not the measured deformation, so in the installation procedure of the remote

monitoring system at this mine it must be considered that the system must be capable of memorizing the deformation regime in the monitored sites.

According to the developed theories in chapter 6, one of the most difficult tasks in the gradient method consists of distinguishing between the variability of measurements which is due to the real changes of deformation in the site and for other reasons (noises). Figure 8.10 shows the difficulty in detection of a real acceleration, taking into account the variability of measurements. This variability can be due to the precision of instrument (measurements) and also can be caused by the real changes in the deformation regime of rock mass.

In this method the monitoring system must be able to detect among the fluctuation of measurements the abnormal variations of deformation which may lead to the collapse of structure. This can be achieved by data processing during a control period e.g. a week or a day. The elaborated calculations which were presented in chapter 6 allow one to define an average central tendency which gives the evolution of deformation during the reference period in the monitored zone. The variability of punctual measurements will be considered as a deviation of measurements and with the help of the elaborated tests in chapter 6, one can detect a measurement which is so much deviated. This method seems a simple method but at the same time is subjective and it depends so much on the scale of drawing when the study is carried out on the curves.

The effective implantation of this method in a warning system first requires a series of long and tedious calculations. Practically, before the design of an automated remote monitoring of structures by the use of CIUS, several data processing subroutines must be implanted in the acquisition-processing link up, as follows:

- a series of data treatment software
- noise elimination subroutines
- auto regressive models

The studies must be conducted on the reliability of the remote monitoring system and also a risk assessment study of mining stopes may be conducted.

During the feasibility studies of the implantation of an automated remote monitoring of structures using the CIUS, some of the tasks such as validation of several data treatment software have been carried out, but the realization of this technique and the installation of a reliable remote monitoring system at this mine needs several developments in data processing techniques.

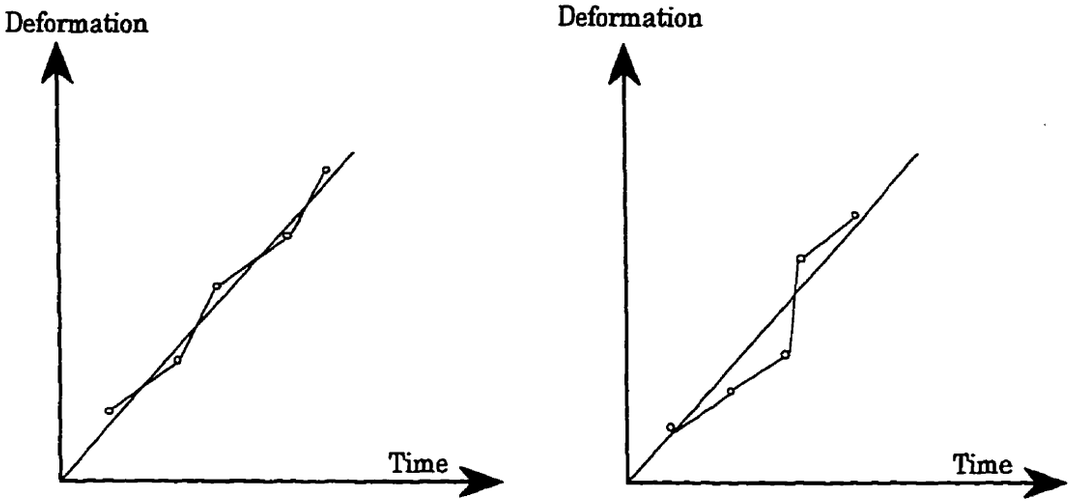

Figure 8.10 Variability of measurements

At the first step a data treatment software (LAIUS) has been developed to treat the unprocessed data, read by the acquisition system in the form of frequency, after being processed, using LAIUS they may be seen in the form of curves, showing the variations of stresses and deformation over time [44].

In order that one can realize the gradient method for detection of anomalies in the deformation rate, it must be known how the rates have been changing in the past periods of time. Having followed the variation of deformation in the pillars in which the CIUS have been installed at Niobec, we can accept the following deformation law as a relationship according to which the deformations have been changing (8-1).

$$\varepsilon = A\left(e^{\frac{-(t-t_0)}{\tau}} - 1\right) \qquad (8\text{-}1)$$

The parameters of this law have been found using the Marquardt algorithm for least-squares estimation of nonlinear parameters [24, 45]. Seeking the parameters of t_0, τ and A, we minimize the sum of squares (SSE).

$$SSE(t_0,\tau A)=\sum_{t=0}^{n}\left[\varepsilon_t-\varepsilon_{(t_0,\tau,A)}\right]^2 \qquad (8\text{-}2)$$

where ε_t is the measured deformation by the CIUS and $\varepsilon_{(t_0,\tau,A)}$ is the predicted value of deformation. The Marquardt's iterative method was applied for finding the parameters of best fitting, using the following equations [24].

$$\frac{\partial\varepsilon(t_0,\tau,A)}{\partial A}=0$$
$$\frac{\partial\varepsilon(t_0,\tau,A)}{\partial t_0}=0 \qquad (8\text{-}3)$$
$$\frac{\partial\varepsilon(t_0,\tau,A)}{\partial \tau}=0$$

These parameters were determined for the two CIUS NIO300 and CIUS NIO600. Table 8.5 shows the parameters of best fitting for the CIUS NIO300. The first series of parameters which are determined by means of a linear regression algorithm, were used as the starting points in the non linear regression algorithm.

Table 8.5 Parameters of minimization

Sensor No.	First Parameters			Best Fitting Parameters		
#	A (μm/m)	τ (Hours)	t_0 (Hours)	A (μm/m)	τ(Hours)	t_0(Hours)
1	54.00	7680.0	213.20	57.33	8226.0	-19.51
2	51.53	7250.4	-48.79	46.61	6714.0	8.28
3	56.15	7704.0	-213.20	52.42	6791.0	164.20
4	47.14	6902.4	91.25	52.22	8935.0	42.54
5	54.45	7692.0	35.98	56.35	9379.0	1.80
6	56.96	9273.6	-172.68	63.40	9302.0	-28.76

Figure 8.11 shows three curves which are drawn using the CIUS' measurements (Original), the first parameters (LR) and the best fitting parameters (NLR) [Appendix 2].

These parameters being known, the gradient method is applied on the following function:

$$Y=f(t)=-\tau\ln\left(1+\frac{\varepsilon}{A}\right)+t_0 \qquad (8\text{-}4)$$

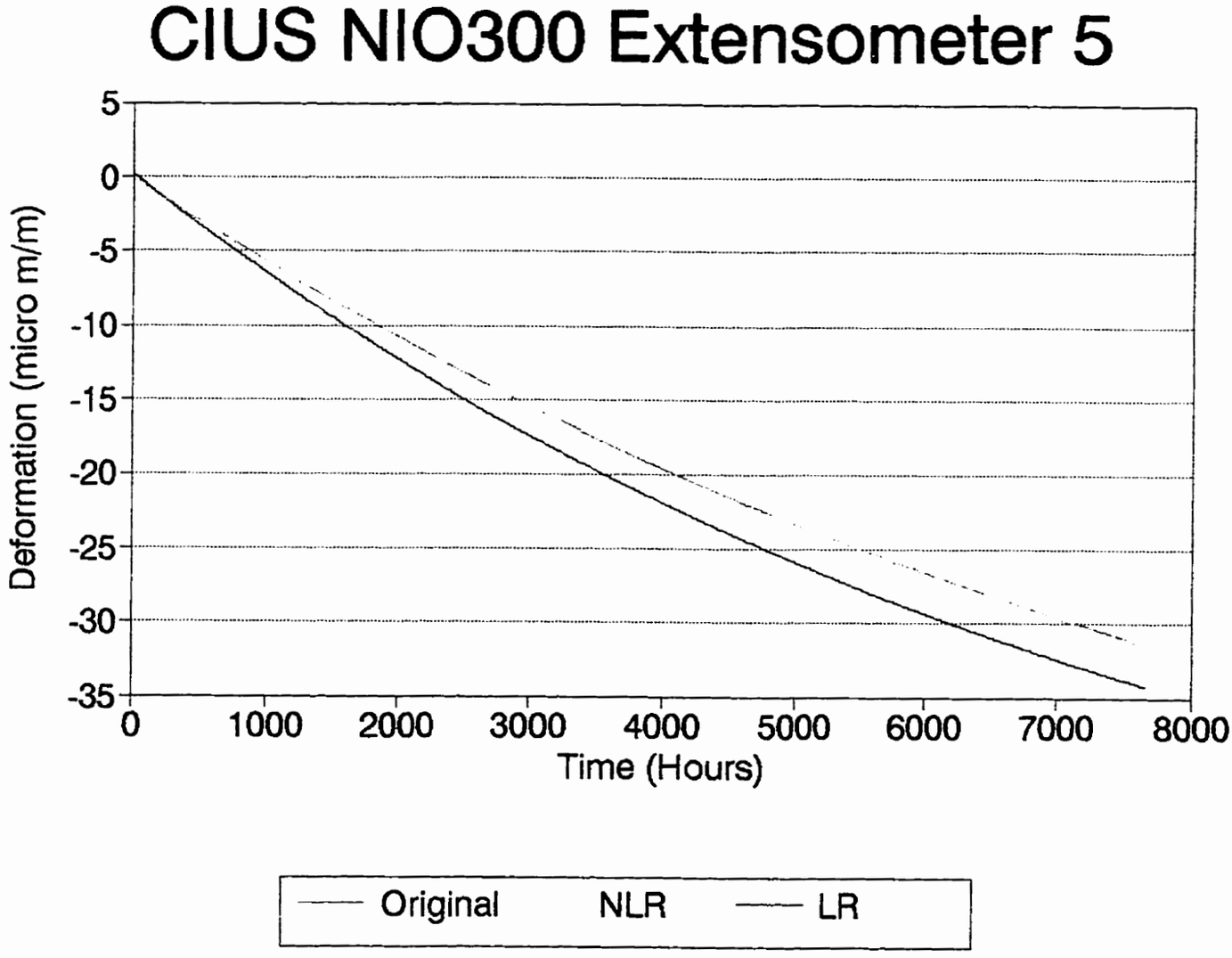

Figure 8.11 The recorded rate and predicted rate of deformation (extensometer No.5)

This is a relation between the measured deformations in terms of time which gives the desired linear adjustment in the gradient method.

Figure 8.12 shows the average line, drawn by the best fitting parameters for the CIUS NIO300 [Appendix 3]. The characteristic of these lines ($Y = b_1t+b_0$) are the slope's lines, the intercepts and the deviation of measurements around the lines (σ).

For applying the gradient method using these lines we consider the average value of deformation during the reference period and it can be presented in the following form:

$$Y = b_1^R t + b_0^R \qquad (8\text{-}5)$$

- the first test to know the rate of deformation in the past periods of time (reference period), must be done before starting the monitoring of our site. That means, knowing how deformations have been changing in the past. The result of this test can be the recognition of an ACCELERATING RATE of deformation or DECELERATING RATE of deformation or in the case that the rate of deformation has been constant the result will be NO MOVEMENT.

The gradient method starts in fact after this step by comparing the observed tendency during the period of controls with that of the reference period, stored in the system's memory.

The deformation during the i^{th} control period can be shown in the form of $Y = b_1^i t + b_0^i$ with a specified deviation (σ^i).

- the second test is a comparison between σ^i (deviation of measurements during the i^{th} control period) and σ^R (deviation of measurements during the reference period). In the case that σ^i is significantly greater than σ^R it can be the sign of either the defectivness of instruments (extensometers, CIUS) or the increase in the amplitudes of sudden jumps in the deformation process for example the sudden jumps of amplitude of deformation after blasting operations. (Figure 8.10).

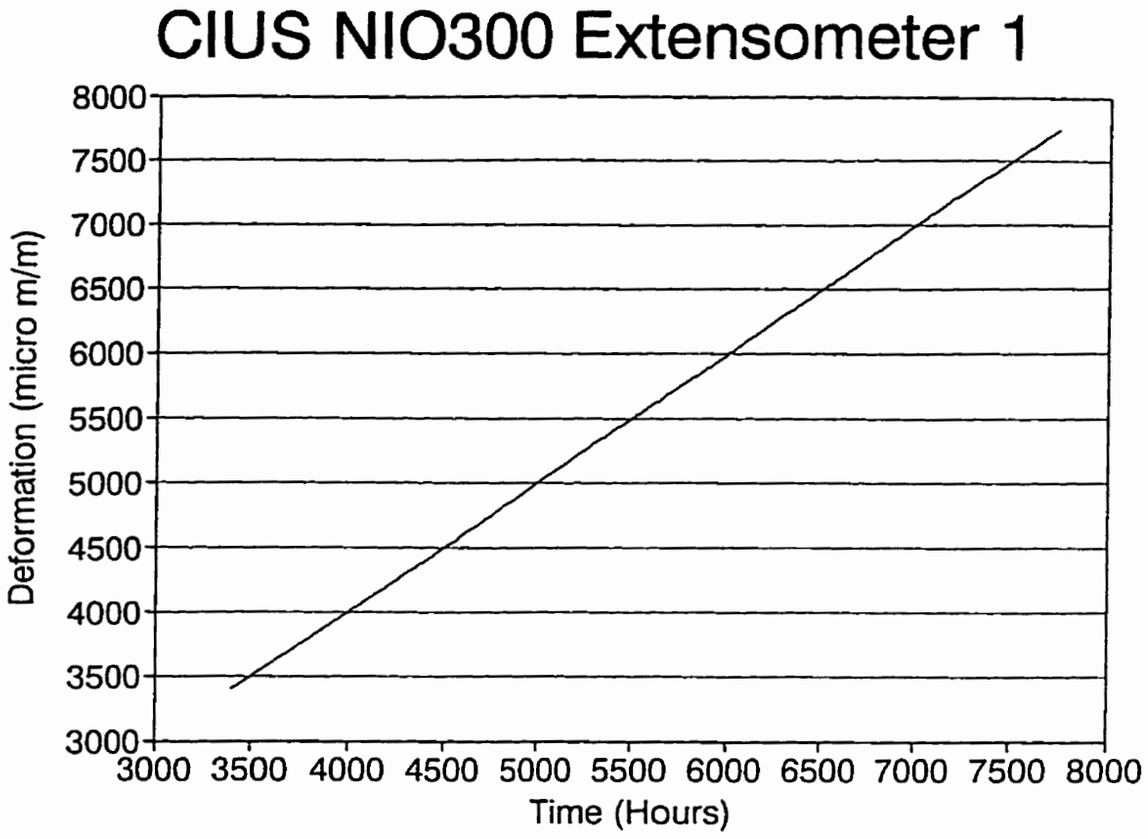

Figure 8.12 Linear adjustment of deformation rate in the CIUS NIO300 (extensometer No.2)

- the third comparison is carried out between the tendencies (slope test), by which we test the concavity of the deformation's curves. The slope test is carried out according to the criteria which were developed in chapter 6. In this test two slopes b_1^i and b_1^R are compared, if the difference between two values are greater than the confidence interval which has been already determined (chapter 6) the system warns the responsible by means of triggering the audio or/and visual warning signals. It means that there is an abnormal evolution of deformation (SLOPE WARNING). Otherwise, there is STABILITY and in this case the data are added to the previous data for determining the new line which will be considered as a next reference for the control period i+1:

$Y = b_1^{i+1}t + b_0^{i+1}$ with σ^{i+1}

In the case of abnormal evolution the line which has been characterized by $Y = b_1^i t + b_0^i$ will be considered as the reference for the period i+1.

This algorithm has been applied using the measurements of CIUS NIO300 and CIUS NIO600. The following parameters were chosen in programming of the gradient method using the measured deformation of these CIUS.

- duration of each control period T is 24hours
- duration of reference period Tr is 45 days (starting March 25, 1993)
- frequency of reading one measurements every 3 hours (Δt=3hours)

Figure 8.13 shows the linear adjustment of deformation in the pillar in which the CIUS NIO600 is installed [Appendix 3]. The rate of deformation on this curves is the slope of the curve and an acceleration of deformation is the difference between two consecutive rates. As it was mentioned earlier, at the end of each control period, we can compare the average rate of deformation during that control period with the average rate of deformation recorded during the previous periods, using the statistical tests which have already been elaborated. The interpretation of this statistical tests are done with two risks (probabilities).

- the risk which is called the first species risk (α), is reaching to conclusion that there is a difference between two rates of deformation recorded during two consecutive periods (reference period and control period), while in fact the detected deviation has been due to the random characteristics of measurements. This risk can be reduced either by opening the tolerance of rate deviation which is considered as an anomaly in rates, or by increasing the number of readings during each control period (chapter 6).

- the second risk which is called the second species risk (β), is defined as the chance of reaching to the conclusion that there is no great difference between two rates or at least it is not equal to the detected value. This risk can be reduced by closing the range tolerance of the accepted value of deviation rates.

These risks have two different meanings but they must be as small as possible. The consequence of the first risk (α) is an unjustified triggering of the warning signal. Obviously, in order that the measuring instrument be operable, practically this risk must be as small as possible. We choose the value of 0.001 for this risk.

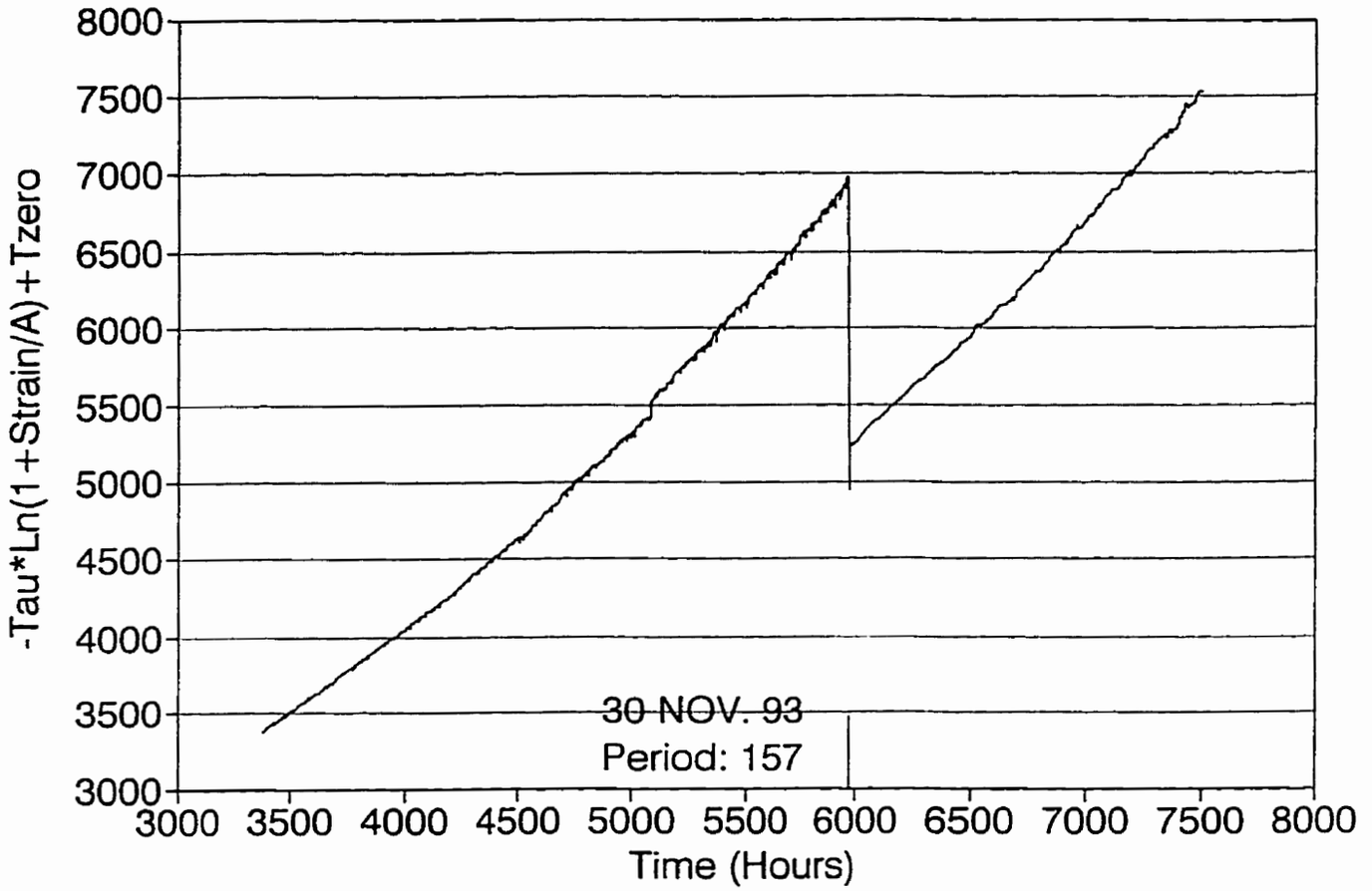

Figure 8.13 Linear adjustment of deformation rate in the CIUS NIO600

The consequence of the second risk (β) is that the system does not trigger the necessary warning, while in fact there is an abnormal evolution of deformation (anomaly). Its value may arbitrary be chosen. In the case of Niobec we chose the value of 0.001.

It must be mentioned that this interpretation technique can only guarantee the detection of an abnormal evolution of deformation which is real and significant of movements, the conformity

of this abnormal evolution with the collapse of structure is an experimental fact which may be verified in different cases, but its probability may not be assessed.

Emphasizing, the effectiveness of such method depends on the period between the opening's collapse and the tripping of the warning signal; this period can vary from nearly zero to several weeks depending on the stability condition of the monitored structures. In this first programming of gradient method for remote monitoring of the Niobec mine's stability, we chose a period of 24 hours (one day).

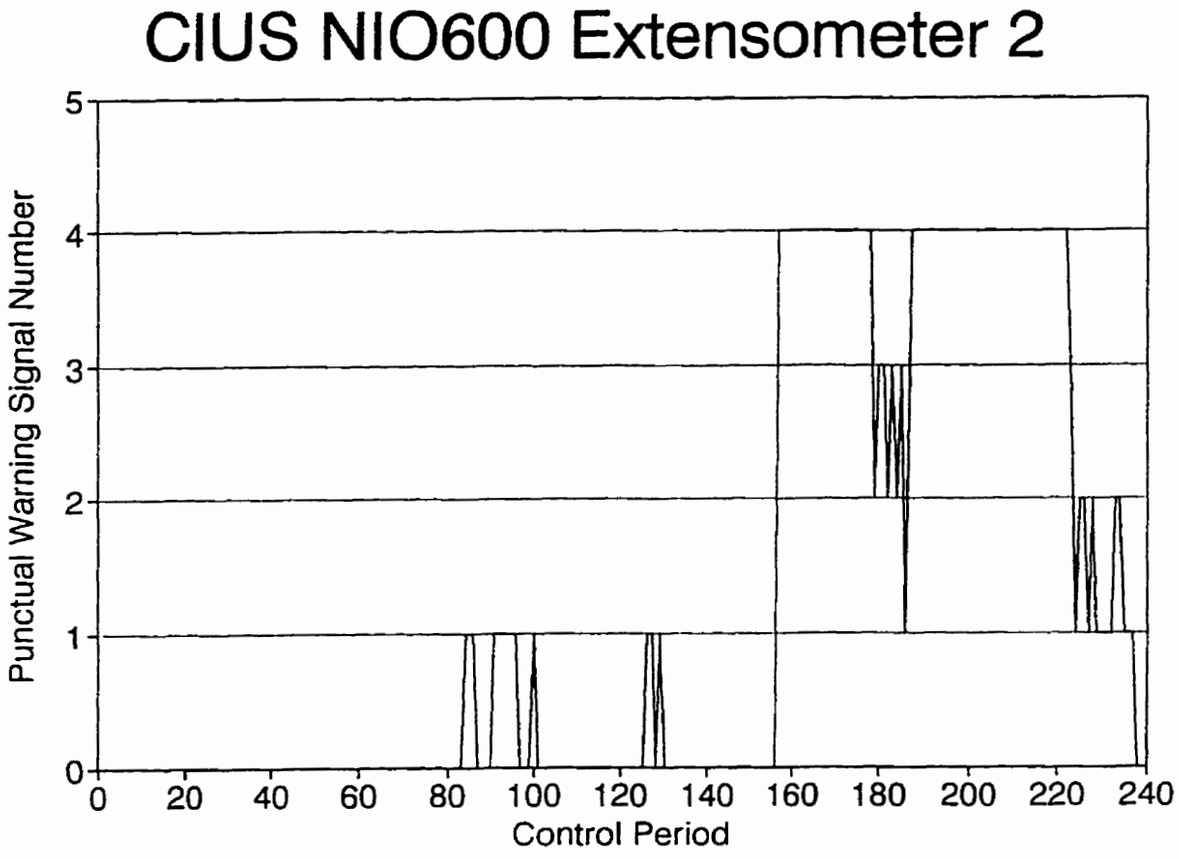

Figure 8.14 Number of punctual warning signals detected by the CIUS NIO600

As it has been already mentioned, the gradient method can be programmed in a warning system using two manners. In the first manner the warning system operates for detection of

anomalies at the end of the fixed period called control period, by comparing their tendencies with the recorded tendency of the reference period (previous periods), in the case of an anomaly, the warning system will trigger the audio or/and visual warning signals indicating the beginning of an accelerating rate of deformation in the monitored zone (SLOPE WARNING).

The second manner of programming in a warning system which operates upon the gradient method is the examination of each reading in order to verify whether or not it is in the confidence interval of the previous readings (punctual test). This warning is punctual and the test is realized after each reading. The punctual test (chapter 6) also is based on the statistical calculations for taking into account the risks α (the risk of triggering of an unjustified warning) and β (risk of concluding a stability while an instability is starting). Figure 8.15 shows a flowchart of the first version of programming the Détecteur d'Anomalies de l'Université de Sherbrooke (DAUS).

In the present version of remote monitoring programming using the CIUS' data, these two manners of programming have been considered. First application of the program using the measurements of the CIUS NIO300 and CIUS NIO600 proved the reliability of program for detection of the anomalies, by detecting the readings which parted from the confidence intervals of the reference lines. Figure 8.13 shows the rate of deformation in the CIUS NIO600 and Figure 8.14 shows the detected number of warning signals.

This method can be programmed for a group of sensors and it is generally assumed that the sensors possess the same variability. The level of warning signals triggering (audio or/and visual) depends on the duration of the abnormal evolution of deformation (acceleration) at the time. So it is possible to consider several levels of warning triggering.

8.4 Development of the remote monitoring system at Niobec

Along with the development of the CIUS, an electronic data acquisition system for signal processing at the source was developed [26]. Each CIUS can be directly connected to this

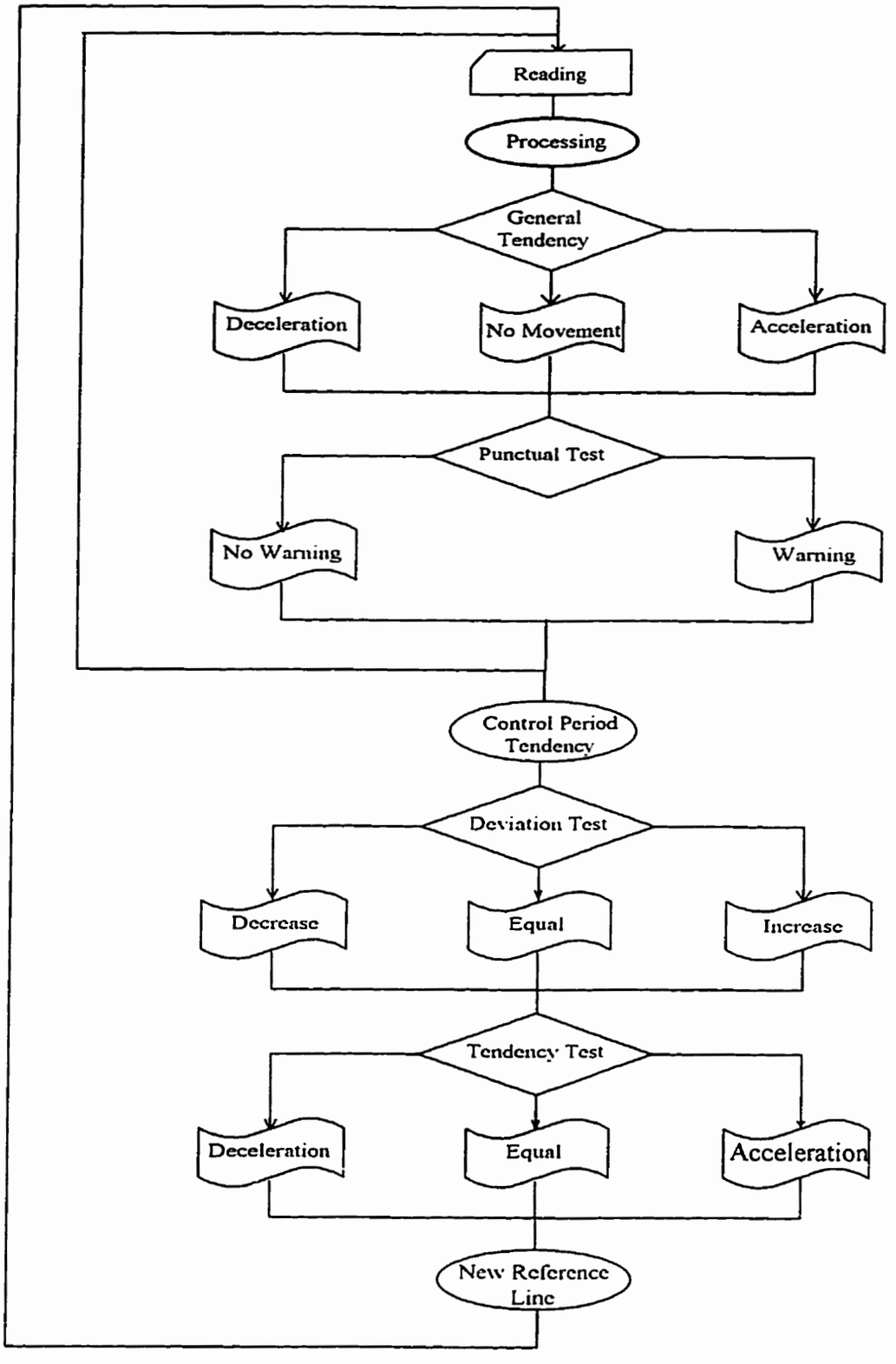

Figure 8.15 Programming of the warning system

electronic acquisition module called also intelligent system. The electronic module comprises three principal blocks acquisition, processing, and communications (Figure 8.16).

Indeed the monitoring of large civil and mining structures implies the acquisition of data over the long distances that separates the measuring instruments from the processing and acquisition center. These long distances introduce signal distortion and involve costs for cables that greatly exceed that of the monitoring system itself. To eliminate these problems, the signal should be digitized and processed at the source for transmission on a minimum of standard wires to a central computer. The developed electronic module at the Université de Sherbrooke offers acquisition, digitizing, verification of recordings (data management) temporary storing and communication with a central computer (PC type). It offers also the continuous remote monitoring of structures, regardless where they are located (Figure 8.16 and 8.19).

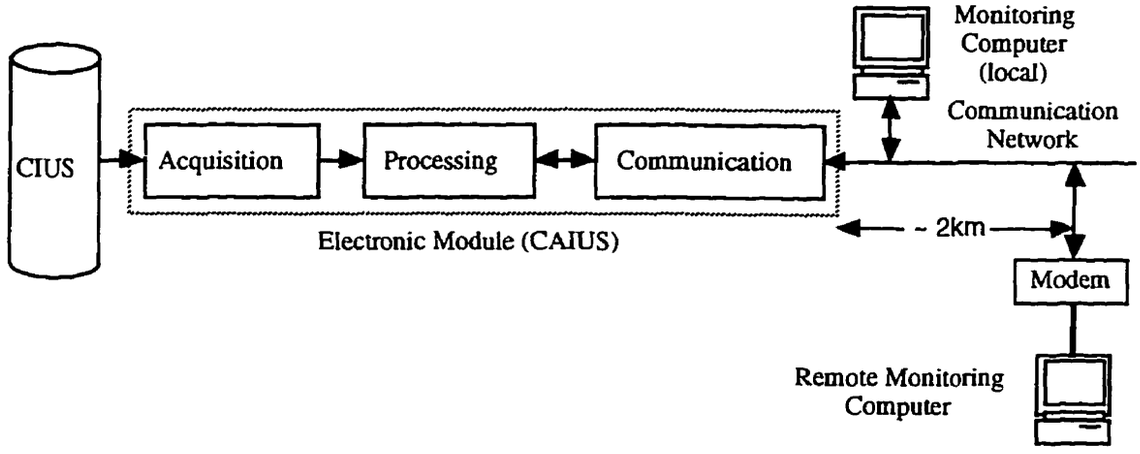

Figure 8.16 Remote monitoring using CIUS and CAIUS

The same computer can remotely manage and operate a minimum 255 electronic modules or 255 instrumented cylinder at the same time.

8.4.1 Description of the Electronic Module

The electronic data acquisition module (Figure 8.17) reads incoming data from the sensors (maximum of 16), processes it, and transmits it in digital form to a local or remote monitoring

computer. The same computer can manage and operate a maximum of 256 electronic modules. Each electronic module (Figures 8.17 and 8.18) comprises three blocks acquisition, processing, and communication [26].

- Acquisition

This block serves as the interface between the sensors and the processing unit. It amplifies, conditions, and digitizes the sent signals from the sensors.

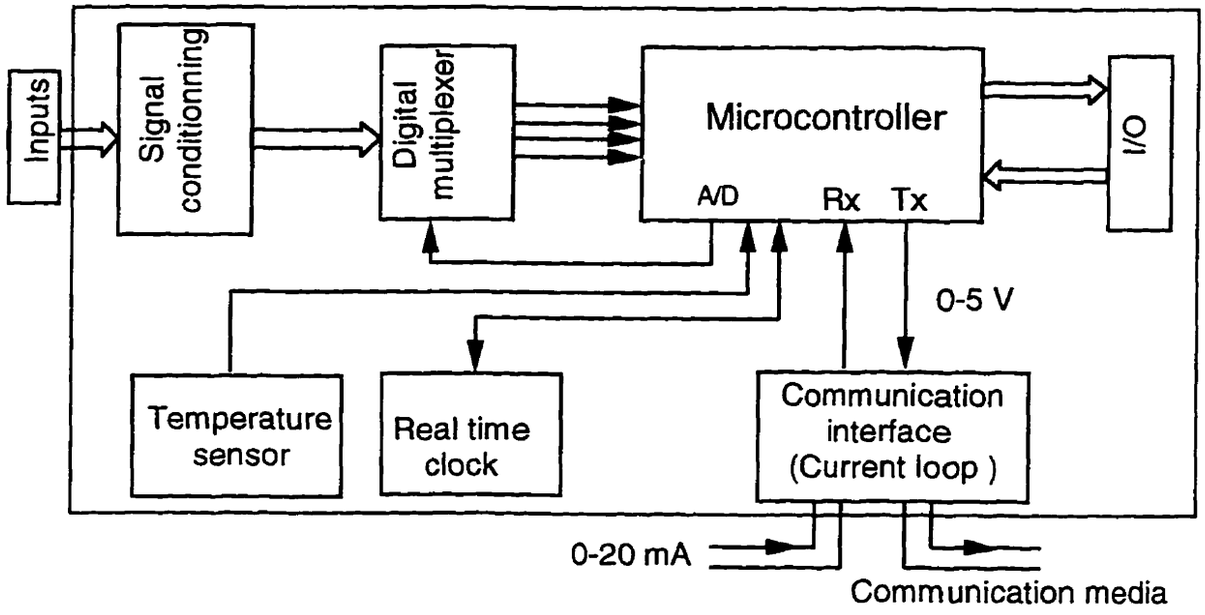

Figure 8.17 Electronic module system

- Processing unit

This is the main part of the electronic module. It is equipped with a micro controller which manages data from the acquisition block. It scans simultaneously all the sensors at a programmable rhythm and can read, process, and store the data from each sensor in a buffer or send it to the monitoring computer if the electronic module is being interrogated. This block also sends alarm signals to the monitoring computer.

Communication

The modules and the monitoring computer are linked via a ring network (Figure 8.18). Data pass in one direction through a two-wire series hookup. The monitoring computer serves as the principal station to which the electronic modules (secondary stations) are slaved. A command/response communication protocol is used, with the primary station sending command frames and the secondary stations answering with response frames.

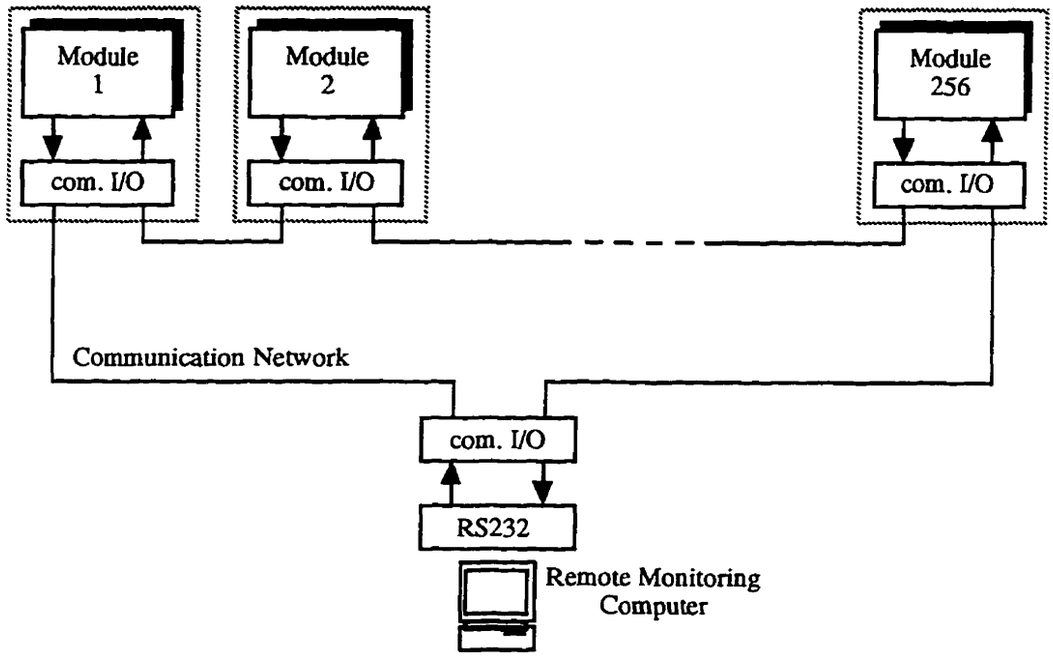

Figure 8.18 Ring topology

Unlike existing data acquisition systems, this electronic module simplifies the wiring by reducing the number of wires connected to the outside, It reduces the cost of installation operation and maintenance. It increases the reliability vis-à-vis the environment. The electronic module is designed, so that treatment and data management is done locally and at the source, for transmitting only the useful information to the outside.

The electronic modules are controlled using a computer and a communication software. The roles of the software are to provide the means for data reception/transmission, to collect data in a user accessible form via processing software, to monitor measuring equipment and to detect/locate any defect in the modules and, the series communication link up.

- Role of the Monitoring Computer

The electronic modules are controlled using a IBM PC™ compatible and communications software. The roles of the software are to provide the means for data reception/transmission, to collect data in a user-accessible form via processing software, to monitor measuring equipment, and detect/locate any defects in the modules and the series communication linkup.

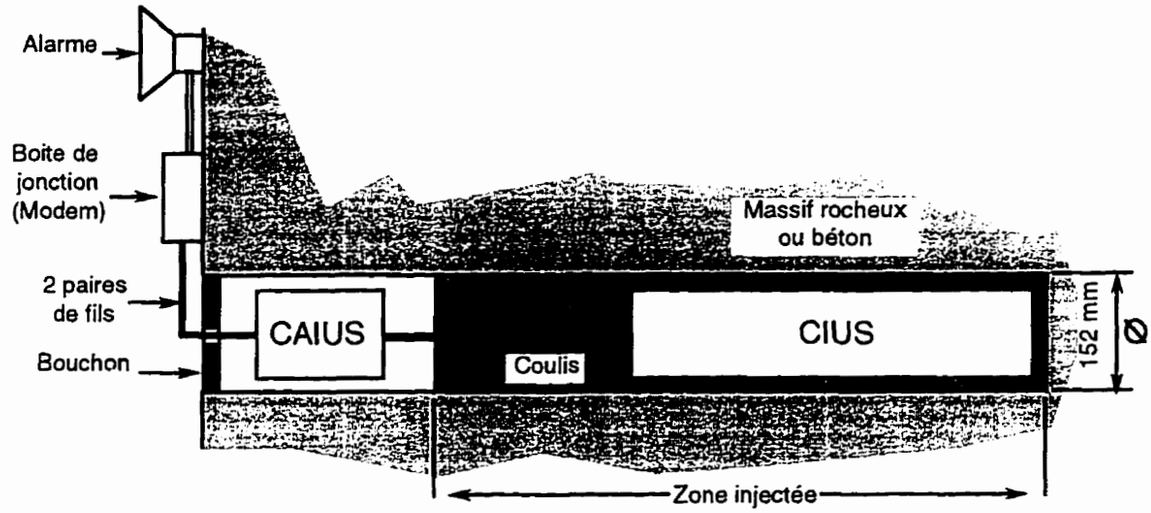

Figure 8.19 Warning system at Niobec

The final development of the remote monitoring system at the Niobec mine can be seen on Figure 8.19 in which the measuring instrument (CIUS) as well as the acquisition system and the warning system together are shown.

CHAPTER 9

9. CONCLUSIONS AND RECOMMENDATIONS

Objectives of the present study

The Niobec mine has been the first place in which the CIUS units were installed in a rocky medium, and has provided many opportunities for the ongoing research works for further development in the CIUS' technique as well as in the data interpretation techniques and in the data acquisition systems. Meanwhile, complying one of the most important aspects of monitoring, the preventive aspect, has been the principal goal of instrumentation at Niobec, where the excessive variation of stresses and deformation may have the direct and important effects on the stability of the productive stopes and pillars as well as on the safety of the personnel and consequently on the productivity and profitability of the mine.

The ability of the CIUS in the detection of excessive stress as well as anomalous deformation response of ground to the mining activities (great blasting operations, extension of excavations, ...) in the rugged conditions at this mine was demonstrated. This ability and the development of a data acquisition system at the Université de Sherbrooke (CAIUS) which makes possible an automated remote monitoring of underground structures in the real time (acquisition, interpretation, processing and management of data, anomaly detection, warning triggering) according to the desirable rhythm and program, has led to the idea that an instability preventive model can be developed to implant in the system.

A probabilistic instability preventive model was developed in which the reliability of remote monitoring system in making decision, regarding the triggering warning signals has been considered. This is the most important part of programming in the programmable systems such as a warning system.

The main objective of this study "feasibility study of the stability remote monitoring of underground structures by means of deformation measurements of the CIUS" showed the

possibility of programming a programmable rock failure warning system based on the gradient method. Meanwhile, it may be told that before applying this model and the final realization of a reliable stability remote monitoring, several developments and works must be conducted in the software part of the system and also in the hardware.

Software development

In the software part of system, the first programming of the gradient method using the CIUS' data (CIUS NIO300, CIUS NIO600) showed the need for the subroutines and programs such as a series of data treatment software in order to filter out the data and eliminate the noises.
The final realization of a reliable continuous remote monitoring needs the implantation of the auto-regressive model in order that the system be able to determine the exact parameters of regime of deformation in the real time.

Hardware development

Considering the hardware link up which consists of the measuring instruments (CIUS) and the acquisition system which includes all the related parts such as the read-out devices, acquisition devices, the wiring, connections and the programmable controller some matters must be considered in the future studies.

Measuring instrument

Regarding the CIUS or any other measuring instrument which is linked to a remote monitoring system and supposed to monitor the stability of mine structures, there are several subjects and possible developments to be considered during the future studies.

The most important characteristic of the mining works are depended on their nature. One of these characteristics may be defined by the mobility of zones in which the mining activities are concentrated which changes during the prescribed functional operation period of a mine.

Considering the productivity period of an underground mine such as Niobec which may be 20-50 years during which the maximum possible volume of the ore body must be extracted. During this relatively long period of time, the exploitable ore body is divided into several zones in different depths and using several stopes. Regarding this characteristic the following points must be considered in the future development of the CIUS.

- The instrument must have dimensions which make it possible its installation in different locations of mine. Therefore the studies must be conducted to miniaturize the CIUS. A study may be conducted for an instrument which is smaller, lighter and more mobile which ease for transportation.

- From the economic point of view, a measuring instrument which is supposed to be used at mines must be either recoverable after first installation in a location for another installation in the new zone or the instrument should have a reasonable price so that it can be installed in all the necessary locations of the mine. This is the most critical problem in the CIUS which must be considered in its future development.

Another important characteristic of the mining works is their rugged environments where the risks of damage to the instruments is relatively high. In this connection, the following points must be considered in the future studies in the development of the CIUS or any other instrument.

- The robustness of instruments and lead out connections must be considered in order to protect them in the harsh environments of mines. This has been already considered in CIUS and it must also be considered in lead out connections (wiring). However with the development of the CAIUS this problem will most be solved.

Complementary studies

An essential and important complementary work which must be conducted in this area is the reliability study of the remote monitoring system, considering all its components (measuring instruments, acquisition and data processing, decision making programs,...).

Finally, an effective remote monitoring in a mine depends originally on the reliability of the system. Further it depends on the possession of a good point of view and engineering knowledge of mining problems in choosing the key locations in mine structures to be instrumented. So a close collaboration must be established between the instrumentation group and mining engineers during future installations.

REFERENCE

[1] Ballivy, G., Saleh, K., Bois, A.P. (1989) Instrumentation d'un piller de la mine de Niobec par le cylindre instrumenté. The Laboratory of Rock Mechanics and Applied Geology of the Université de Sherbrooke, Technical Report, GR-89-11-2, 43 p.

[2] Ballivy, G., Benmokrane, B., Poulin, R., Saleh, K. (1990) Une nouvelle technique d'inclusion pour la mesure à long terme des déformations dans des barrages en béton. Revue canadienne de génie civil, Vol. 17, No. 6, pp. 919-930.

[3] Ballivy, G., Saleh, K., Bois, A.P., Ghorbal, A., Hajiabdolmajid, V. (1995) Mesure des déformations et des variations de contraintes des piliers des mines dans des conditions statique et dynamique. Proc. of Rock Mechanics and Strata Control Session, pp. 267-276, 97th CIM Annual Meeting, Halifax, Canada.

[4] Ballivy, G., Bois, A.P., Hajiabdolmajid, V., Saleh, K. (1995) Auscultation de la mine Niobec: une méthode de conception coherent. Proc. of the 8th International Society of Rock Mechanics Congress, Vol. 2, pp. 521-526, Tokyo, Japan.

[5] Barous, S. (1981) Le Syaleb ou comment prévoir les éboulements miniers? Revue de l'Industrie Minérale, Les techniques, Vol. 9, No.81, pp. 669-77.

[6] Beieniawski, Z.T., Maschek, R.K. (1975) Monitoring the behavior of rock tunnels during construction. The Civil Engineering in the South Africa, Vol. 17, No. 10, pp. 255-264.

[7] Beieniawski, Z.T. (1984) Rock mechanics design in mining and tunneling A.A.Balkema, Rotterdam.

[8] Blake, W., Leighton, F. (1970) Recent development and applications of the microseismic method in deep mines. Proc. of 11th Symp. on Rock Mech. Berkeley, New York, AIME, pp. 429-443.

[9] Boresetto, M., Fanalli, M. (1991) An application of Voight empirical model for the prediction of soil and rock instabilities Landslides, Bell (ed.) Balkema, Rotterdam, pp. 335-341.

[10] Cornelius, R. R. (1992) Feasibility study for the materials science approach to volcano eruption prediction. Ph. D. Thesis in Geosciences, The Pennsylvania State University, University Park.

[11] Cornelius, R. R., Scott, P. A. (1993) A materials failure relation of accelerating creep as empirical description of damage accumulation. Rock Mechanics and Rock Engineering, Vol. 26, No. 3, pp. 233-252.

[12] Cornelius, R. R., Voight, B. (1989) Determination of eruption-prediction constants for accelerated creep or seismicity. Geol. Soc. Amer. Abst. Programs, Vol. 21, No. 13.

[13] Cornelius, R. R., Voight, B. (1990) Feasibility of material failure approach to eruption prediction for Mount St. Helens, 1985 and 1986. EOS Trans. Amer. Geophys. Union 71, 1693.

[14] Crouch, J.L. (1974) Analyses of rock bursts in cut-and-fill stopes. AIME Transactions Vol. 256, pp. 298-302.

[15] Cruden, D. M., Masoumzadeh, S. (1987) Accelerating creep of the slopes of a coal mine. Rock Mechanics and Rock Engineering Vol. 20, pp. 123-135.

[16] Dejean, M., Josien, J.-P. (1981) Télésurveillance des excavations-Analyse décision d'une télésurveillance-Application au cas du stot du village de Rochonvillers. Rapport Cerchar 79.76.2530, 110, 39 p.

[17] Dejean, M., Schwartzmann, R. (1981) Les excavations souterraines à faible profondeur - Cinq ans d'expérience dans l'évolution et la surveillance de leur stabilité, Advanced Tunnelling Technology and Subsurface Use, Vol. 1, No. 2, pp. 133-137.

[18] Dutta, P.K. (1985) Some recent developments in vibrating wire rock mechanics instrumentation. 26th United States symposium on rock mechanics, Rapid City, Vol. 2, pp. 1043-1054.

[19] Farmer, I.W. (1968) Engineering properties of rocks. London, Spon.

[20] Frantti, G. E. (1977) Seismissions and surface waves related to geological structures. Proc. of 1st Conf. on Acoustic Emission/Microseismic Activity in Geol. Struct. and Materials, Penn. State University, Clausthal, W. Germany, Trans Tech. Publications.

[21] Fukuzono, T. (1985) A new method for predicting the failure time of a slope. Proc., 15th Int. Conference and Field Workshop on Landslides, Tokyo, pp. 145-150.

[22] Gagnon, G. (1979) The St-Honoré Carbonatite Complex and its Niobium Deposits, Field Guide Book Lithology and Tectonic of Precambrian Rocks and Carbonatites from Saguenay Lac St-Jean, Geological Association of Canada, Québec, PQ, Canada, pp. 15-29.

[23] Gagnon, G., Gendron, L.A. (1977) The geology and current development of St-Honoré Niobium (Columbium) Deposits. Communication présentée à la 78th CIM Annual Meeting, Ottawa, Canada, 26 p.

[24] Gallant, A. R. (1975) Nonlinear Regression. The American Statistician, Vol. 29, No. 2. pp. 73-81.

[25] Gauthier, A., Gagnon, G., Bonneau, J. (1979) Le complexe de Carbonatite de St-Honoré: une nouvelle image. Communication prèsentée au Congrès AGC/AMC, Quebec, Symposium sur les Carbonatites.

[26] Ghorbal A., (1992) Développement d'un système d'acquisition de données pour l'auscultation des infrastructures (roche ou béton), Sherbrooke, Master Thesis, 79 p.

[27] Glories, P., Dejean, M. (1983) Télésurveillance des ouvrages de génie civil et miniers-Mise au point et essais du dispositif Cerchar à mine de Rochonvillerrs. Revue de l'Indusrie Miniérale-Les techniques, pp. 131-137.

[28] Gwyther, R. L., Gladwin, M.T., Hart, R.H.G. (1992) A shear-stain anomaly following the loma prieta earthquake. Nature, Vol. 356, pp.142-144.

[29] Hajiabdolmajid, V. (1994) Instrumentation de la mine Niobec à l'aide du Cylindre Instrumenté du l'Université de Sherbrooke (CIUS), Programmation des alarmes. The Laboratory of Rock Mechanics and Applied Geology, Sherbrooke University, Technical Report, GR-94-07-1, 14 p.

[30] Hartly, H.O., Booker, A. (1965) Non-linear least squares estimation, The Annals of Mathematical Statistics, Vol. 36, pp. 638-650.

[31] Hardy, H.R.Jr. (1977) Monitoring the stability of geological structures using near-surface micro-seismic transducers. Proc. of 1st Conf. on Acoustic Emission/Microseismic Activity in Geol. Struct. and Materials, Penn. State University, Clausthal, W. Germany, Trans Tech. Publications.

[32] Hawkes, I. (1975) Hydrofracturing stress measurements and the design of the Heimsk Creek Powerhouse. 16th Symp. on Rock Mech. Minneapolis, USA.

[33] Hawkes, I., Moxon, S. (1966) The measurement of in-situ rock stress using the photoelastic biaxial gauge with the core relief technique. Int. J. Rock Mech. & Min. Sci. Vol. 2, pp. 405-419.

[34] Hayashi, S. (1991) Forecasting occurrence time of slope failure Landslides. Bell (ed.) Balkema, Rotterdam, pp. 965-970.

[35] Herget, (1988) Stresses in Rock. A.A. Balkema, Rotterdam, Netherlands.

[36] Hoek, E., Brown, E.T.(1980) Underground excavations in rock, London, Institute of Mining and Metallurgy, 527p.

[37] Jaeger, J.C., Cook, N.G.W. (1969) Fundamentals of rock mechanics. London, Methuen.

[38] Jeremic, M.L. (1975) In situ stress measurements. Manuscript, University of Alberta, Edmonton, Canada.

[39] Jeremic, M.L. (1987) Ground Mechanics in Hard Rock Mining. A.A. Balkema, Rotterdam, Netherlands.

[40] Josien, J.-P. (1977) Surveillance de la stabilité d'une excavation par des mesures de déformation - Choix d'une méthode d'alarme. Annales des mines, Vol. 3, pp. 51-62.

[41] Kuroki, K., Ishikawa, K., Nishikawa, J. (1995) Forecast time and analysis of rupture mechanism using video-tape records for a rock failure of a cut slope. Proc. 8th international society of rock mechanics congress, Tokyo, Japan, pp. 399-402.

[42] Linde, A.T., Suyehiro, K., Miura, S., Sacks, I.S., Takagi, A. (1989) Episodic aseismic earthquake precursors. Nature, Vol. 334, pp. 513-15.

[43] Londe, P. (1973) The role of rock mechanics in the reconnaissance of rock foundations, water seepage in rock slopes and the stability of rock slopes. Quarterly Journal of Engineering Geology, Vol. 5, pp. 57-127.

[44] Ludovic, A. (1995) Logiciel d'analyse et d'interpretation pour le Cylinder Instrumenté de l'Université Sherbrooke, Technical Report GR-95-7-01, 29 p.

[45] Marquardt, D. W. (1963) An Algorithm for least-squares estimation of nonlinear parameters. Journal of Society of Industrial Application of Mathematics, Vol. 11, No.2, pp. 431-441.

[46] McCreath, D. (1975) Borehole insertion devices for stress determination. Report to Subcommittee of Rock Mechanics Instrumentation, Manuscript, ACRES Consulting Service, Toronto.

[47] McKavanagh, R.M. & R.A. Godsou (1978) Determination of design parameters and an automated rock noise location system for use in 11 level MICAF, Mount Isa Mines. Commonwealth Scient. and Ind. Research Organization, Division of Applied Geomechanics.

[48] Obert, L. (1977) The microseismic method. Discovery and early history. Proc. of 1st Conf. on Acoustic Emission/Microseismic Activity in Geol. Struct. and Materials, Penn. State University, Clausthal, W. Germany, Trans Tech. Publications.

[49] Obert, L., Duvall W.I. (1967) Rock mechanics and the design of structures in rock. New York, Wiley.

[50] Roy, D.W., Gagnon, G., Archambault, G., Thivierge, S. (1979) Tardi-tectonique de la Carbonatite de St-Honoré. Congres GAC/MAC, Quebec.

[51] Saito, M. (1969) Forecasting time of slope failure by tertiary creep. Proc. 7th International Conference on Soil Mechanics and Foundation Engineering, Mexico City, Vol. 2, pp. 677-683.

[52] Saito, M. (1980) Semi Logarithmic Representation for Forecasting Slope Failure. Proc. 3rd International Symposium on Landslides, New Delhi, Vol. 1, pp. 321-324.

[53] Schultz, M. (1982) The role of microseismic monitoring in the prevention of rockbursts. Engineering thesis, Laurentian University, Sudbury, Canada.

[54] Schwartzmann, R. (1987) Surveillance et télésurveillance des anciennes exploitations. Revue de l'industrie minérale-Mines et carrières-Les techniques, pp. 433-438.

[55] Schwartzmann, R. (1990) Surveillance et sécurité des ouvrages et des sites en génie civil et minièrs, Surveillance à long terme et télésurveillance des anciennes exploitations abandonnées. Nancy, 10 p.

[56] Schwartzmann, R., Bivert, B. (1986) Surveillance des carrières souterraines abandonnées par des mesures de déformation. Revue de l'Industrie Minérale-Mines et Carrières-Les techniques, pp. 293-303.

[57] Singh, D.P. (1975) A study of creep of rocks. Int. J. Rock Mech. Min. Sci. & Geomech. Abstr.

[58] Tilling, R. I. (1988) Lessons from materials science. Nature Vol. 332, pp. 108-109.

[59] Unembu, D. (1989) Instrumentation de barrage en béton en service par la technique d'inclusion instrumentée et injectée, Sherbrooke, M.Sc. Thesise, Université de Sherbrooke, 102 p.

[60] Vallée, M. Dubuc, F. (1970) The St-Honoré Carbonatite Complex, Quebec. CIM transactions, Vol. LXXIII, pp. 245-258.

[61] Varnes, D. C., (1983) Time-Deformation Relations in Creep to Failure of Earth Materials. Proc. 7th South East Asian Geotechnical Conference, Vol.2, pp.107-130.

[62] Voight, B. (1988): A method for prediction of volcanic eruptions. Nature Vol. 332, pp. 125 130.

[63] Voight, B. (1989) A relation to describe rate-dependent material failure. Science Vol. 243, pp. 200-203.

[64] Voight, B., Nebil, O., Kirby, Y. (1989) Deformation and failure-time prediction in rock mechanics. Proc. of 26th US symposium rock mechanics congress, pp. 919-929.

[65] Voight, B., Cornelius, R. R. (1991) Prospects for eruption prediction in near real time. Nature Vol. 350, pp. 695-698.

[66] Yu, T. R. (1983) Rock mechanics to keep mine productive. Can. Min. J., pp. 61-66.

[67] Zavodni, Z. M., Broadbent, C. D. (1980) Slope Failure Kinematics. Bulletin Canadian Institute of Mining, Vol. 73, No. 816, pp. 69-74.

[68] Zienkiewicz, O.C. (1968) Continuum mechanics as an approach to rock mass problems. In Rock mechanics in engineering practice, London, Wiley.

APPENDIX 1

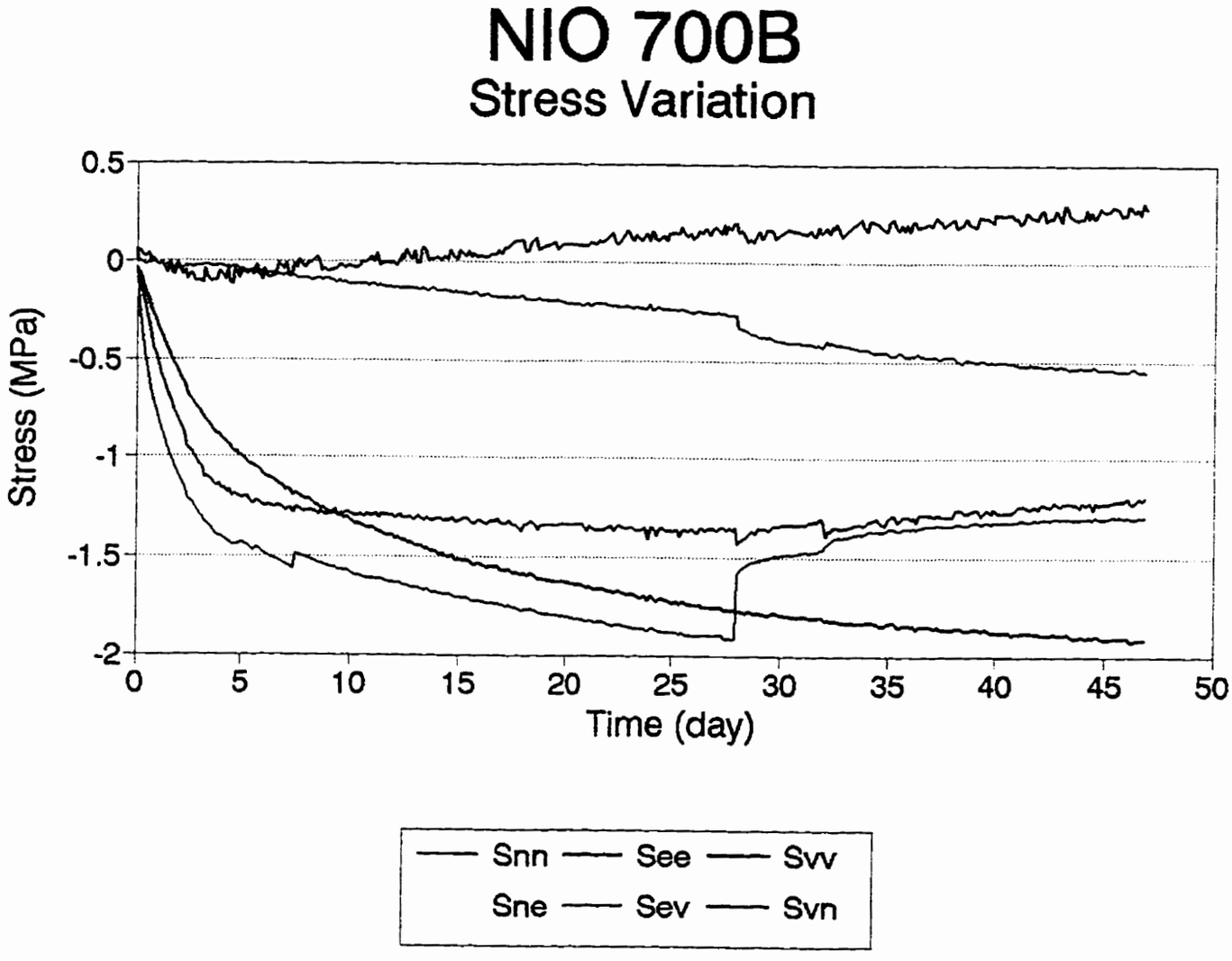
NIO 700B
Stress Variation
Stress (MPa)
0.5
0
-0.5
-1
-1.5
-2
0
5
10
15
20
25
30
35
40
45
50
Time (day)
Snn
See
Svv
Sne
Sev
Svn

NIO 700B
Deformation Variation

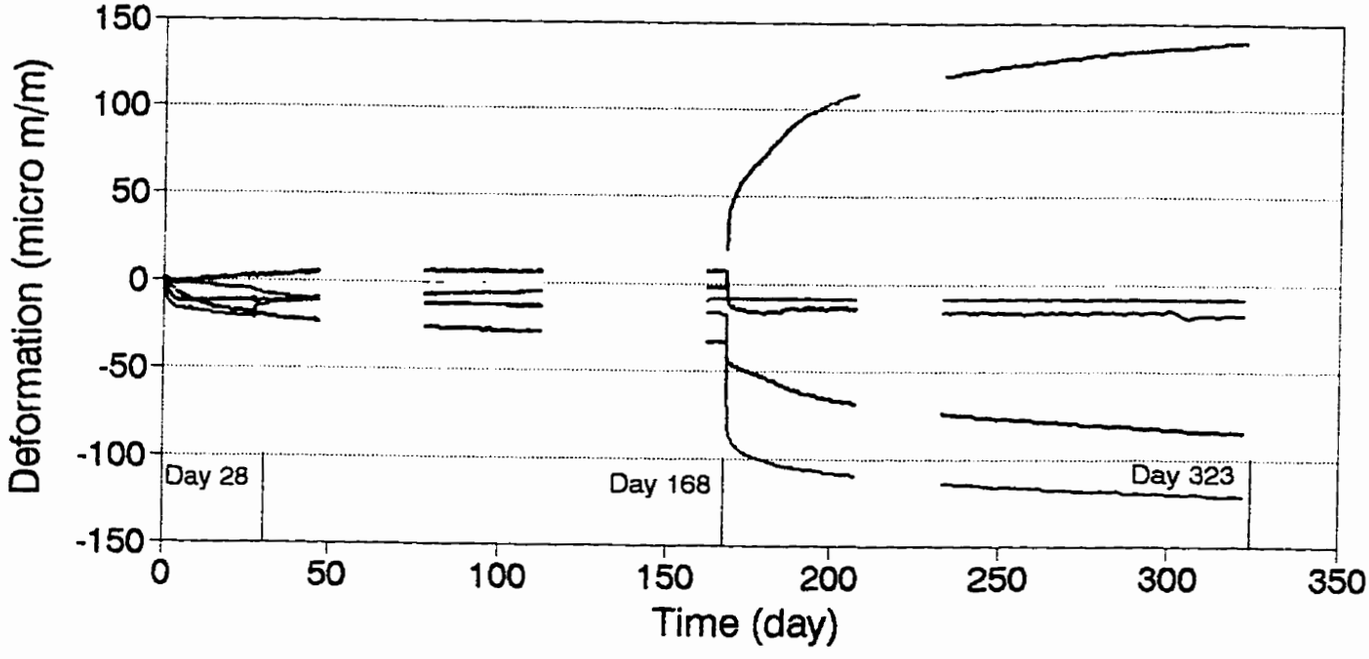

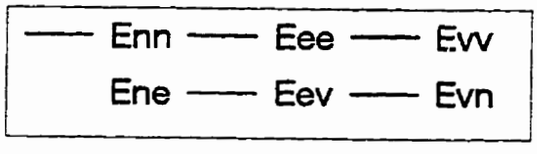

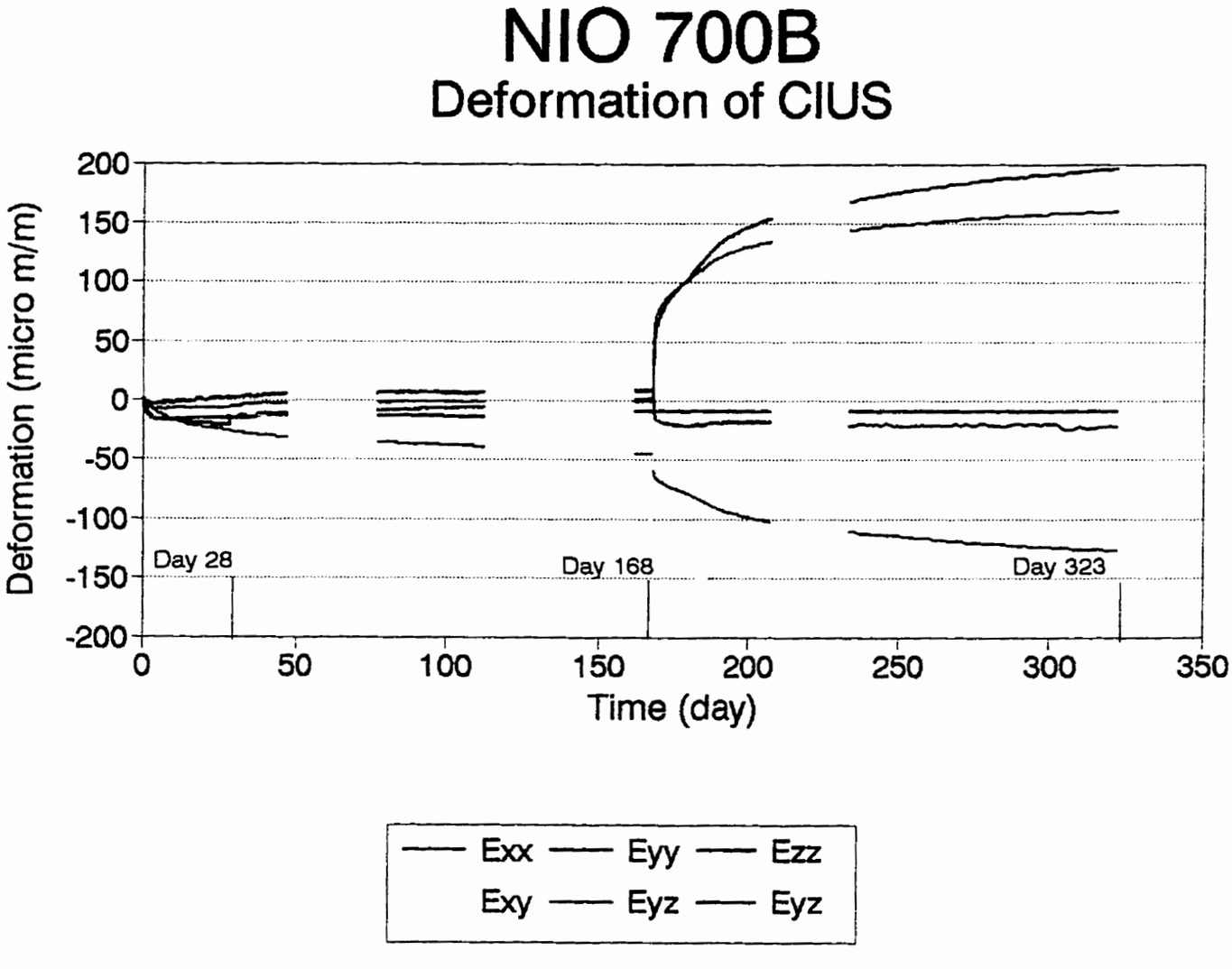
NIO 700B
Deformation of CIUS
Deformation (micro m/m)
200
150
100
50
0
-50
-100
-150
-200
Day 28
Day 168
Day 323
0
50
100
150
200
250
300
350
Time (day)
Exx
Eyy
Ezz
Exy
Eyz
Eyz

NIO 700B

Deformation of Extensometers

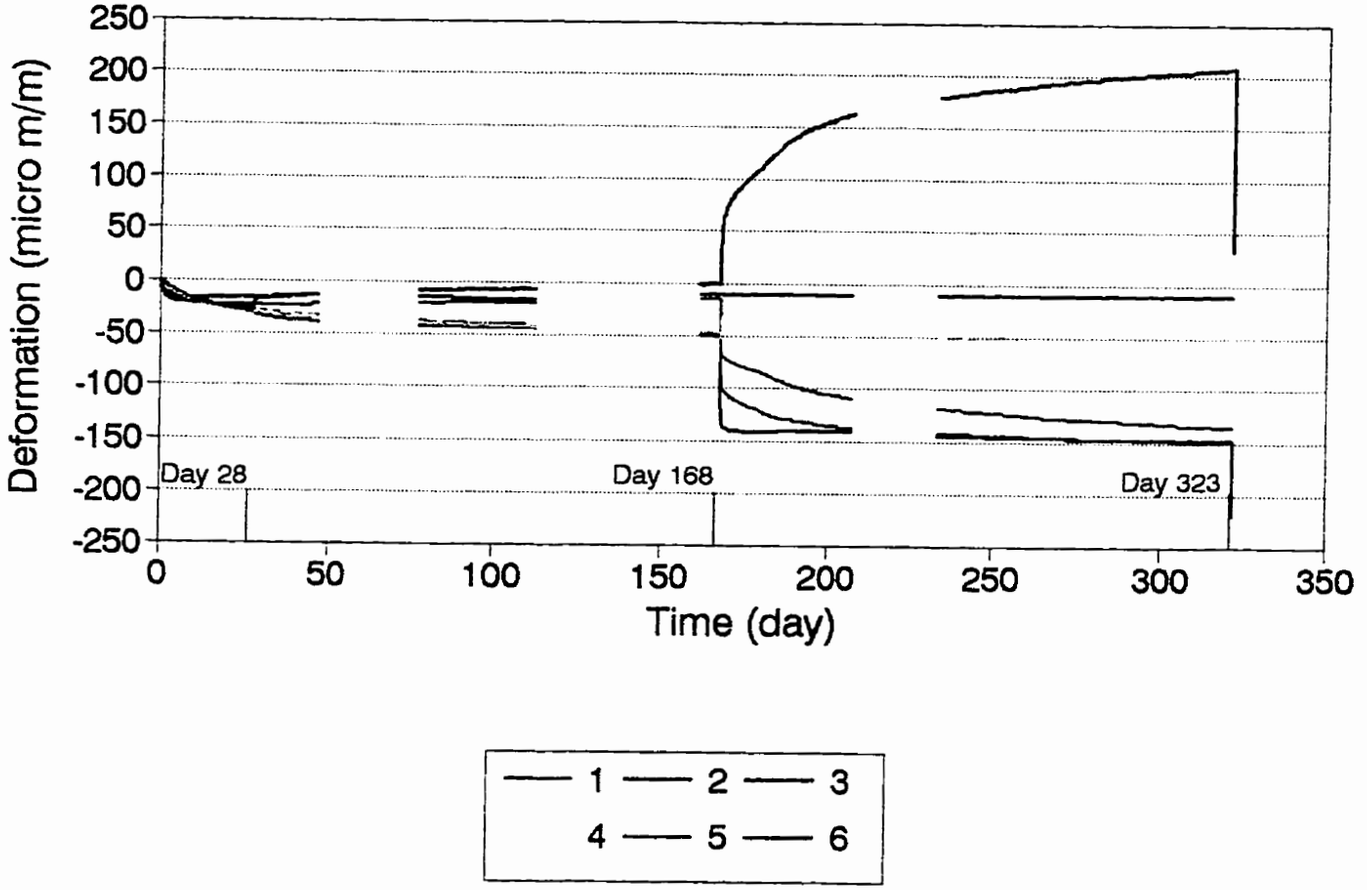

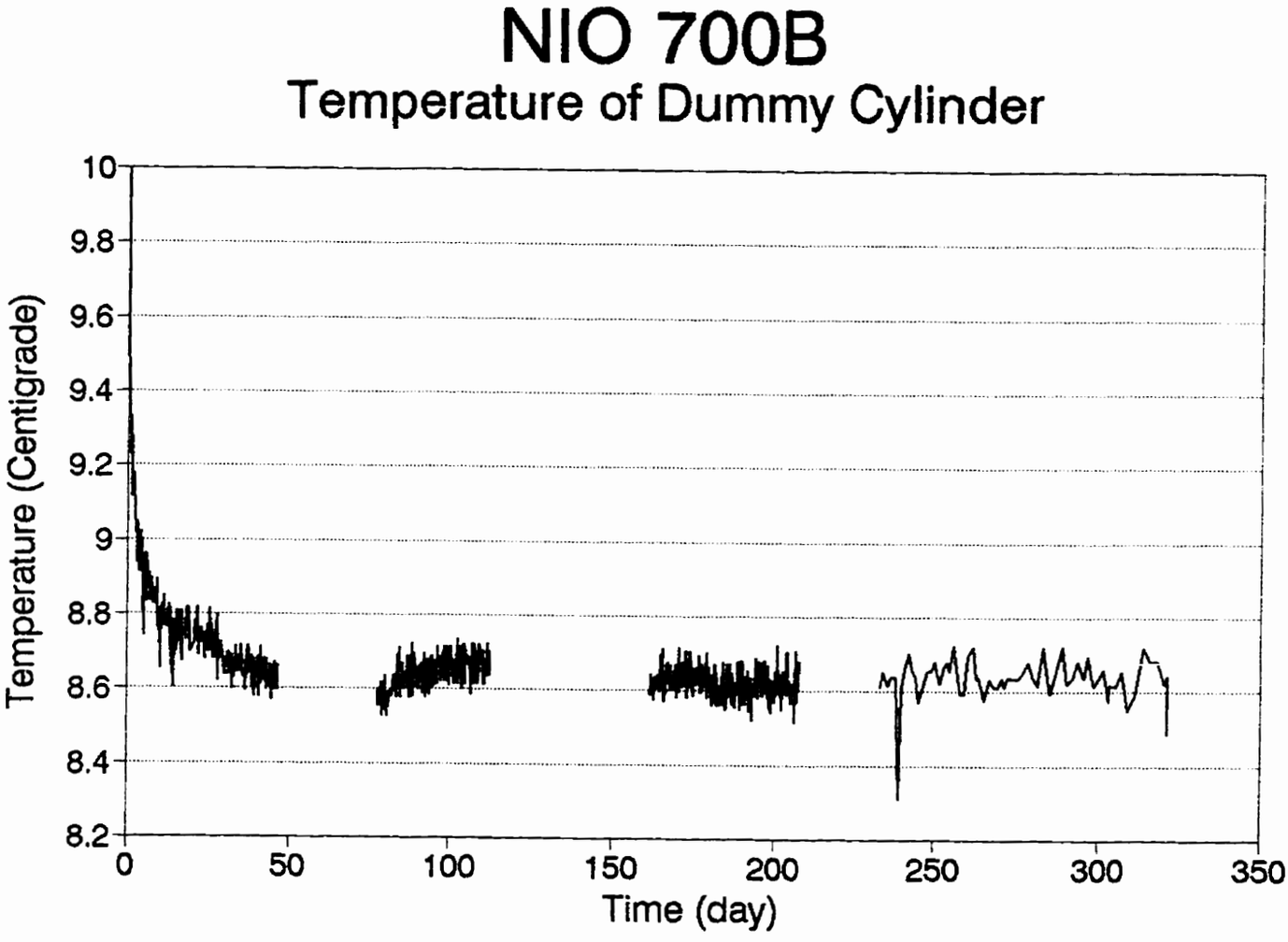
NIO 700B
Temperature of Dummy Cylinder
Temperature (Centigrade)
10
9.8
9.6
9.4
9.2
9
8.8
8.6
8.4
8.2
0
50
100
150
200
250
300
350
Time (day)

APPENDIX 2

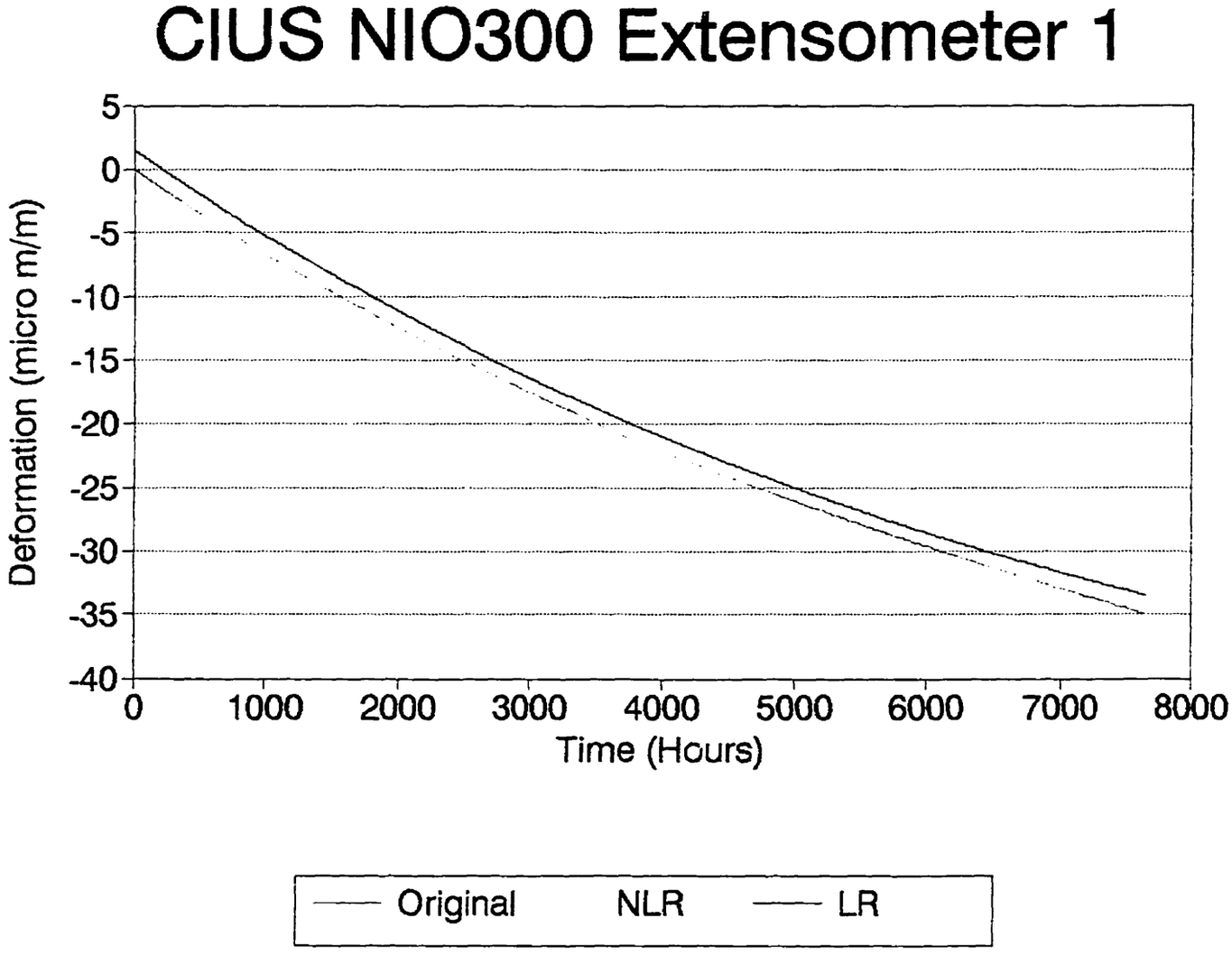
CIUS NIO300 Extensometer 1
Deformation (micro m/m)
5
0
-5
-10
-15
-20
-25
-30
-35
-40
0
1000
2000
3000
4000
5000
6000
7000
8000
Time (Hours)
Original
NLR
LR

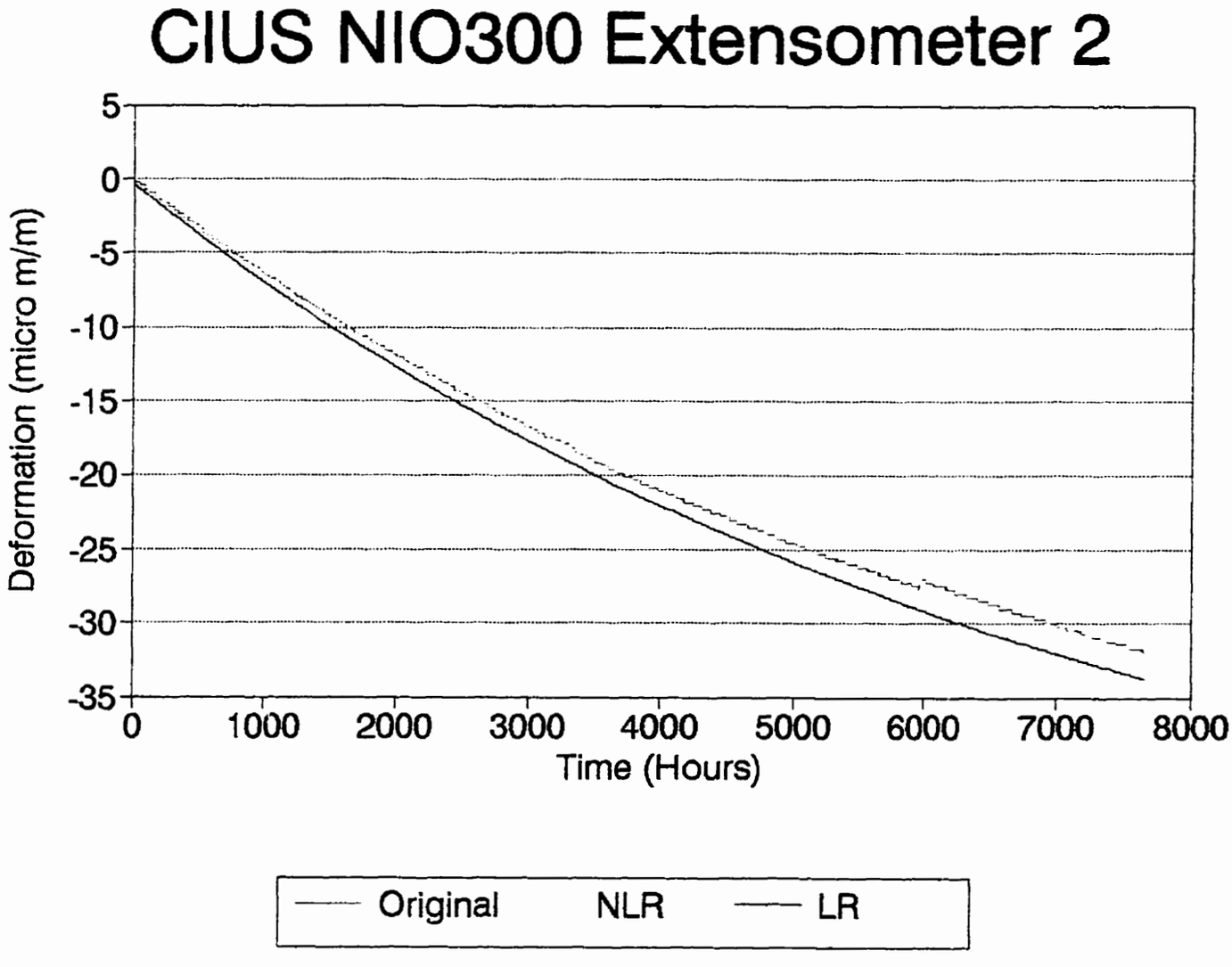
CIUS NIO300 Extensometer 2
Deformation (micro m/m)
5
0
-5
-10
-15
-20
-25
-30
-35
0
1000
2000
3000
4000
5000
6000
7000
8000
Time (Hours)
Original
NLR
LR

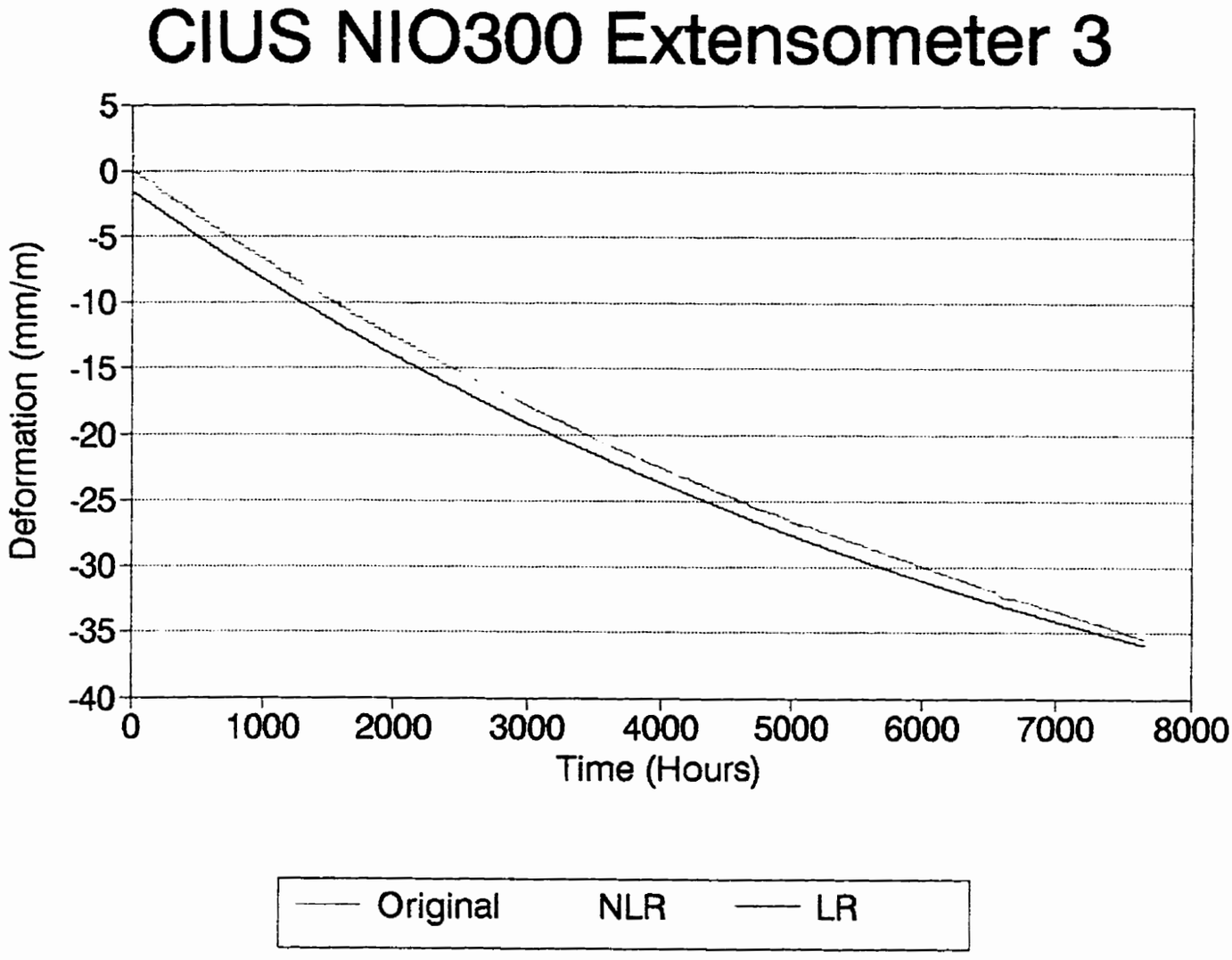
CIUS NIO300 Extensometer 3
Deformation (mm/m)
5
0
-5
-10
-15
-20
-25
-30
-35
-40
0
1000
2000
3000
4000
5000
6000
7000
8000
Time (Hours)
Original
NLR
LR

CIUS NIO300 Ext

0 000 2000 3000 4

Time (Hours)

Original N

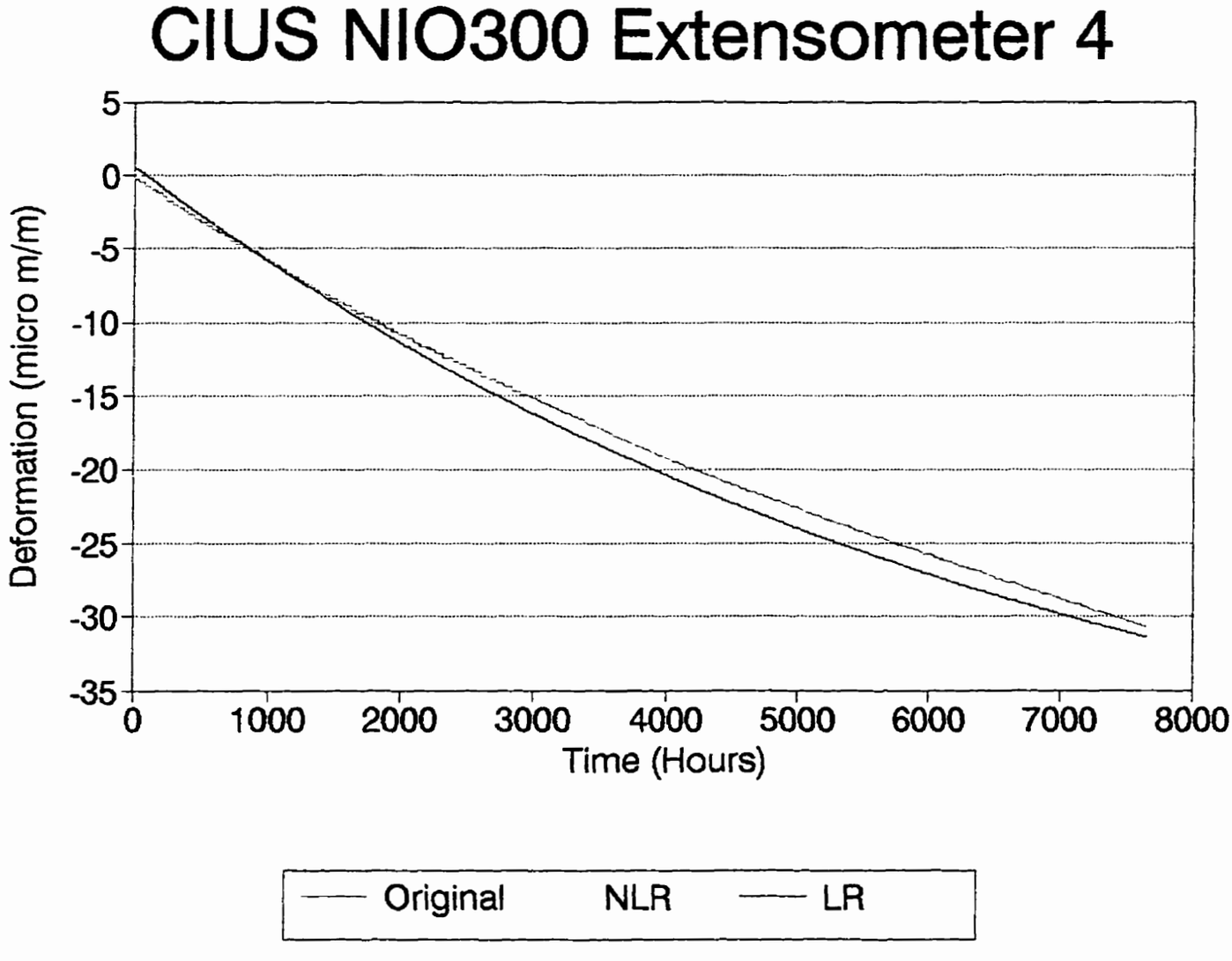
CIUS NIO300 Extensometer 4
Deformation (micro m/m)
5
0
-5
-10
-15
-20
-25
-30
-35
0
1000
2000
3000
4000
5000
6000
7000
8000
Time (Hours)
Original
NLR
LR

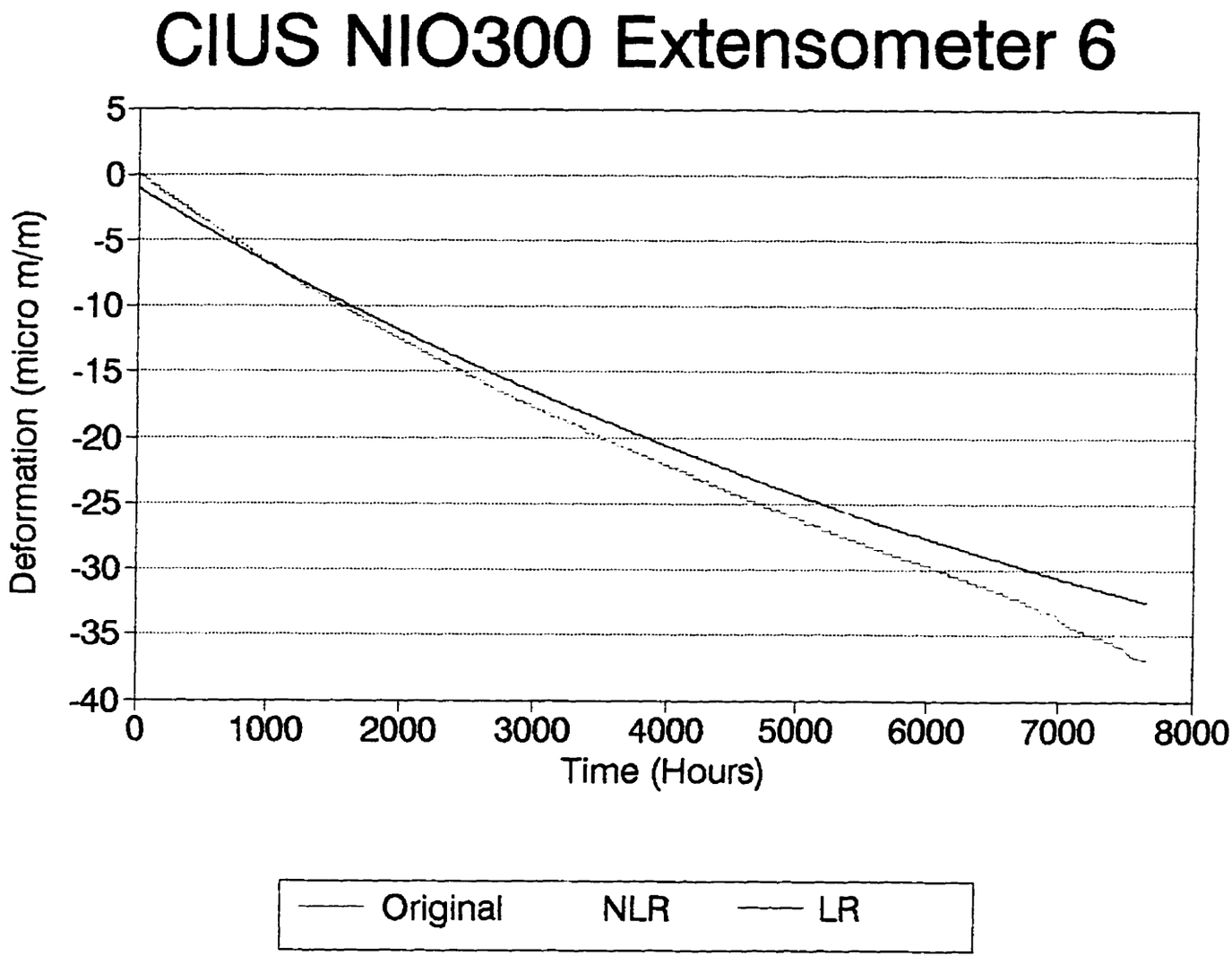
CIUS NIO300 Extensometer 6
Deformation (micro m/m)
5
0
-5
-10
-15
-20
-25
-30
-35
-40
0
1000
2000
3000
4000
5000
6000
7000
8000
Time (Hours)
Original
NLR
LR

APPENDIX 3

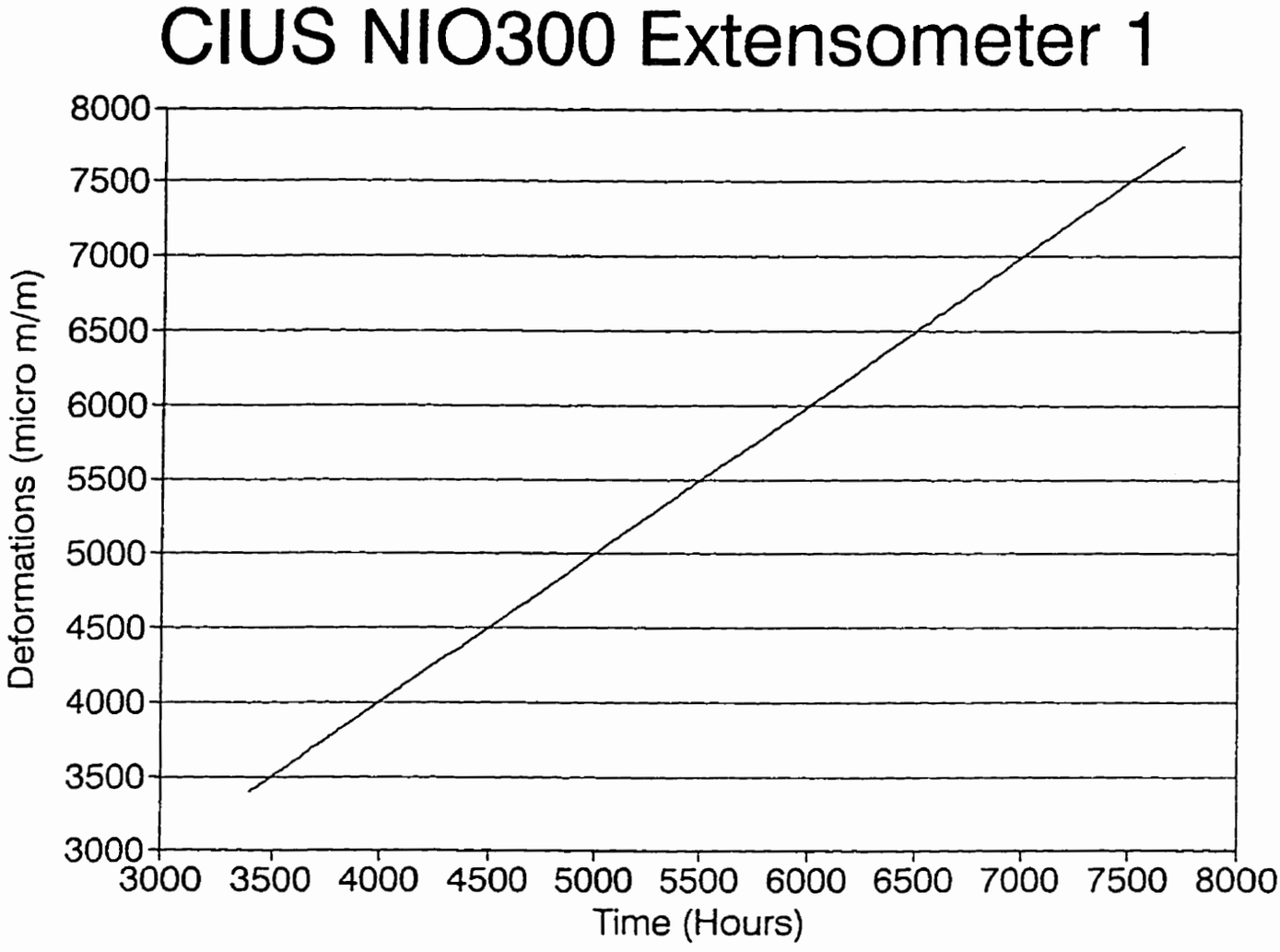
CIUS NIO300 Extensometer 1
Deformations (micro m/m)
8000
7500
7000
6500
6000
5500
5000
4500
4000
3500
3000
3000 3500 4000 4500 5000 5500 6000 6500 7000 7500 8000
Time (Hours)

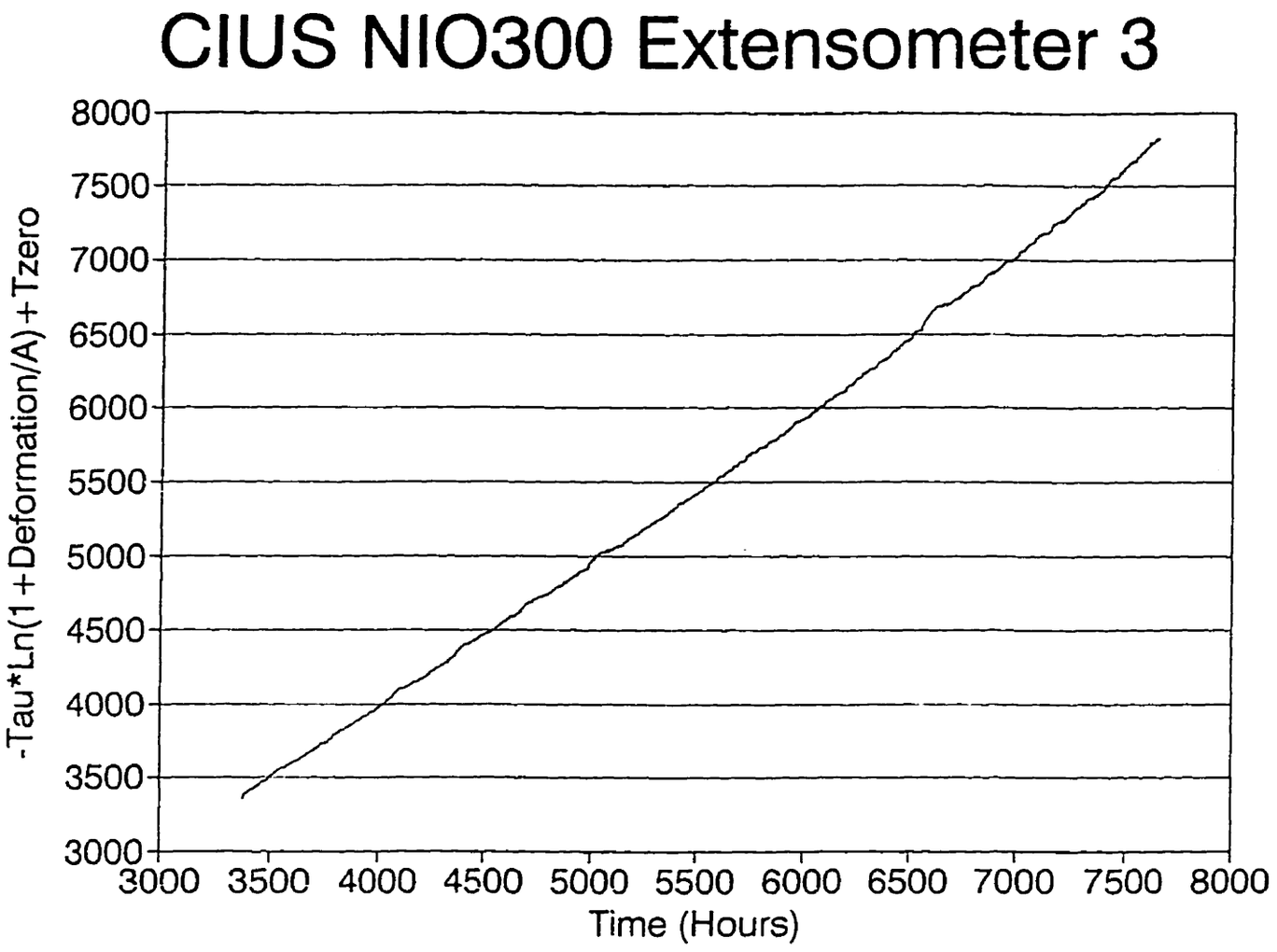
CIUS NIO300 Extensometer 3
-Tau*Ln(1+Deformation/A)+Tzero
8000
7500
7000
6500
6000
5500
5000
4500
4000
3500
3000
3000 3500 4000 4500 5000 5500 6000 6500 7000 7500 8000
Time (Hours)

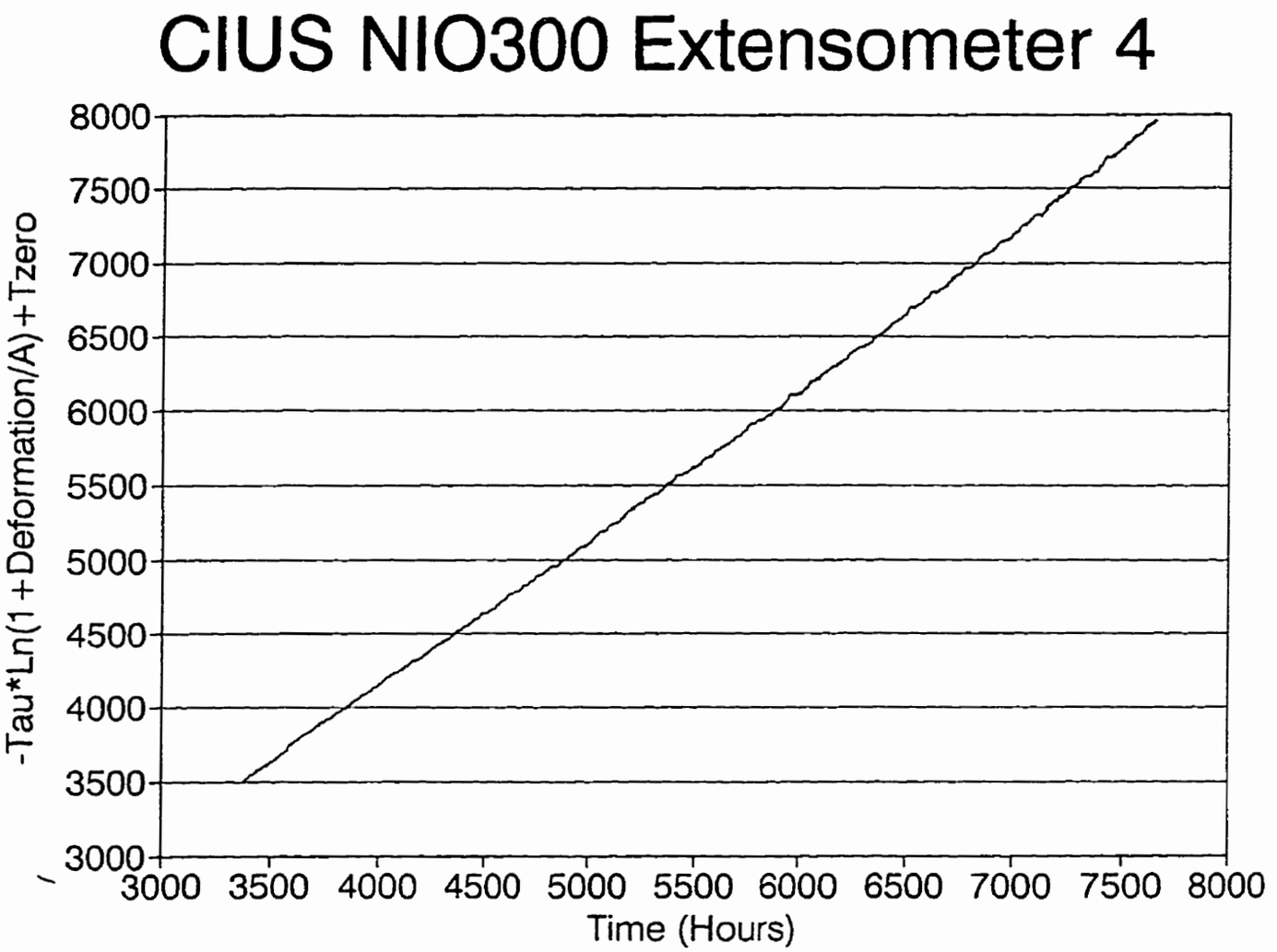
CIUS NIO300 Extensometer 4
-Tau*Ln(1+Deformation/A)+Tzero
8000
7500
7000
6500
6000
5500
5000
4500
4000
3500
3000
3000 3500 4000 4500 5000 5500 6000 6500 7000 7500 8000
Time (Hours)

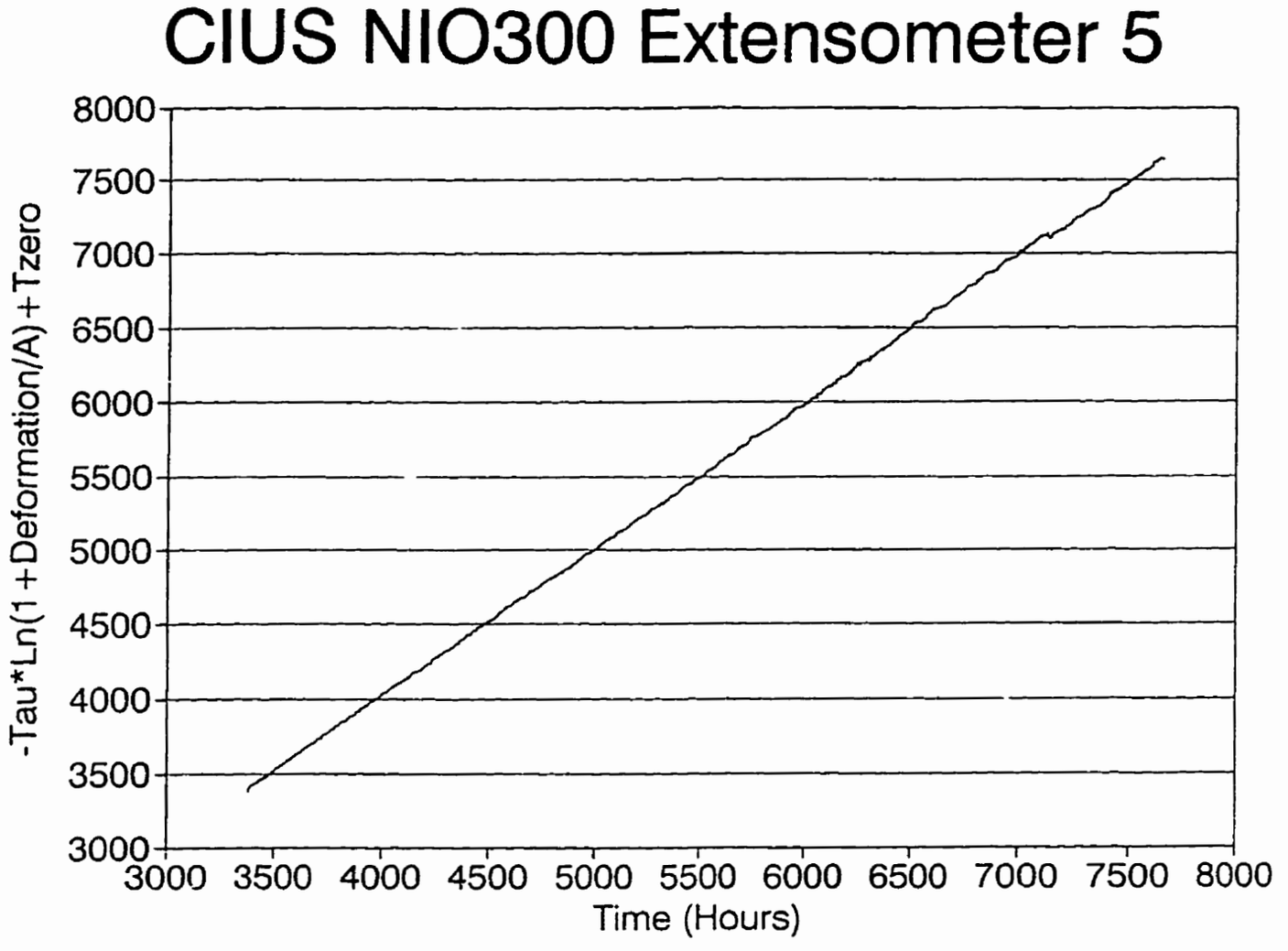
CIUS NIO300 Extensometer 5
-Tau*Ln(1+Deformation/A)+Tzero
8000
7500
7000
6500
6000
5500
5000
4500
4000
3500
3000
3000 3500 4000 4500 5000 5500 6000 6500 7000 7500 8000
Time (Hours)

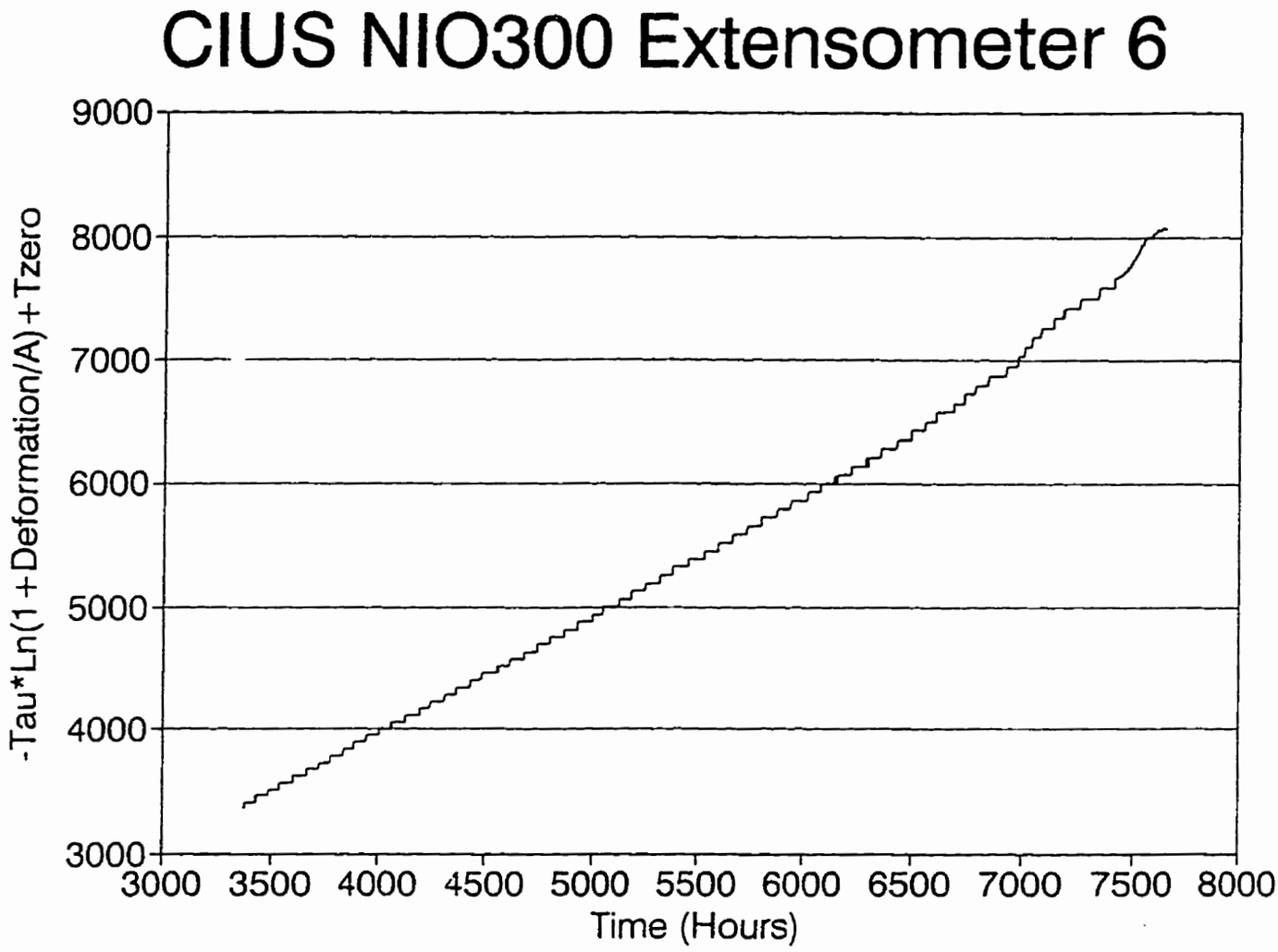
CIUS NIO300 Extensometer 6
-Tau*Ln(1+Deformation/A)+Tzero
9000
8000
7000
6000
5000
4000
3000
3000 3500 4000 4500 5000 5500 6000 6500 7000 7500 8000
Time (Hours)

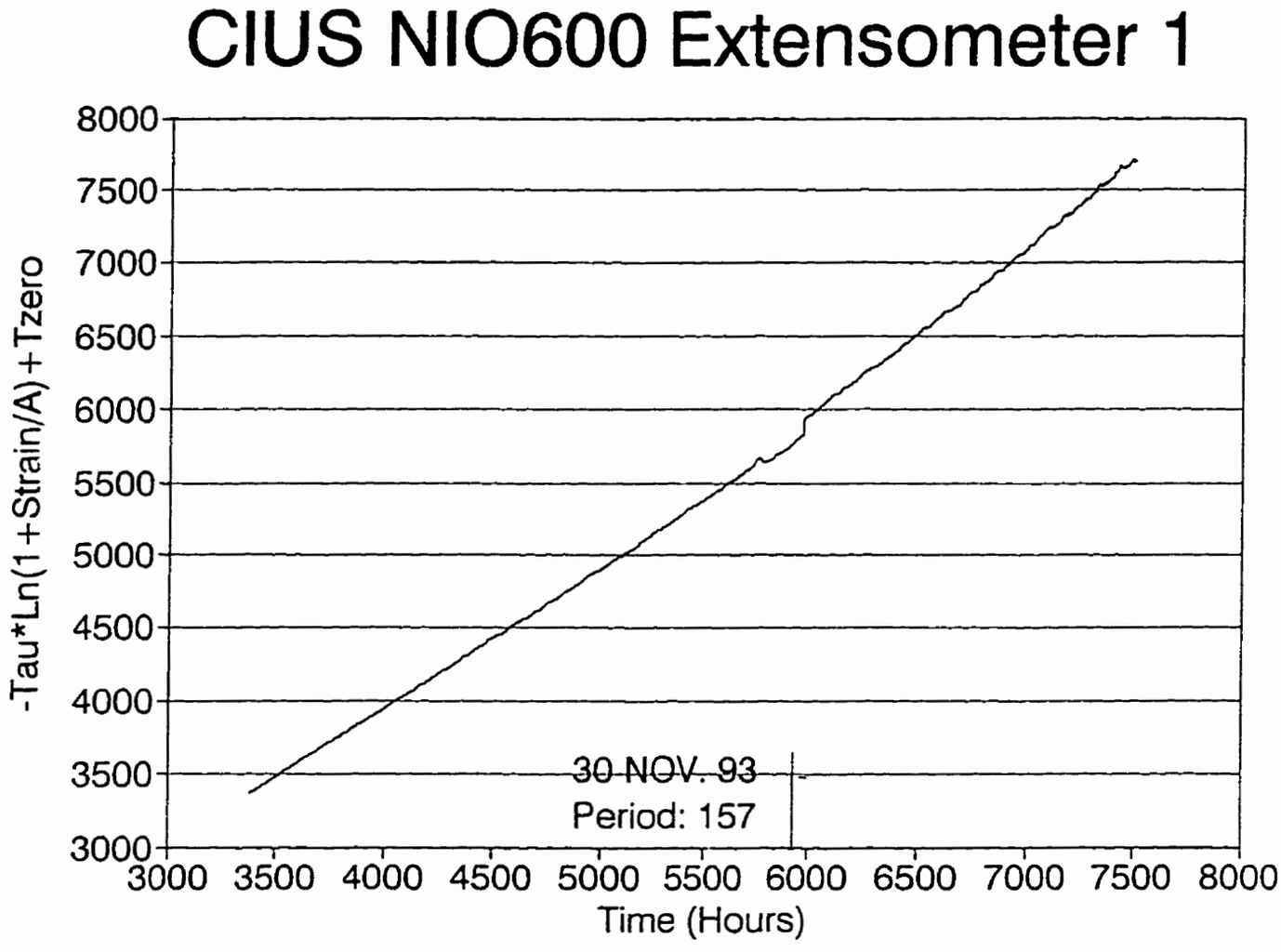
CIUS NIO600 Extensometer 1
-Tau*Ln(1+Strain/A)+Tzero
8000
7500
7000
6500
6000
5500
5000
4500
4000
3500
3000
30 NOV. 93
Period: 157
3000 3500 4000 4500 5000 5500 6000 6500 7000 7500 8000
Time (Hours)

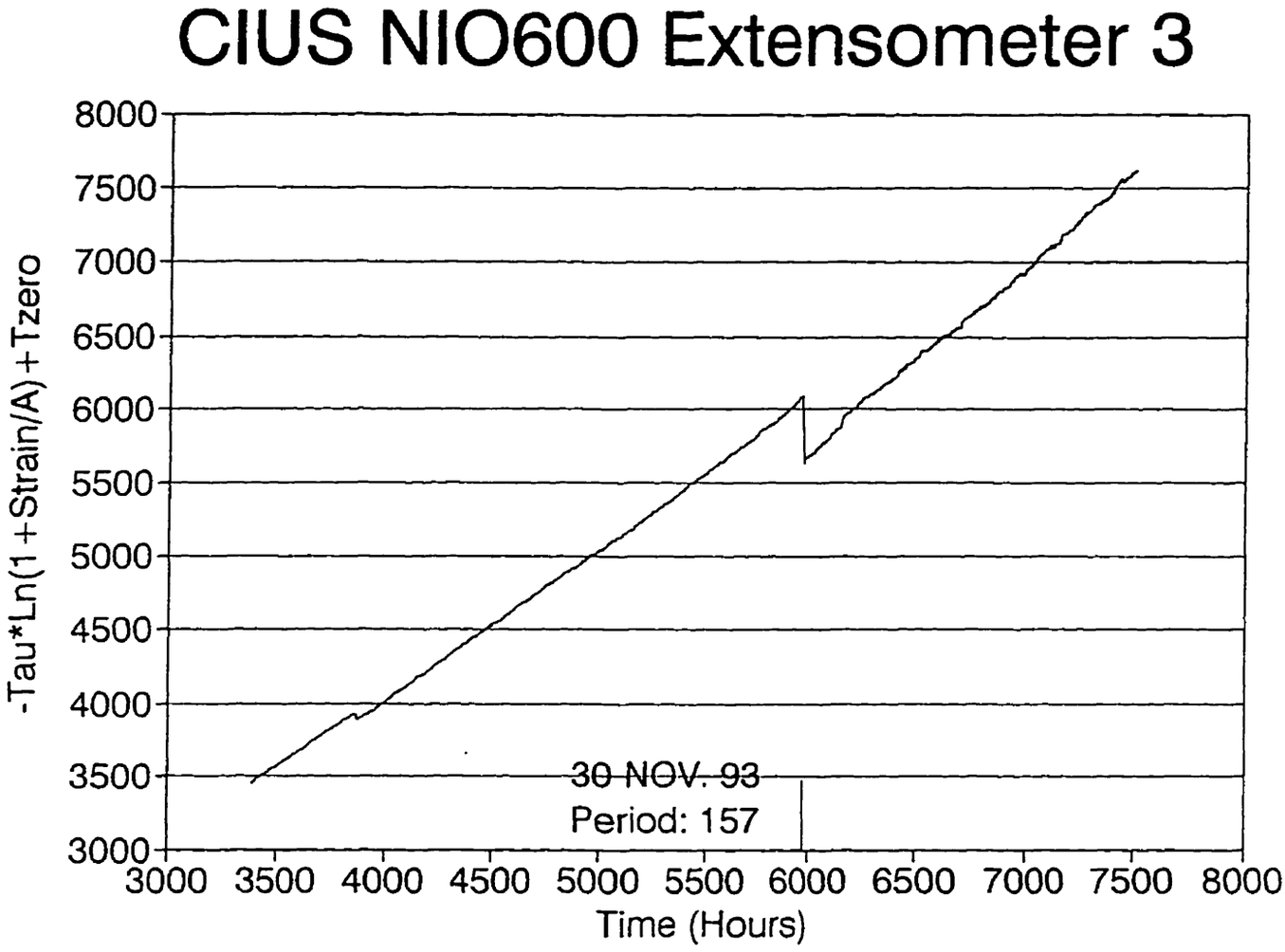
CIUS NIO600 Extensometer 3
-Tau*Ln(1+Strain/A)+Tzero
8000
7500
7000
6500
6000
5500
5000
4500
4000
3500
3000
3000 3500 4000 4500 5000 5500 6000 6500 7000 7500 8000
Time (Hours)
30 NOV. 93
Period: 157

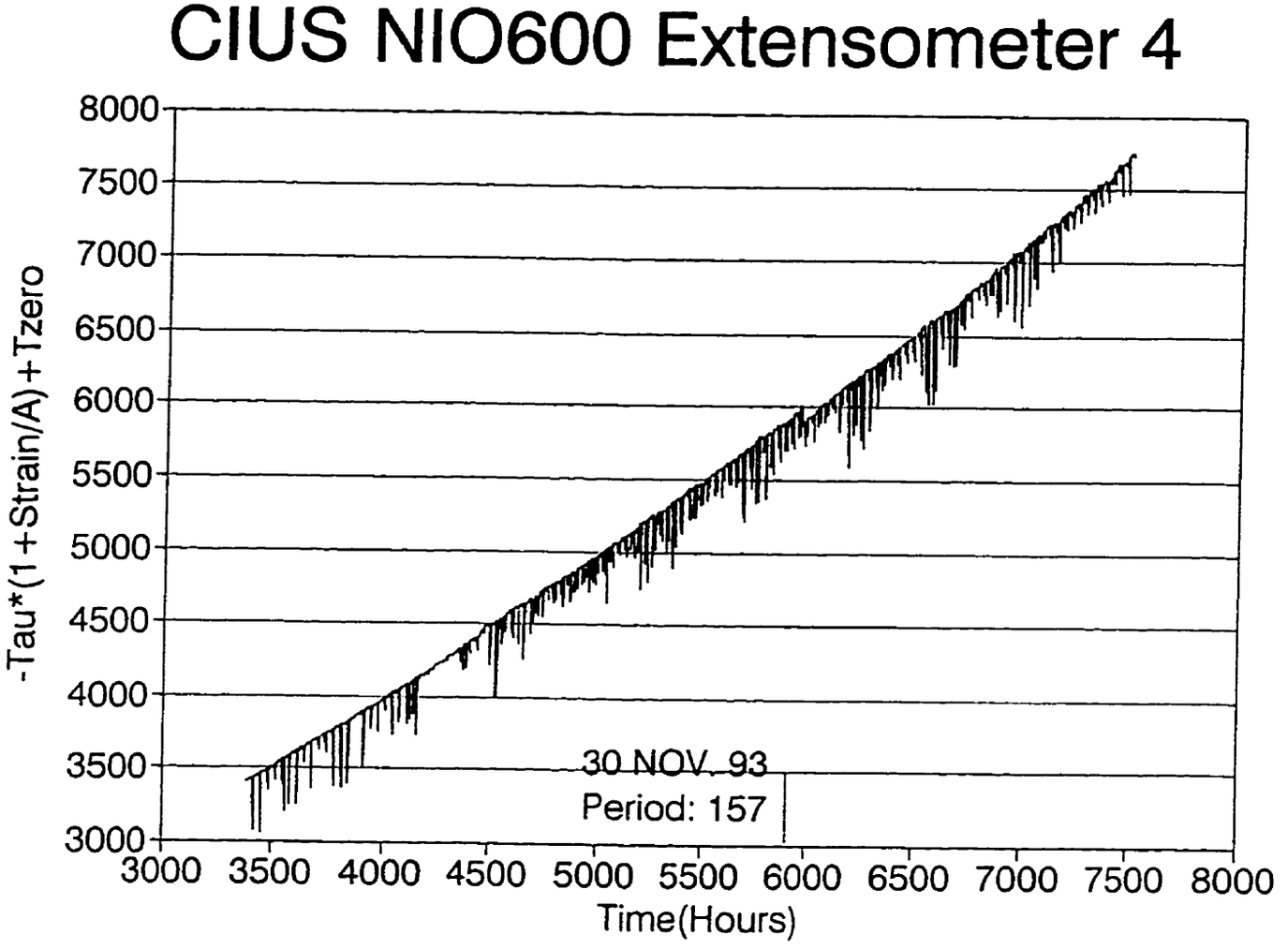
CIUS NIO600 Extensometer 4
-Tau*(1+Strain/A)+Tzero
8000
7500
7000
6500
6000
5500
5000
4500
4000
3500
3000
3000 3500 4000 4500 5000 5500 6000 6500 7000 7500 8000
Time(Hours)
30 NOV. 93
Period: 157

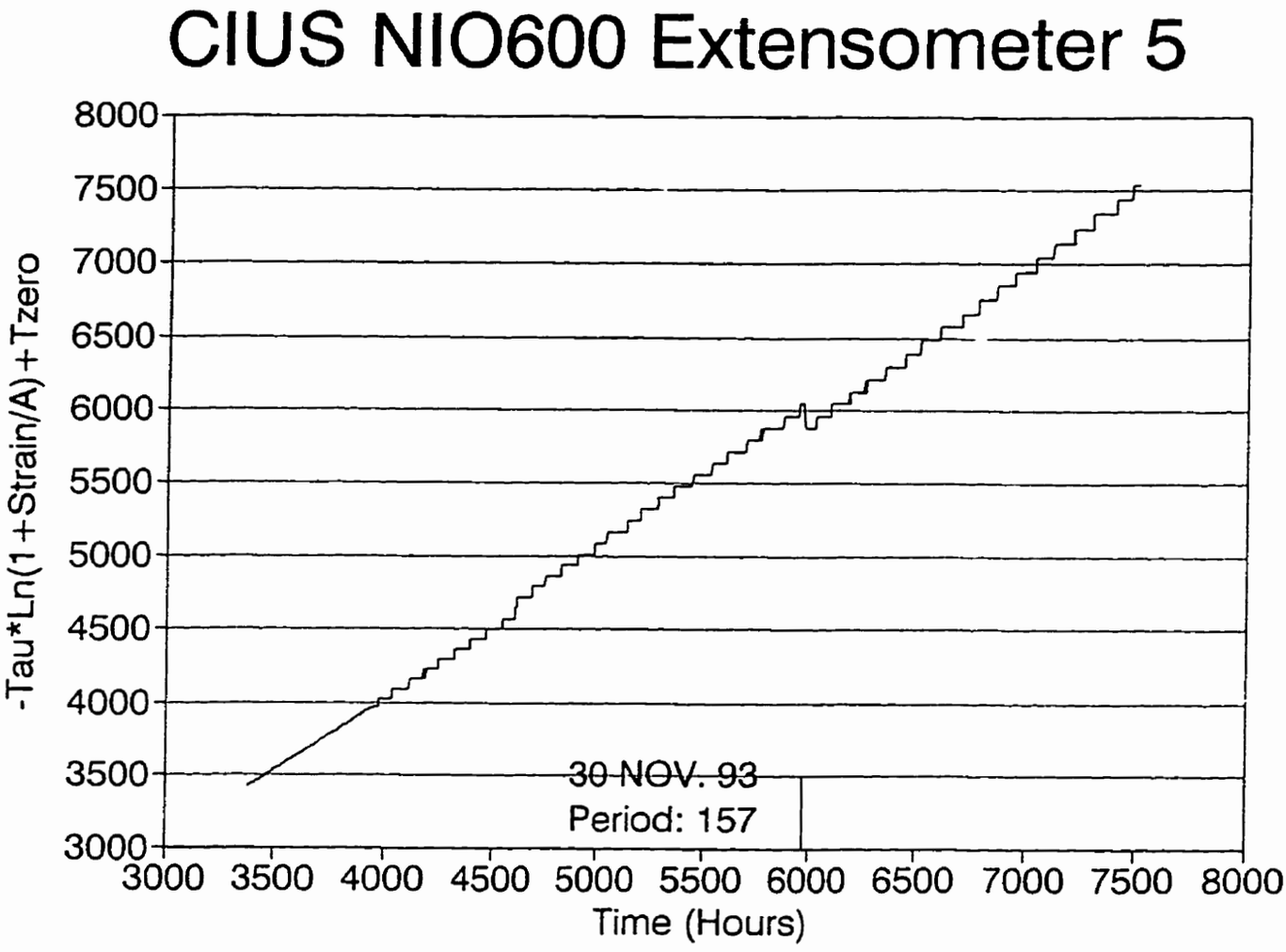
CIUS NIO600 Extensometer 5
-Tau*Ln(1+Strain/A)+Tzero
8000
7500
7000
6500
6000
5500
5000
4500
4000
3500
3000
30 NOV. 93
Period: 157
3000 3500 4000 4500 5000 5500 6000 6500 7000 7500 8000
Time (Hours)